Sjors van der Stelt

RISE AND FALL OF PERIODIC PATTERNS

IN A GENERALIZED KLAUSMEIER-GRAY-SCOTT MODEL

Sjors van der Stelt

Rise and Fall of Periodic Patterns

in a Generalized

Klausmeier-Gray-Scott Model

Rise and Fall of Periodic Patterns

in a Generalized

Klausmeier-Gray-Scott Model

ACADEMISCH PROEFSCHRIFT

ter verkrijging van de graad van doctor

aan de Universiteit van Amsterdam

op gezag van de Rector Magnificus

prof. dr. D.C. van den Boom

ten overstaan van een door het college voor promoties ingestelde

commissie, in het openbaar te verdedigen in de Aula der Universiteit

op vrijdag 27 januari 2012, te 13.00 uur

door

Sjors van der Stelt

geboren te Amsterdam

Promotiecommissie

Promotor: prof. dr. A. Doelman

Copromotores: dr. G.M. Hek
                   dr. J.D.M. Rademacher

Overige leden: prof. dr. G.J.B. van den Berg
                   prof. dr. A.J. Homburg
                   prof. dr. ir. M.G. Rietkerk
                   prof. dr. R.P. Stevenson
                   prof. dr. J.J.O.O. Wiegerinck

Faculteit der Natuurwetenschappen, Wiskunde en Informatica

Contents

Chapter 1

Introduction

Semi-arid ecosystems, ecosystems with an annual precipitation of 250-500 mm, are typically found at the edge of deserts, marking the landscape between deserts and dry steppes on the one side and greener ecosystems such as grass savannas, montane forests and temperate broadleaf forests on the other side. One striking fact observed in semi-arid ecosystems is the presence of patterned vegetation, that has been discovered by aerial photographs in the 1950s [52, 53] in sub-Saharan Africa. These patterns have subsequently been reported in many semi-arid ecosystems in Africa, the Americas and Australia, and are estimated to cover about 30% of the emerged surface of the earth. The composition of the vegetation varies wildly from one ecosystem to another and can comprise of grass, scrubs, bushes or trees [51, 53]. Also, the occurence of these patterns is not specific to the type of soil [51].

It is confirmed widely that semi-arid ecosystems which exhibit vegetation patterns run the risk of a sudden collapse to become deserts or dry steppes when a vital system parameter crosses a threshold value, in particular, this occurs when either the precipitation rate crosses a threshold value in a downward movement or the grazing pressure by cattle crosses a threshold value in an upward movement [41, 46]. Ecologists tend to speak of a catastrophe since this process is irreversible: when, for example, a valley with striped vegetation patterns has turned into a desert after years of severe drought, then, after years when rain begins to fall gradually again, it generally does not turn back into a vegetated ecosystem.

★

Early attempts to formulate a model for semi-arid ecosystems are by using cellular automata [91] or by mean field models [51]. In 1999, C.A. Klausmeier was the first to model the dynamic interplay between water infiltration and vegetation density by a reaction-(advection-)diffusion system [46]. His model describes a positive feedback between water infiltration and vegetation density and captured the irreversibility of the catastrophe described above. He introduced a 2-component system to describe

patterns in semi-arid ecosystems, the components representing water infiltration u and vegetation density v. In unscaled form, the model he introduced reads as follows:

$$\begin{cases} u_t = k_0 u_x + k_1 - k_2 u - k_3 k_5 u v^2 \\ v_t = d_v v_{xx} - k_4 v + k_5 u v^2 \end{cases} \tag{0.1}$$

where $u(x,t), v(x,t) : \mathbb{R} \times \mathbb{R}_+ \to \mathbb{R}$ and $k_i \geq 0$, $i = 1, \ldots, 5$, $d_v \geq 0$. The change of water infiltration u_t is assumed to be governed by advection caused by the gradient slope of the area, modeled by $k_0 u_x$, a constant precipitation rate k_1, an evaporation rate that is linear in the water infiltration $-k_2 u$, and the infiltration feedback, modeled by $-k_3 k_5 u v^2$. It assumes that the change of vegetation density is controlled by a diffusive spread of biomass, modeled by a diffusion term $d_v v_{xx}$, a linear natural death rate $-k_4 v$ and the infiltration feedback $k_5 u v^2$, that has a positive effect on the vegetation. Since the spread of biomass occurs on a much slower time scale than the advection of surface water, it is natural to assume $d_v \ll k_0$. Though the model is simplistic in nature, it is able to capture essential features of semi-arid ecosystems, such as the emergence of patterned vegetation.

We notice that Klausmeier's original model [46] assumed two-dimensional spatial variation in x and y of both vegetation density v and water infiltration u. In this thesis, we focus on the one-dimensional dynamics of Klausmeier's original model, so we have simplified the two-dimensional spatial variance by assuming a constant variation in the direction of the spatial y-variable. We also assume that both u and v vary on an infinite domain $\mathbb{R}$ instead of a bounded domain $[0, L]$ with $L \in (0, \infty)$. This assumption is natural, since the scale of the observed patterns is relatively small compared to the size of the domain (cf. [41, 46, 52, 53, 74], and [8] and the references therein).

We extend the model as follows. The model assumes the existence of some slope or gradient that lets the water flow downhill and the growing vegetation migrate uphill. However, patterns have been observed in semi-arid ecosystems without a slope [52, 53, 100]. In order to model the spread of water on a terrain without a specific preference for the direction in which the water flows, we have added a term that models porous media flow, and obtain

$$\begin{cases} u_t = d_u (u^\gamma)_{xx} + k_0 u_x + k_1 - k_2 u - k_3 k_5 u v^2; \\ v_t = d_v v_{xx} - k_4 v + k_5 u v^2, \end{cases} \tag{0.2}$$

where it is assumed that $\gamma \geq 1$. Since the spread of biomass occurs on a much slower scale than the (nonlinear) diffusion of water, it is natural to assume $0 < d_v \ll d_u$. For ecosystems without a slope, we set $k_0 = 0$. In this thesis we choose either $\gamma = 1$ or $\gamma = 2$. The choice $\gamma = 1$ models the random motion of water as diffusion, whereas the model with $\gamma = 2$ models the motion of water as porous media flow.

In order to reduce the number of parameters, we rescale the model. Set

$$U = \frac{k_2}{k_1} u; \quad V = \frac{k_2 k_3}{k_1} v, \tag{0.3}$$

and further

$$T = \frac{k_1^2 k_5}{k_2^2 k_3} t; \quad X = \left[d_u \frac{k_3}{k_5} (\frac{k_1}{k_2})^{\gamma-3} \right]^{-\frac{1}{2}} x. \tag{0.4}$$

We obtain

$$\begin{cases} U_t &=& U_{xx}^\gamma &+& CU_x &+& A(1-U) &-& UV^2 \\ V_t &=& \delta^{2\sigma} V_{xx} &-& BV &+& UV^2, \end{cases} \tag{0.5}$$

with

$$A = k_2 \frac{k_2^2 k_3}{k_1^2 k_5}; \quad B = k_4 \frac{k_2^2 k_3}{k_1^2 k_5}; \quad C = k_0 \frac{k_2^2 k_3}{k_1^2 k_5} \left[d_u \frac{k_3}{k_5} \left(\frac{k_1}{k_2} \right)^{\gamma-3} \right]^{-\frac{1}{2}}$$

and

$$\delta^{2\sigma} = \frac{d_v}{d_u} (\frac{k_2}{k_1})^{\gamma-1} \quad (\sigma > 0).$$

One has $0 < \delta \ll 1$, since $0 < d_v \ll d_u$. Notice that there is a redundancy in the introduction of $\delta^{2\sigma}$. In chapter 2 it will become clear why it is convenient to define the rescaled diffusion coefficient this way. The system parameters A, B, C and γ are chosen according to the characteristics of the ecosystem under study. In particular, ecosystems without a slope are modelled by setting $C = 0$ and ecosystems on a terrain that has a slope are modelled by setting $C \neq 0$. We may view C as a parameter that measures the rate of advection (or the rate of the slope of the terrain), A as a parameter that controls the precipitation and B as a parameter that describes the extinction rate of the biomass. A priori, there is no reason to assume that the parameters A, B and C are $\mathcal{O}(1)$ with respect to δ, in fact, the relative magnitudes of A, B and C will play a crucial role in the analysis of chapter 2 (see also [56]).

We need to make one crucial remark. The expression for A depends on the rainfall k_1 via $A \sim k_2^3/k_1^2$. At first sight, this may seem contradictory, since in the rescaled model (0.5) we consider A as a parameter that measures the rainfall. In order to understand this, consider the expression for B: since B is proportional to $B \sim k_2^2/k_1^2$ and it is assumed that B and the other k_j, $j = 3, 4, 5$, are constant, we conclude $k_1 \sim k_2$ and therefore

$$A \sim \frac{k_2^3}{k_1^2} \sim \frac{k_1^3}{k_1^2} = k_1.$$

Hence, we see that A is proportional to the rainfall k_1.

The above rescaling is motivated by the fact that equation (0.5) reduces to the Gray-Scott model if we set $C = 0$ and $\gamma = 1$ (see [5, 23, 56] and the references therein). More generally, by either setting $\gamma = 1$ or $\gamma \geq 1$ and either $C = 0$ or $C > 0$, the model (0.5) comprises four types of equations. We will refer to the equations in (0.5) as *the Generalized Klausmeier-Gray-Scott model* or shortly, GKGS-model. A schematic picture of the four classes of the GKGS-system is given in Figure 1.1.
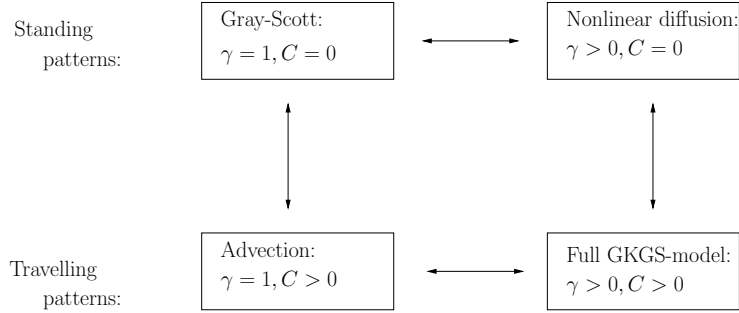
Figure 1.1: A schematic picture of the GKGS-model. On the top line, the models without advection ($C = 0$) are depicted. These models generate small amplitude symmetric Turing patterns that are modulated according to a real GLE. On the bottom line, the models with a nontrivial advection rate $C > 0$ are depicted. For these models, the appearance of the travelling periodic patterns is described by a complex GLE. (See section 2.1.4.)

Like the Gray-Scott model, the GKGS-model (0.5) has three spatially homogeneous background states for $A > 4B^2$:

$$U_0 = 1, V_0 = 0, \quad U_{\pm} = \frac{1}{2A}\left(A \mp \sqrt{A^2 - 4AB^2}\right), V_{\pm} = \frac{1}{2B}\left(A \pm \sqrt{A^2 - 4AB^2}\right).$$
$$(0.6)$$

The state $(U_0, V_0) = (1, 0)$ represents the desert (since $V_0 \equiv 0$). At $A_{\mathrm{sn}} = 4B^2$, the equilibria (U_+, V_+) and (U_-, V_-) collapse and disappear in a fold, or saddle node bifurcation. Hence, for $A < A_{\mathrm{sn}}$, the desert $(U_0, V_0) = (1, 0)$ is the only background state, while for $A > A_{\mathrm{sn}}$, we have three background states, among which the homogeneously vegetated state (U_+, V_+) and the desert state (U_0, V_0) are homogeneously stable and the homogeneously vegetated state (U_-, V_-) is homogeneously unstable.

★

Now that we have introduced the model that is studied in this thesis, and since it is our final aim to gain insight in the fall and rise of vegetation patterns in semi-arid ecosystems, we first dedicate a few words to the use and practice of mathematical modelling in general in §1.1. Then, in §1.2, we describe some important characteristics of the model. In §1.3 we aim to explain in a simple setting the methods that we have used in this thesis to study the GKGS-model (0.5) – in fact, each of the subsections of §1.3 tries to explain in layman's terms what is going on in chapters 2, 3 and 4. The concepts in sections 1.2 and 1.3 will sometimes be explained with models other than the GKGS-model (0.5) as examples, since we thought it easier for the reader to grasp the basic ideas when they are applied to a simpler setting. Then, finally, we give a brief outline of the thesis in §1.4.

1.1   On mathematical modelling

Despite the famous words of Galileo[1], one of the most challenging tasks of the applied sciences[2] is the formulation of mathematical models that properly describe the system under study. As of now, many complex natural systems such as wind circulation, the forming of clouds and rivers, oceanic currents, phytoplankton growth and decay, leaf arrangements on trees, cellular growth, formation and meltdown of polar ice caps, stripe pattern formation on the skin of African mammals, tides and many, many more are only partly understood. Mathematical models aiming to describe these natural phenomena can only do so to a limited extent. For example, none of the models in use is able to give precise predictions on the future state of the system under study – most notably among which are models that aim to describe the future state of the global climate.

This section is written in order to shortly explain the difficulties that come with the description of natural systems. We will lay bare some of the restrictions of mathematical modelling. Also, we will try to shed light on how results based on mathematical models can be useful.

We start with the important remark that there is a difference between models that are phenomenological and those that are not. Models such as Newton's laws or Maxwell's laws describe closed systems. Therefore, these 'laws' are verifiable[3], that is: one can make predictions based on model calculations and measure if a physical model shows the behaviour that it predicts for the (closed) system. These models usually form part of a well accepted general theory.

Phenomenological models are models that describe open systems. They usually do not derive from first principles[4] as they are often debatable. These models can in principle be validated in the sense that they do not contradict accepted theory [65]. However, due to the openness of the systems they describe they can never be fully verified [65]. In fact, almost all models for complex natural systems that are used today are phenomenological models (though not always to the same extent[5]).

At least three causes for the abundance of phenomenological models can be pointed out [47]. First, our theoretical understanding of many natural processes is limited. Second, most models suffer from a lack of complete observations. Parameter uncertainty and uncertainty of the initial and boundary conditions are caused by the lack

---

[1] "The laws of nature are written in the language of mathematics."

[2] We define applied sciences as sciences that make extensive use of mathematical models in order to understand physical (observable) systems, such as chemistry, physics, biology, ecology, economics, climatology or (geophysical) fluid dynamics.

[3] However, Popper [69] disagrees with this and remarks that no law in the natural sciences can ever be verified. According to [69], the laws of nature are open only to falsification and corroboration.

[4] Laws that are part of generally accepted physical theory are said to be derivable from first principles.

[5] In climate science, for example, there exist simple phenomenological two-component models that focus on very specific processes that are part of the climate and that are not able to precisely predict the climate, while on the other hand, there are fully coupled atmosphere-ocean general circulation models (AOGCMs) that do make predictions and projections that are relatively precise.

of complete observations. Third, simplifications of some model assumptions have to be made due to computational constraints or accessibility to mathematical analysis.

As an example one may consider the central theme of this thesis: semi-arid ecosystems. As of now, we have no complete theoretical understanding of the infiltration feedback between water infiltration and plant density. The equations of the GKGS-model (0.5) model the infiltration feedback by $\pm uv^2$, but theoretical ecologists agree that this is only a very coarse way of modelling [41]. Generally speaking, the water uptake is parametrized by environmental conditions such as the soil type, physical characteristics of the root system, temperature, precipitation rate, competition among different trees, and surely others. Also, the relatively simple nature of the GKGS-model entails that its parametrization can only be approximate: for example, it is not clear how the parameter d_v can be drawn from field data.

These complications generally cannot be undone by just enlarging or simplifying the model. For example, throwing more data at the problem naturally asks for more complicated models. However, more complicated models generally suffer from greater computational difficulties and are generally harder to analyze. Also, assigning meaning to empirical tests of the model becomes increasingly difficult with an ever larger number of parameters.

Lack of access to the phenomena of interest prevents us to verify some outcomes of the mathematical model that we propose. However, models can certainly be useful [65]. First, models may corroborate a hypothesis by offering evidence to results that have already been partly established otherwise. Second, models may elucidate shortcomings of other models. And third, models can be used for sensitivity analysis: "what if" scenarios such as worst and best case scenarios can be used to shed light on what could happen with the phenomena of interest.[6]

As an example of the first, we turn our attention to the saddle-node bifurcation of the homogeneously vegetated states (U_-, V_-) and (U_+, V_+) of the GKGS-system (0.5). If A decreases through A_{sn} and the stable state (U_+, V_+) disappears, then increasing A again does not bring the system back into a vegetated state. It is precisely this hysteretical behaviour of the model (0.5) that corroborates the irreversible character of the catastrophe that has been observed in nature [41, 74].

As another example of the first, we consider the GKGS-model again. One may formulate the hypothesis that it is not necessary to model the flow of water with porous media flow, as we have done in the GKGS-model (0.5), since it would not give more insight than the model for $\gamma = 1$. As will be made more precise in chapter 2 and later in chapter 3, the dynamics of the GKGS-system (0.5) with diffusion ($\gamma = 1$) is qualitatively identical to the dynamics of the GKGS-system (0.5) for porous media flow ($\gamma = 2$). This corroborates the hypothesis that the spread of water in a two-component model comprising water infiltration and vegetation density can in fact be modelled with diffusion, instead of (the more complicated) porous media flow.

---

[6]One usually refers to these scenarios as *projections*, in contrast to predictions. For example, the reports of the IPCC (see [42]) contain projections of the average global temperature based on, for example, assumptions about future CO_2 levels.
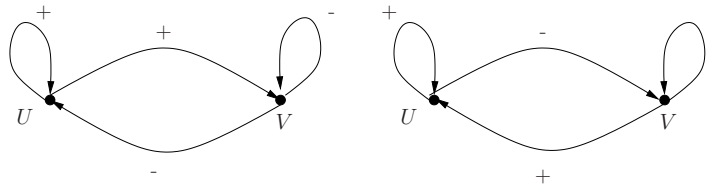
Figure 1.2: Graphical display of the feedbacks within the activator-inhibitor mechanism (left) and the positive feedback mechanism (right).

This way we have corroborated our initial hypothesis that modeling water flow in the GKGS-model (0.5) can be modelled well by diffusion.

1.2 Some important characteristics of the model

1.2.1 Positive feedback

The GKGS-model (0.5) exhibits the important feature of a positive feedback between the water infiltration and the plant density [31, 41, 46]. From a modelling perspective, this positive feedback mechanism makes sense: water infiltration in vegetated ground is much faster than in unvegetated ground, so the water infiltration is enhanced by both water infiltration and vegetation density. Mathematically, positive feedback and activator-inhibitor structures of PDE systems are captured by the sign structure of the linearization $\mathcal{P}$ about a relevant homogeneous background state [31]:

$$
\begin{aligned}
\text{Activator-inhibitor mechanism:} \quad &\mathcal{P} = \begin{pmatrix} + & - \\ + & - \end{pmatrix}. \\
\text{Positive feedback mechanism:} \quad &\mathcal{P} = \begin{pmatrix} - & - \\ + & + \end{pmatrix}.
\end{aligned}
\tag{2.1}
$$

See Figure 1.2 for a graphical display of the feedback mechanisms that define these two different types of systems. Assuming we are not far from the background state (U_+, V_+), we are sure that the homogeneous dynamics of the GKGS-system (0.5) is mainly given by the derivative at (U_+, V_+),

$$
DF|_{U_+, V_+} = \mathcal{P} = \begin{pmatrix} -A - V_+^2 & -2B \\ V_+^2 & B \end{pmatrix}.
\tag{2.2}
$$

From (2.2) we see that the GKGS-system has a positive feedback, since it has the structure of a positive feedback mechanism as displayed in $(2.1)_2$.

1.2.2 Turing instability

A.M. Turing[7], mostly known for cracking the German code during the Second World War and remembered as one of the founding fathers of today's computers,

---

[7]The reader may know that A.M. Turing tragically committed suicide, after being released from a prison sentence brought upon him by the British autorities because of an alleged violation of the

has also made an important contribution to the science of pattern formation. In an attempt to clarify the occurence of Fibonacci sequences in plant morphology (known as phyllotaxis – see for a modern treatment [26, 27, 28, 2, 50]), he introduced a concept that is now known as a Turing instability. Loosely speaking, a Turing instability happens when a homogeneous background state that is stable with respect to homogeneous perturbations loses its stability when perturbed by spatially periodic perturbations. Turing's vital discovery was, in modern terms, that this can happen in a two-component PDE for which both components diffuse at *different rates*. Though the basic idea can now be viewed as rather simple, one should understand that this discovery came as rather a surprise: it was known that solutions to Cauchy problems for the heat equation flatten out in the course of time, and that they do so precisely due to the presence of diffusion in the heat equation. Turing's discovery meant that adding diffusion to a two-component model can destabilize homogeneous solutions, thereby allowing for pattern growth – which is in sharp contrast to the effect that initial conditions in one-component models such as the heat equation flatten out in the course of time.

Later, in chapter 2 we will rigorously deduce that the GKGS-system (0.5) undergoes a Turing instability (in fact, it undergoes a Turing-Hopf instability; which basically means that the emerging patterns are travelling). Here, we seek to explain this concept in the context of a linear reaction-diffusion model

$$\begin{array}{rclclcl} u_t & = & D_1 u_{xx} & + & (\mu - 1)u & + & v \\ v_t & = & D_2 v_{xx} & - & \mu u & - & v \end{array} \qquad (2.3)$$

where $x \in \mathbb{R}$, $t \in \mathbb{R}_+$, $u, v : \mathbb{R} \times \mathbb{R}_+ \to \mathbb{R}$ and $\mu \geq 0$, $D_1, D_2 > 0$. System (2.3) is of purely theoretical interest, only meant to introduce the concept of the Turing bifurcation and as far as we know, it does not represent a real model for any natural process. It is assumed that the equilibrium $(0, 0)$ is homogeneously stable – that is, the equilibrium $(0, 0)$ is stable with respect to perturbations that have no spatial structure. A necessary and sufficient condition for the equilibrium $(0, 0)$ to be homogeneously stable is

$$\det \begin{pmatrix} \mu - 1 & 1 \\ -\mu & -1 \end{pmatrix} = 1 > 0 \quad \text{and} \quad \mathrm{tr} \begin{pmatrix} \mu - 1 & 1 \\ -\mu & -1 \end{pmatrix} = \mu - 2 < 0, \qquad (2.4)$$

which gives the condition

$$\mu < 2. \qquad (2.5)$$

If $\mu = 2$, the equilibrium undergoes a Hopf bifurcation.

Criminal Law Amendment Act 1885 that, in fact, prohibited homosexual behaviour of any kind, be it private or public. We refer the reader to [40] for an intriguing account on both his life and his scientific work (also for the nonmathematician).

By computing the Fourier transform of (2.3)[8] with respect to x we derive the *dispersion relation*. The dispersion relation associated to (2.3) is determined by the eigenvalues of the matrices

$$\mathcal{M}(k) = \begin{pmatrix} \mu - 1 - D_1 k^2 & 1 \\ -\mu & -1 - D_2 k^2 \end{pmatrix}. \tag{2.6}$$

The determinant of $\mathcal{M}(k)$ is easily computed,

$$\det \mathcal{M}(k) = D_1 D_2 k^4 + (D_1 + D_2) k^2 + 1 - D_2 \mu k^2.$$

Now, the background state $(0,0)$ loses stability if one of the eigenvalues of $\mathcal{M}(k)$ crosses the imaginary axis, which happens if $\det \mathcal{M}(k) = 0$. Assume we increase μ from zero upwards. The determinant of $\mathcal{M}(k)$ equals zero at

$$\mu = D_1 k^2 + \frac{D_1 + D_2}{D_2} + \frac{1}{D_2 k^2}. \tag{2.7}$$

Remembering that μ increases from zero, the first value of μ for which there exists a k such that μ can be written as in (2.7) is the minimum of $\mu = \mu(k)$. By differentiation of (2.7), we see that the minimum of $\mu(k)$ is at

$$k_*^2 = \frac{1}{\sqrt{D_1 D_2}} \qquad \text{and} \qquad \mu_* = \left(1 + \sqrt{\frac{D_1}{D_2}}\right)^2. \tag{2.8}$$

Therefore, the instability sets in at $\mu = \mu_*$ and the unstable mode has wavenumber $k = k_*$.

For completeness, we remark that it is immediately clear from (2.8) that $D_1 \neq D_2$, since if $D_1 = D_2$ then condition (2.5) is violated. This is always true: a reaction diffusion system can undergo a Turing instability only if the diffusion rates are different.

Remark System (2.3) undergoes a Hopf instability if $\mu = 2$. Therefore, we substitute μ_* into condition (2.5) and obtain an inequality which is stronger than the above requisite that $D_1 \neq D_2$:

$$D_1 < (3 - 2\sqrt{2}) D_2.$$

If this inequality is not satisfied, then the equilibrium $(0,0)$ undergoes a Hopf bifurcation first and the Turing instability takes place when the equilibrium is already Hopf unstable.

1.3 Methods

1.3.1 Nonlinearities: the Ginzburg-Landau approach

If we were studying a solution to a linear model, then every instability and in particular the Turing instability, would yield perturbations that grow indefinitely and

---

[8] For a study of the stability of patterns, the reader is referred to [39],[76] and [96].

exponentially in time and the solution would become unbounded (in every nontrivial norm of the Banach space of solutions that we consider). However, in nature one never witnesses such behaviour. This is precisely because such instabilities occur in systems that are inherently *nonlinear*.

Intuitively, one can understand this as follows. Usually a perturbation is initially very small and therefore the dynamics are mainly determined by the linear terms of the model, which tell the solution to grow (exponentially) in time. However, after some time the perturbed solution becomes larger and the nonlinear terms come into play. These nonlinear terms usually prevent ongoing exponential growth of the initial perturbation in some way. Exactly *how* this happens is a field that is under thorough study and heavily depends on the premises of the problem under study. In fact, it is safe to say that most of the modern theory of dynamical systems and the field of PDEs deals with the study of nonlinearities.[9]

This section aims to describe at least one method to deal with a PDE for which the nonlinear terms are taken into account. This method is a reduction method: the basic idea is to reduce the analysis of the full PDE to the study of a much simpler and well studied equation that is known as the *Ginzburg-Landau equation*. In order for this method to be applicable, three assumptions have to be satisfied. The first is that the solution $u(x, y, t)$ is defined for a domain that is cylindrically shaped, i.e. $y \in \Omega$ with Ω bounded (in our case, $\Omega = \emptyset$) and $x \in \mathbb{R}$, $t \in [0, \infty)$.

The second assumption is that the spectrum of the differential operator associated to the linearization about the perturbed solution satisfies the hypotheses as formulated in §2.1 in [55] or in §2.2 in [11]. As this serves as an introduction to the subject and the exact hypotheses are quite technical, we refrain from repeating the spectral assumption here. However, as a mental image, one may have the following facts in mind. First, it is important to keep in mind that in the neighbourhood of the most unstable mode, the spectrum should be parabolically shaped, as is suggested in Figure 1.3. Second, one should be aware that the spectral assumptions entail that the unstable mode associated to the perturbed solution is of the form $E = e^{\mathrm{i}k_* x}$ associated to an eigenvalue $\mathrm{i}\omega_*$ and that either $k_* \neq 0$ or $\omega_* \neq 0$ or both. In fact, in this thesis, it will always be so that $k_* \neq 0$, so that the unstable mode has nontrivial spatial structure.

The third important condition is the assumption that the critical parameter μ is only slightly unstable: it is assumed that $\mu = \mu_* + \varepsilon^2$ with $0 < \varepsilon \ll 1$. This way, we are able to 'balance' the linear terms with the nonlinear terms, as we will see shortly. Notice that this condition severely restricts the applicability of the Ginzburg-Landau approach: if $|\mu - \mu_*|$ is of order larger than ε^2, the method can no longer be applied. Still, it enables us to describe the emerging periodic patterns right after the bifurcation has taken place. Later in this thesis, in chapter 3, we will develop numerical techniques that enable us to describe patterns far from equilibrium, i.e. patterns for which $|\mu - \mu_*| > \varepsilon^2$. We will come back to this later in the introduction (see section 1.3.2).

---

[9]To Stanislaw Ulam are attributed the words "Using a term like nonlinear science is like referring to the bulk of zoology as the study of non-elephant animals.". Cf. [38].
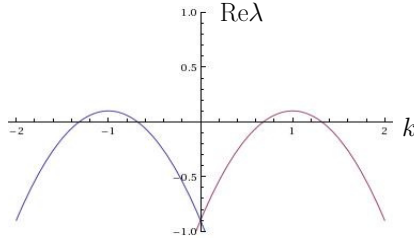
Figure 1.3: Sketch of a critical branch of the essential spectrum locally near the unstable modes. Near the unstable modes, the spectrum is parabolically shaped.

As an example, we consider the Swift-Hohenberg equation

$$u_t + (1 + \partial_{xx})^2 u = \mu u - u^3. \tag{3.1}$$

The Swift-Hohenberg (3.1) equation serves in many ways as the most natural example to show the Ginzburg-Landau formalism. The dispersion relation associated to the spectrum of the background state $u_0 = 0$ of (3.1) reads

$$\lambda + (1 - k^2)^2 = \mu. \tag{3.2}$$

From (3.2) we derive that $\lambda(k) < 0$ for all $k \in \mathbb{R}$ if and only if $\mu < \mu_* := 0$. Hence, at $\mu = \mu_*$ we have

$$\lambda = 0 \qquad \text{and} \qquad k_* = \pm 1. \tag{3.3}$$

The interested reader may verify that the spectrum of the linearisation about the background state $u = 0$ indeed satisfies the spectral assumptions from [55] or [11].

The basic idea then goes as follows. (Here, we closely follow the unpublished notes [20].) Assume that $\mu = r\varepsilon^2$. Then from the dispersion relation (3.2) it is clear that there exist two intervals centered around $k_* = \pm 1$ for which $\lambda = \lambda(k, r\varepsilon^2) > 0$: $I_- \cup I_+ = (-1 + \varepsilon K_-(\varepsilon), -1 + \varepsilon K_+(\varepsilon)) \cup (1 + \varepsilon K_-(\varepsilon), 1 + \varepsilon K_+(\varepsilon))$, with $K_\pm = \pm \frac{1}{2}\sqrt{r} + \mathcal{O}(\varepsilon)$. Therefore, an unstable and exponentially growing linear mode $e^{ikx + [r\varepsilon^2 - (1-k^2)^2]t}$ with $k \in I_- \cup I_+$ can be written as

$$e^{i(1+\varepsilon K)x + [r\varepsilon^2 - (1-(1+\varepsilon K)^2)^2]t} = e^{iK(\varepsilon x) + (r - 4K^2 + \mathcal{O}(\varepsilon))(\varepsilon^2 t)} e^{ix} = \mathcal{A}_{\text{lin}}(\varepsilon x, \varepsilon^2 t) e^{ix} \tag{3.4}$$

Thus, the specific spectral structure associated to the Swift-Hohenberg equation more generally described by the spectral assumptions in [11, 55] enforce that each linearly unstable mode can be written as a slow modulation (in time and space) of the most unstable mode e^{ix}.

The above modulation $\mathcal{A}_{\mathrm{lin}}$ varies on a slow temporal and slow spatial scale given by

$$\xi = \varepsilon x, \quad \tau = \varepsilon^2 t. \tag{3.5}$$

In order to derive a Ginzburg-Landau equation, we plug in a linear wave of the form

$$\varepsilon^\eta \mathcal{A}_{\mathrm{lin}}(\xi, \tau) e^{\mathrm{i}x} \tag{3.6}$$

into the full (nonlinear) equation (3.1). Using the shorthand $E = e^{\mathrm{i}x}$, this gives

$$\partial_t u = \varepsilon^{\eta+2} \mathcal{A}_{\mathrm{lin},\tau} E + \text{c.c.} + \text{h.o.t.}$$

and

$$u^3 = \varepsilon^{3\eta}[\mathcal{A}_{\mathrm{lin}}^3 E^3 + 3\mathcal{A}_{\mathrm{lin}}|\mathcal{A}_{\mathrm{lin}}|^2 E] + \text{c.c.} + \text{h.o.t.}.$$

Let us now come back to the discussion at the begin of this section. In order to balance the exponential growth induced by the linear terms, the nonlinear terms have to be of the same order of magnitude. This is only so if $3\eta = \eta + 2$, i.e. if $\eta = 1$. Therefore, we assume a that there exists a modulation $\mathcal{A} = \mathcal{A}(\tau, \xi)$ such that a solution of the form

$$u \sim u_0 + \varepsilon \mathcal{A}(\xi, \tau) E + \text{c.c.} + \text{h.o.t.} \tag{3.7}$$

can be plugged into the equation (3.1). This assumption is usually called the 'Ansatz'. (In the case of the Swift-Hohenberg equation (3.1), we have $u_0 = 0$.)

Plugging Ansatz (3.7) into the PDE and working out the expansion results in an equation of the form[10]

$$
\begin{aligned}
\mathcal{A}_\tau \;=\;& a\mathcal{A}_{\xi\xi} + r\mathcal{A} + b|\mathcal{A}|^2\mathcal{A} \\
&+\; \varepsilon\{c\mathcal{A}_{\xi\xi\xi} + rd\mathcal{A}_\xi + c|\mathcal{A}|^2\mathcal{A}_\xi + f\mathcal{A}^2\bar{\mathcal{A}}_\xi\} \\
&+\; \varepsilon^2\{\ldots + g|\mathcal{A}|^4\mathcal{A}\} + \mathcal{O}(\varepsilon^3)
\end{aligned}
$$

with r from $|\mu - \mu_*| = r\varepsilon^2$ and $a, b, c, d, e, f, g \in \mathbb{R}$. At highest order, this equation is known as the *Ginzburg-Landau equation* (GLe):

$$\mathcal{A}_\tau = a\mathcal{A}_{\xi\xi} + r\mathcal{A} + b|\mathcal{A}|^2\mathcal{A} \tag{3.8}$$

As an example, the GLe for the Swift-Hohenberg equation near criticality reads

$$\mathcal{A}_\tau = 4\mathcal{A}_{\xi\xi} + r\mathcal{A} - 3|\mathcal{A}|^2\mathcal{A} \tag{3.9}$$

The GLe (3.9) has a very rich family of solutions [12, 94], though many of these solutions are not stable. For example, the only stable stationary solutions of the GLe for the Swift-Hohenberg equation (3.9) are the simple 'linear' spatially periodic patterns and a simple front solution – all quasi-periodic and homoclinic solutions are unstable [15, 34].

---

[10]We do not prove this here – the reader interested in the details of the derivation procedure should consult [20] for an elaborate intuitive account and [55] or [11] for the general abstract approach.

The GLe and other modulation equations had already been derived as early as the 60s [59, 82, 90], but it lasted untill the early 90s before the first proofs of its persistency and validity appeared [93, 7]. Though we have tried in this section to explain some of the intuition behind the Ginzburg-Landau approach, it is not at all immediately clear why the Ansatz (3.7) gives a good approximation of the solutions of the full PDE (3.1) (that is, we must prove the *validity* of the GLe). Also, it is not clear whether matters of stability, and more generally the dynamics of (3.1) is fully described by the GLe (that is, we must prove the *persistence* of the GLe).

For the general setting, assume we analyze a PDE of the from

$$u_t = \mathcal{L}(\mu, u) + \mathcal{N}(\mu, u) \tag{3.10}$$

with $u \in \mathbb{R}^n$, $x \in \mathbb{R}$, $t \in [0, \infty)$ and $\mathcal{L}$ a linear operator, $\mathcal{N}$ a nonlinear operator. Assume at some $\mu = \mu_*$ a bifurcation takes place that satisfies the spectral assumptions from [55]. Then a (complex) GLe can be derived of the form

$$\mathcal{A}_\tau = a \mathcal{A}_{\xi\xi} + r\mathcal{A} + b|\mathcal{A}|^2 \mathcal{A} \tag{3.11}$$

$a, b \in \mathbb{C}$ and τ and ξ as in (3.5).

In the early nineties the first proofs of versions of the following theorem were delivered[11]:

Theorem 3.1 (Validity) *Assume $\mathcal{A}_0(\xi)$ is an arbitrary initial condition for the GLe (3.11) that is, via Ansatz (3.7), associated to an initial condition $u_{\mathcal{A}_0}(\xi)$ for the full PDE (3.10). We denote by $u(x,t)$ the solution to the PDE (3.10) that has $u_{\mathcal{A}_0}(\xi)$ as initial condition. Also, we denote by $\mathcal{A}(\xi, \tau)$ the solution to the GLe (3.11) that takes $\mathcal{A}_0(\xi)$ as initial condition and denote by $u_{\mathcal{A}}(x,t)$ the Ansatz (3.7) associated to $\mathcal{A}(\xi, \tau)$. Then there exist C_1, C_2 such that on $t < \frac{C_1}{\varepsilon^2}$ we have*

$$||u(x,t) - u_{\mathcal{A}_0}(x,t)||_X \leq C_2 \varepsilon^2.$$

(We do not define the Banach space X here, but see [93, 7].)

Besides this, partial results of the following theorem have been proved (see ([55]):

Theorem 3.2 (Persistence) *Assume that $\mathcal{A}_*$ is a spectrally stable solution to the GLe (3.11). Then it holds that:*

1. **(Persistence)** *There is a solution $u_*(\mathcal{A}_*)$ of the orginal PDE (3.10) that is approximated by $\mathcal{A}_*$ via the Ansatz.*

2. **(Persistence stability)** *The solution from 1 is spectrally stable: if $\mathcal{A}_*$ is a spectrally stable solution of the GLe (3.11), then $u_*(\mathcal{A}_*)$ is a spectrally stable solution of the PDE (3.10).*

---

[11]We intentionally leave out some technicalities for the sake of clarity.
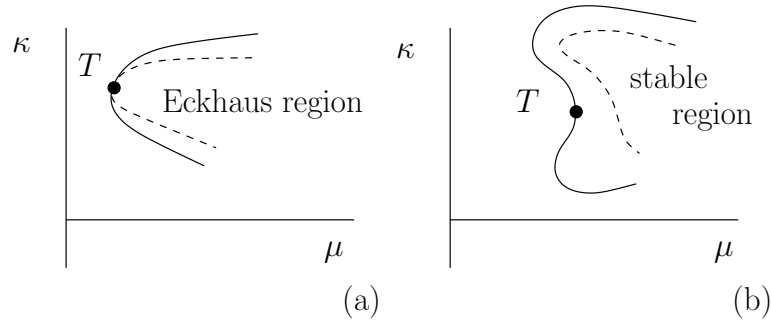
Figure 1.4: (a) A supercritical Turing bifurcation. The realm of periodic patterns is bordered by the solid curve, the Eckhaus band of stable periodic patterns is indicated by the dashed curve. The Turing bifurcation is indicated by the black dot. (b) A possible configuration in (μ, κ)-space when the bifurcation is subcritical. Again, the solid line indicates the border of the existing patterns, the dashed curve indicates the border of the stable periodic patterns. In this example, the region of stable patterns detaches from the Turing bifurcation.

3. **(Nonlinear stability)** *If the solution $u_*(\mathcal{A}_*)$ of the PDE (3.10) induced by $\mathcal{A}_*$ is spectrally stable, then it is also nonlinearly stable.*

Having these theorems at hand, we can reduce the analysis of the original PDE (3.10) to the study of the GLe (3.11). For example, in the case of a real GLe there exists an Eckhaus band of stable periodic patterns, thus, a similar band of stable patterns must exist in the full system. See Figure 1.4(a). Also, if the Ginzburg-Landau equation is subcritical the corresponding bifurcation in the original PDE (3.10) is subcritical too. See Figure 1.4(b).

1.3.2 Spatially periodic patterns for $|\mu - \mu_*| \gg \varepsilon^2$

If $|\mu - \mu_*| \gg \varepsilon^2$, the Ginzburg-Landau approach of section 1.3.1 breaks down. As of now, no concise and general theory has been built to tackle the far-from-equilibrium dynamics of general PDEs or general RDEs [61]. Even if we restrict ourselves to the description of spatially periodic patterns, such a theory does not exist. For example, one wants to know how the Eckhaus region of stable periodic patterns introduced in §1.3.1 extends to the region that is far-from-equilibrium, i.e. the region where the assumption that $|\mu - \mu_*| = \mathcal{O}(\varepsilon^2)$ is violated. More specifically, one wants to know which destabilization mechanisms destabilize stable periodic patterns in regions that are far-from-equilibrium. A full (graphical) description of the stable spatially periodic patterns (parametrized by their nonlinear wavenumber κ) for each value of μ and the instabilities that destabilize these patterns is called a *Busse balloon* and a significant part (in particular, chapter 3) of this thesis is devoted to the construction of Busse balloons of the GKGS-system (0.5). See Figure 1.5.

Busse balloons are named after the physicist F. Busse who introduced the concept in

the seventies [4]. As far as we know, only partial representations of Busse balloons have been published before [6, 30, 56]. This thesis (see chapter 3) contains a series of complete Busse balloons for the GKGS-system (0.5).

A Busse balloon gives a complete picture of all the instabilities that spatially periodic patterns can undergo. Therefore, it gives a complete overview of the instabilities that trigger the rise and fall of periodic vegetation patterns in semi-arid ecosystems. However, it is not immediately clear what happens to a stable periodic pattern if it approaches the boundary of the Busse balloon. Forcing the wavenumber to be fixed, this will ultimately lead to a destabilization of the periodic pattern, though generally, without forcing, we expect that it will transform into a periodic pattern with a different (smaller) wavenumber. This way, transforming gradually into periodic patterns with ever smaller wavenumbers, we expect it to move into the singular region, where the patterns are strongly localized and desertification ultimately happens. See Figure 1.5. In order to gain insight into this process, one needs to supply the Busse balloons with PDE simulations that describe the PDE dynamics of periodic patterns near the boundary. The Busse balloons that we have constructed and that are presented in chapter 3 give full insight into the instabilities that occur to the stable periodic patterns; therefore, they form a fundamental first step in the analysis of the dynamics along the curve of (sideband) instabilities that forms the boundary of the Busse balloon.

The methods we have used are based on relatively small extension(s) of the methods introduced in [70]. They will be elaborately described in chapter 3 and can also be found in [70], so due to the technical nature of the methods, we refrain from doing this here.

1.3.3   Hopf dances

In chapter 4, we describe in detail a generic destabilization mechanism that we have found numerically for the Gray-Scott system (i.e. the GKGS-system for $\gamma = 1$ and $C = 0$). Also, we analytically describe the destabilization mechanism for the generalized Gierer-Meinhardt system [37, 22]. The Hopf dance appears for a class of two-component, singularly perturbed reaction-diffusion equations that we describe in chapter 4. Here, it suffices to think about the Gray-Scott system – both the Gray-Scott system and the Gierer-Meinhardt system belong to this class of reaction-diffusion systems, though we stress that the GKGS-model for $C \neq 0$ does not: an essential ingredient is that the system possesses the reversibility symmetry $x \to -x$. In this section, we briefly explain the basic idea that underlies the Hopf dance.

Assume the Gray-Scott system (or any other system of the class described in chapter 4, for that matter) is solved by some spatially periodic solution $(U_{per}(x), V_{per}(x))$ with wavelength $2L$,
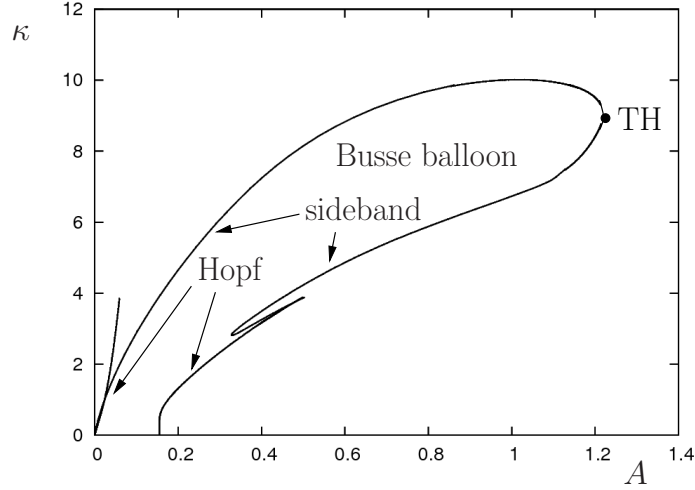
Figure 1.5: A Busse balloon for the GKGS-model (0.5) with $B = C = 0.2$ and $\gamma = 1$. The boundary exists of a branch of sideband instabilities that is crossed by a curve of Hopf bifurcations on the left and a curve of Hopf bifurcations on the right.

$$0 = U_{\mathrm{per},xx} + (1 - A)U_{\mathrm{per}} - U_{\mathrm{per}}V_{\mathrm{per},xx}^2$$
$$0 = \delta^2 V_{\mathrm{per},xx} - BV_{\mathrm{per},xx} + U_{\mathrm{per}}V_{\mathrm{per},xx}^2$$

We are interested in the (spectral) stability of this solution, so we perturb it by

$$(U(x,t), V(x,t)) = (U_{per}(x) + u(x)e^{\lambda t}, V_{per}(x) + v(x)e^{\lambda t})$$

To first order, this leads to the equation

$$\lambda u = u_{xx} - Au - V_{\mathrm{per},xx}^2 \cdot u - 2U_{\mathrm{per}}V_{\mathrm{per}} \cdot v$$
$$\lambda v = \delta^2 v_{xx} - Bv + V_{\mathrm{per},xx}^2 \cdot u + 2U_{\mathrm{per}}V_{\mathrm{per}} \cdot v$$

This linearization about the periodic solution $(U_{per}(x), V_{per}(x))$ defines a linear first order (ODE) problem by

$$\phi(x) = (u(x), p(x) = u_x(x), v(x), q(x) = v_x(x)) : \mathbb{R} \to \mathbb{C}^4,$$

and a $2L$-periodic 4×4 matrix $\mathcal{A}(x)$,

$$\phi_x = \mathcal{A}(x; \lambda, 2L)\phi. \tag{3.12}$$
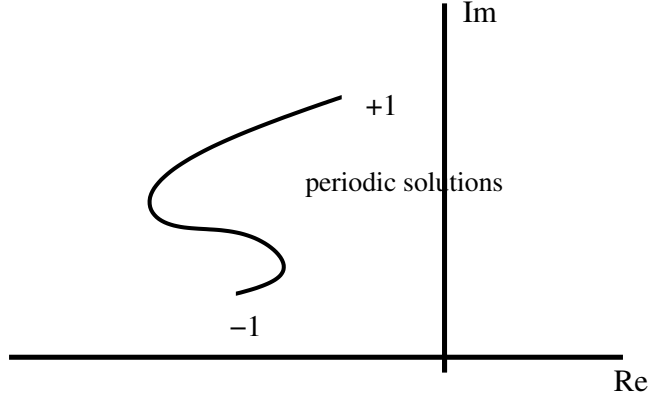
Figure 1.6: The loops – continuous images of $\mathbb{S}^1$ – collapse to line segments due to the reversible symmetry. The endpoints are γ-eigenvalues associated to $\gamma = \pm 1$.

The reversibility symmetry entails that the if $\phi(x)$ is a solution, then $R\phi(x) := \phi(-x)$ is also a solution. It follows from Floquet Theory (see [95]) that solutions to (3.12) are of the form

$$\phi(x) = \psi(x)e^{cx}, \quad c \in \mathbb{C} \quad \text{with } \psi(x) \text{ 2L-periodic in } x.$$

Now, since we only allow for bounded perturbations $\phi(x)$, it follows that $c \in i\mathbb{R}$. Hence, for $\gamma = e^{2Lc}$,

$$\phi(x + 2L) = \gamma\phi(x), \quad \gamma \in \mathbb{S}^1$$

We can now define the notion of γ-eigenvalue.[12]

Definition 1.3.1 [35] $\lambda \in \mathbb{C}$ *is a γ-eigenvalue if the linear system (3.12) has a solution $\phi(x; \lambda)$ such that*

$$\phi(x + 2L; \lambda) = \gamma\phi(x; \lambda) \quad \text{for a } \gamma \in \mathbb{S}^1.$$

It turns out that the spectrum associated to the stability problem (3.12) consists entirely of γ-eigenvalues [34].

It follows from the above that the spectrum $\sigma(U_{per}, V_{per})$ consists of (up to countably many) 'loops' $\lambda(\mathbb{S}^1)$, i.e. continuous images of $\mathbb{S}^1$ (some of these 'loops' could go to infinity and need not be closed). However, the reversibility of the system causes these loops to collapse to curves with endpoints.

Lemma 1.3.2 *If λ is a γ-eigenvalue, then λ is also a $\bar{\gamma}$-eigenvalue.*

---

[12]Notice that there is the risk of confusion with the parameter γ that describes the nonlinear diffusion of (0.5). However, the notion of γ-eigenvalue has become quite standard and so we will abide to this terminology.
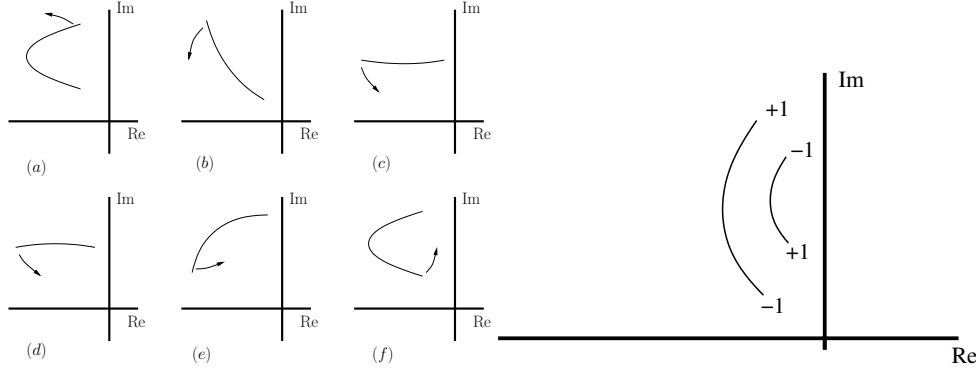
Figure 1.7: Left: The 'snaking' Hopf curves in the Busse balloon. There are no instabilities corresponding to γ-eigenvalues for $\gamma \neq \pm 1$ and all codimension 2 points exist as instabilities. Right: A stable spectral branch just before it crosses the imaginary axis, depicted twice after a half turn. The spectral branch crosses the imaginary axis only for γ-eigenvalues λ with $\gamma = \pm 1$.

Proof. If $\phi(x)$ is a solution of the linear problem, then by the reversibility, $\hat{\phi}(x) := R\phi(-x)$ is also a solution:

$$\hat{\phi}(x) = R\phi(-x) = (u(-x), -p(-x), v(-x), -q(-x)).$$

Let λ be a γ-eigenvalue, i.e. there is a $\phi(x; \lambda)$ s.t.

$$\phi(x + 2L; \lambda) = \gamma\phi(x; \lambda).$$

Then

$$\hat{\phi}(x + 2L; \lambda) = R\phi(-x - 2L; \lambda) = \frac{1}{\gamma}R\phi(-x; \lambda) = \bar{\gamma}\phi(x; \lambda).$$

$\square$

Hence 'generic loops' become curves with endpoints. See Figure 1.6.

Using the Evans function, we are also able to derive that near the homoclinic 'end point' of the Busse balloon the curve is actually, to first order, a line segment that shrinks and rotates as the wavenumber of the periodic pattern decreases towards 0. Moreover, if it is (almost) vertical, it is slightly bent towards the imaginary axis (see the right side of Figure 1.7). (We do not delve into the details here; an exposition on this can be found in chapter 4.) Therefore, either the $+1$ or the -1 'endpoint' of the critical spectral branch will be the first to cross the imaginary axis and since the rotation speed increases with a factor $1/k$ (here k is the linear wavenumber), there is an accumulating succession of countably many codimension 2 points at which the $+1$ and -1 endpoints simultanuously move through the imaginary axis. In Figure 1.8 the typical 'in-phase' respectively 'out-of-phase' character of the -1, resp. $+1$ Hopf bifurcations are sketched.

1.4 Outline

This thesis is the start of the study of the generalized Klausmeier-Gray-Scott system for vegetation patterns. Our primary focus is on the rise and fall of spatially periodic patterns.

In chapter 2, we consider the rise of patterns. As explained in section 1.3.1 of this introduction, the emerging patterns can be consistently described by studying Ginzburg-Landau equations. This chapter appeared as the first part of the article *Rise and fall of periodic patterns for a Generalized Klausmeier-Gray-Scott model* that has been submitted to *Journal of Nonlinear Science* for publication. The main mathematical approach we use here is the Ginzburg-Landau equation in its role as modulation equation.

In chapter 3, we present a series of Busse balloons for different ecologically relevant parameter values. This chapter forms the second part of the paper *Rise and fall of periodic patterns for a Generalized Klausmeier-Gray-Scott model.* The Busse balloons have been constructed by extensive use of the methods developed in [70].

In chapter 4, we study the generic Hopf dance mechanism that we have found for the Gray-Scott system which is, in fact, generic for a class of reversible two-component, singularly perturbed reactions-diffusion equations and has also been recovered for the GKGS-model with nonlinear diffusion. This chapter will appear as *Hopf dances near the tips of Busse balloons* in the journal *Discrete and Continuous Dynamical Systems S*. The main mathematical approach used in this chapter is the Evans function.

We must point out that this thesis mainly focuses on a description of the existence and stability of periodic patterns generated by (0.5). From a practical point of view, theoretical ecologists are naturally interested in the sudden collapse of semi-arid ecosystems to the desert state. Therefore, future studies of the GKGS-system should at least in part focus on the dynamics of periodic patterns near the boundary of the Busse balloon and especially the singular region where A and κ are small (the region for small A and small κ), as this is basically where desertification takes place.

Also, many other interesting solutions such as N-pulses and N-fronts, as well as more complicated patterns generated by (0.5), are not dealt with in this thesis.

An interesting question is raised when we ask what happens if A decreases and a periodic pattern with fixed wavenumber κ approaches the boundary of the Busse balloon. PDE simulations of the dynamics near the boundary will be needed here. More on this and other possible future work will be addressed in chapter 5.
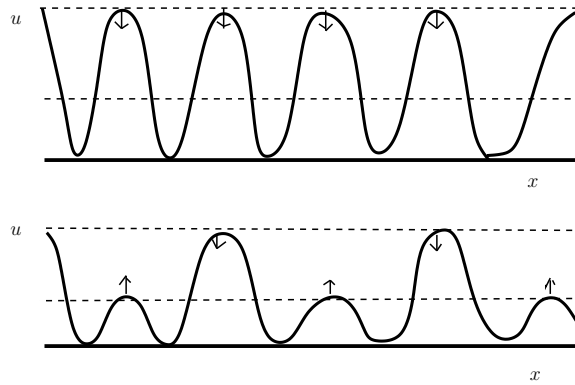
Figure 1.8: Above: A sketch of the in-phase dynamics of a periodic pattern that has become unstable due to a perturbation associated to $\gamma = 1$. Below: The out-of-phase dynamics caused by a perturbation associated to $\gamma = -1$.

Chapter 2

Ginzburg-Landau equations for the GKGS-system

This chapter is a first step in the analysis of GKGS model for vegetation patterns. In the first part (§2.1) of this chaper, we describe analytically the emergence of spatially periodic vegetation patterns in a Turing-Hopf bifurcation of the stationary state (U_+, V_+) by deriving a complex Ginzburg-Landau Equation (GLE) for each of the four classes in Figure 1.1. The derivation of the GLE as modulation equation for a Turing bifurcation in reaction-diffusion equations is a well-known, but certainly nontrivial procedure (see for instance [56] for the Turing bifurcation in the Gray-Scott model). Here we show that this procedure can also be applied to reaction-diffusion-advection equations with nonlinear diffusion (of porous media type) – to our knowledge a similar analysis does not yet exist in the literature (see §2.1.4). We derive that the Turing-Hopf bifurcation is supercritical for ecologically relevant parameter combinations in each of the four classes, regardless the values we choose for B and C. Moreover, we have evaluated the associated (and analytically determined) Benjamin-Feir-Newell criterion ([81] & §2.1.4) from which it follows that there always exists a band of stable periodic patterns near a Turing(-Hopf) bifurcation for ecologically relevant parameter combinations. Note that this is quite remarkable, given the dimensions of the parameter space. It is found however that the Turing(-Hopf) bifurcation becomes subcritical if $\gamma > \gamma_{ss} \approx 13$. Though this might not be of any interest to the ecologist, we notice that it is, however, an interesting mathematical fact: the nonlinearity of the diffusion is able to trigger a change from super- to subcriticality while a change of C, the parameter that measures the advection rate (and that is therefore related to the gradient of the slope), is not. Also, we show that the Klausmeier model appears as a limit case of the GKGS-model for large C and derive an explicit Ginzburg-Landau equation for the Klausmeier model that shows the Turing-Hopf bifurcation of the Klausmeier system to be supercritical.

2.1 Linear analysis

Before we embark upon a study of the onset of patterns in the GKGS-system, let us introduce some terminology that will be used throughout the article. Reaction-diffusion-advection systems as (0.5) naturally allow for spatially periodic solutions. These spatially periodic patterns or *wave trains* are solutions $u(x,t)$ that can be written as $u(x,t) = u_{\mathrm{per}}(\kappa x + \Omega t)$ and that satisfy $u_{\mathrm{per}}(\xi) = u_{\mathrm{per}}(\xi + 2\pi)$. Here κ is called the *(nonlinear) wavenumber* and Ω is the *(nonlinear) frequency*. A wave train is called a *background state* or *stationary state* when both its wavenumber and frequency are zero, i.e., when $u(x,t) \equiv u_{\mathrm{per}}(0)$ for all $x \in \mathbb{R}$, $t \in [0,\infty)$. It is called a *Turing pattern* if its frequency is zero, i.e., when $u(x,t) = u_{\mathrm{per}}(\kappa x)$ for all $x \in \mathbb{R}$, $t \in [0,\infty)$: Turing patterns have standing profiles. A generic wave train has $\kappa \neq 0$ and $\Omega \neq 0$ and will therefore have a traveling profile with velocity Ω/κ.

In this section we derive critical parameter values for which the stationary state (U_+, V_+) 0.6 undergoes a Turing-Hopf instability and derive a leading order form for $0 < \delta \ll 1$ of the GKGS-model (0.5) near the Turing-Hopf bifurcation. The stationary state (U_-, V_-) is always unstable, as can be readily checked. Subsequently, we derive a Ginzburg-Landau equation for the slowly modulating amplitude of the periodic pattern that appears at the Turing-Hopf instability. In order to employ a leading order analysis in (0.5) for $0 < \delta \ll 1$, we follow [56] and scale the parameters by

$$A = a\delta^{\alpha}, \quad B = b\delta^{\beta} \quad \text{and} \quad C = c\delta^{\nu}, \tag{1.1}$$

with $\alpha, \beta > 0, \nu \in \mathbb{R}$ and $a, b, c = \mathcal{O}(1)$ with respect to δ. The background state (U_+, V_+) can then be written out to leading order in δ as

$$(U_+, V_+) = \left(\frac{b^2}{a} \delta^{2\beta - \alpha}, \frac{a}{b} \delta^{\alpha - \beta} \right) + \text{h.o.t.}. \tag{1.2}$$

We notice that the two states $(U_\pm, V_\pm)$ only exist if $A \geq A_{\mathrm{sn}} = 4B^2$, or equivalently, $a \geq 4b^2 \delta^{2\beta - \alpha}$. Since δ is assumed asymptotically small, boundedness of a yields the condition

$$2\beta - \alpha \geq 0, \tag{1.3}$$

with equality allowed only if $a \geq 4b^2$.

2.1.1 The Turing and Turing-Hopf instabilities

The linearized GKGS-system about the stationary state $u_+ = (U_+, V_+)$ can be written abstractly as

$$u_t = \mathcal{D}u_{xx} + \mathcal{C}u_x + \partial_u F(u_+; A, B)u =: \mathcal{L}[\partial_x]u, \tag{1.4}$$

with $u = (U,V)$, $F(U,V;A,B) := (A(1 - U) - UV^2, -BV + UV^2)$, $\mathcal{D}$ the matrix defined by $\mathcal{D} = \mathrm{diag}(\gamma U_+^{\gamma-1}, \delta^{2\sigma})$ and $\mathcal{C}$ the matrix defined by $\mathcal{C} = \mathrm{diag}(C, 0)$.
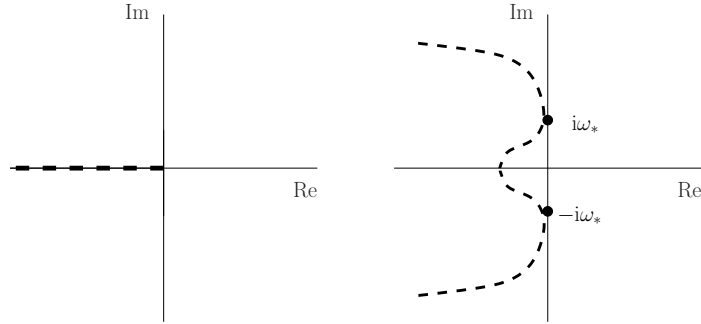
Figure 2.1: The thick lines denote possible typical configurations of a spatially periodic perturbation of the background state at marginal stability in the complex λ-plane. On the left, the spectrum near the origin is real, as is typical for the (reversible) GKGS-model with $C = 0$. On the right, $C \neq 0$.

We consider the spectrum $\operatorname{spec} \mathcal{L}[\partial_x]$ of the operator $\mathcal{L}[\partial_x]$ defined in (1.4) and define the matrix $\mathcal{M}$ by

$$\mathcal{M}(a, c, \mathrm{i}k) := \begin{pmatrix} -\gamma(U_+)^{\gamma-1}k^2 + \mathrm{i}c\delta^\nu k - V_+^2 - \delta^\alpha a & -2b\delta^\beta \\ V_+^2 & -\delta^{2\sigma}k^2 + \delta^\beta b \end{pmatrix}. \qquad (1.5)$$

Notice that $\mathcal{M}(a, c, \mathrm{i}k) = \mathcal{L}[\mathrm{i}k]$. As can be seen by computing the Fourier transform of (1.4) w.r.t. x, a complex number $\lambda \in \mathbb{C}$ belongs to the L^2-spectrum of $\mathcal{L}[\partial_x]$ if there exists a $k \in \mathbb{R}$ such that

$$d(\lambda, \mathrm{i}k) := \det[\mathcal{M}(a, c, \mathrm{i}k) - \lambda] = 0. \qquad (1.6)$$

Equation (1.6) is called the (linear) *dispersion relation* of (0.5) about (U_+, V_+). We refer to k as the (linear) wavenumber. It is associated to a Fourier mode of the perturbation of the background state (U_+, V_+). Recall the nonlinear wavenumber κ is the wavenumber of the bifurcating wave train itself. We can now make a basic definition, analogous to [80].

Definition 2.1.1 $\mathcal{L}[\partial_x]$ *is called* marginally stable *with critical Fourier mode* $u_0 e^{\mathrm{i}k_* x}$ *associated to the unique critical eigenmode* $\mathrm{i}\omega_*$, *up to complex conjugation, if:*

1. $d(\mathrm{i}\omega_*, \mathrm{i}k_*) = 0$,
2. $d(\mathrm{i}\omega_*, \mathrm{i}k) \neq 0$ *for all* $k \neq \pm k_*$,
3. $d(\lambda, \mathrm{i}k) \neq 0$ *for all* $k \in \mathbb{R}$ *and all* $\lambda \in \mathbb{C}$ *with* $\lambda \neq \mathrm{i}\omega_*$ *and* $\operatorname{Re}\lambda \geq 0$.

Two possible spectral configurations of the background state (U_+, V_+) at marginal stability are depicted in Figure 2.1. Definition 2.1.1 does not provide an explicit scheme to determine marginal stability. In practice, one uses the following necessary

(though a priori not sufficient) conditions to derive marginal stability of $\mathcal{L}$ with respect to eigenfunction $U_0 e^{ik_* x}$ and eigenvalue $i\omega_*$:

$$\text{Re}\lambda|_{k=k_*} = 0 \quad \text{and} \quad \left.\frac{\partial \text{Re}\lambda}{\partial k}\right|_{k=k_*} = 0. \tag{1.7}$$

We call the instability a *Turing-Hopf* instability if the wavenumber and its associated frequency of the eigenmode at marginal stability are nonzero, $k_* \neq 0$, $\omega_* \neq 0$, and we call the instability a *Turing* instability if the frequency of the eigenfunction at marginal stability is zero, i.e., $\omega_* = 0$ and $k_* \neq 0$ (see Figure 2.1). It will be confirmed in §2.1.2 and §2.1.3 that (U_+, V_+) undergoes a Turing instability to Turing patterns if $C = 0$ and a Turing-Hopf instability to generic wave trains if $C \neq 0$.

2.1.2   Critical parameters for the GKGS-model with $C = 0$

First we derive the critical parameter a_* and critical wavenumber k_* at which the stationary state (U_+, V_+) undergoes a Turing instability for the GKGS-model with $C = 0$. For $C = 0$, the dispersion relation (1.6) can be written as

$$
\begin{aligned}
d(\lambda, ik) &= \det[\mathcal{M}(a, 0, ik) - \lambda I] \\
&= \lambda^2 - \text{tr}\mathcal{M}(a, 0, ik)\lambda + \det\mathcal{M}(a, 0, ik). \tag{1.8}
\end{aligned}
$$

If Definition 2.1.1 for marginal stability holds, then the trace $\text{tr}\mathcal{M}(a, ik) = \lambda_- + \lambda_+$ cannot be positive. Substitution of the leading order formulation for V_+ yields

$$-\gamma\delta^{(2\beta-\alpha)(\gamma-1)}\left(\frac{b^2}{a}\right)^{\gamma-1} k^2 - \frac{a^2}{b^2}\delta^{2(\alpha-\beta)} - \delta^\alpha a - \delta^{2\sigma}k^2 + \delta^\beta b \leq 0. \tag{1.9}$$

Recall $a, b > 0$. For this inequality to hold, also at $k = 0$, it is needed that either $2(\alpha - \beta) \leq \beta$ or $\alpha \leq \beta$. Since the weakest of these conditions suffices, we impose

$$2\alpha \leq 3\beta. \tag{1.10}$$

Notice that this condition is stricter than (1.3). We are now in the position to formulate the following proposition concerning marginal stability.

Proposition 1 *Let $C = 0$, $\gamma \geq 1$ and $0 < \delta \ll 1$, and define $g := 3 - 2\sqrt{2}$. The background state (U_+, V_+) of (0.5) is marginally stable for σ, $a = a_*$ and $k = k_*$ satisfying*

$$
\begin{aligned}
(2\gamma + 1)\beta - (\gamma + 1)\alpha &= 2\sigma \\
k_*^2 &= \tfrac{1}{2}(1-g)b\delta^{-2\gamma\beta+(\gamma+1)\alpha} \\
a_*^{\gamma+1} &= g\gamma b^{2\gamma+1}, \tag{1.11}
\end{aligned}
$$

to leading order in δ.

Notice that we recover Proposition 3.1 of [56] for the Gray-Scott model if we set $\gamma = 1$.

Proof. We first show that, as expected from the reversible symmetry for $C = 0$, an instability always occurs through the origin so that it suffices to consider the simple case $\lambda = \omega_* = 0$ at $k = k_*$.

Suppose that $d(\mathrm{i}\omega, \mathrm{i}k) = 0$ and note that $\mathcal{M}(a, 0, \mathrm{i}k)$ is real. According to (1.8)

$$\mathrm{Im}\, d(\mathrm{i}\omega, \mathrm{i}k) = \omega \mathrm{tr}\mathcal{M}(a, 0, \mathrm{i}k) = 0,$$

so that either $\omega = 0$ (which means $\lambda = 0$) or $\mathrm{tr}\mathcal{M} = 0$. The latter implies

$$\mathrm{tr}\mathcal{M}(a, 0, \mathrm{i}k) = -(\gamma(U_+)^{\gamma-1} + \delta^{2\sigma})k^2 + \mathrm{tr}\mathcal{M}(a, 0, 0) = 0,$$

which has real roots k if and only if $\mathrm{tr}\mathcal{M}(a, 0, 0) > 0$, which is clearly not the case by (1.9).

Therefore it suffices to consider $\lambda = 0$ and prove that there exist a_* and k_* such that

$$\begin{array}{rcl} \det \mathcal{M}(a_*, 0, \mathrm{i}k_*) & = & 0 \\ \frac{\partial}{\partial k} \det \mathcal{M}(a_*, 0, \mathrm{i}k_*) & = & 0 \end{array} \tag{1.12}$$

From $(1.12)_2$ we get

$$k_*^2 = -\frac{\delta^{2\sigma}V_+^2 + \delta^{2\sigma+\alpha}a_* - \gamma\delta^\beta U_+^{\gamma-1}b}{2\gamma\delta^{2\sigma}U_+^{\gamma-1}} \tag{1.13}$$

Substitution of this expression in $(1.12)_1$ yields

$$k_*^2 = \frac{-2\delta^\beta b(V_+^2 - \delta^\alpha a_*)}{\delta^{2\sigma}V_+^2 + \delta^{2\sigma+\alpha}a_* - \gamma\delta^\beta U_+^{\gamma-1}b}. \tag{1.14}$$

Before we solve a_* from the combination of (1.13) and (1.14) we first determine its magnitude. Since k_*^2 in (1.13) is positive, one obtains by using the leading order expression (1.2),

$$\frac{a_*^2}{b^2}\delta^{2(\alpha-\beta+\sigma)} + a_*\delta^{2\sigma+\alpha} - \gamma b\left(\frac{b^2}{a_*}\right)^{\gamma-1}\delta^{\beta+(2\beta-\alpha)(\gamma-1)} < 0. \tag{1.15}$$

It follows from (1.10) that $2(\alpha - \beta + \sigma) < 2\sigma + \alpha$, which means that condition (1.15) would be satisfied if $\beta + (2\beta - \alpha)(\gamma - 1) \leq 2(\alpha - \beta + \sigma)$. Using (1.2) and (1.10), we deduce from (1.13) that k_*^2 is $\mathcal{O}(\delta^{\beta-2\sigma})$, and from (1.14) that k_*^2 is $\mathcal{O}(\delta^{2(\alpha-\beta)-(2\beta-\alpha)(\gamma-1)})$. Hence, we find a condition on the magnitude of the parameters at the Turing instability,

$$(2\gamma + 1)\beta - (\gamma + 1)\alpha = 2\sigma. \tag{1.16}$$

By substituting this in condition (1.15), we get

$$a_*^{\gamma+1} < \gamma b^{2\gamma+1}.$$

We can now consider the leading order expressions of (1.13) and (1.14), and conclude

$$\left(\frac{a_*^2}{b^3} - \gamma \left(\frac{b^2}{a_*} \right)^{\gamma-1} \right)^2 = 4\gamma \frac{a_*^2}{b^3} \left(\frac{b^2}{a_*} \right)^{\gamma-1}.$$

Solving this for a_* gives two solutions of which only one satisfies condition $a_*^{\gamma+1} < \gamma b^{2\gamma+1}$, hence

$$a_*^{\gamma+1} = g\gamma b^{2\gamma+1},$$

which also yields the leading order expression for k_*^2.

Since the spectral curves $\lambda_\pm(k^2)$ are solutions of the quadratic equation in λ (1.8), it is straightforward to show that $d(0, k_*)$ indeed satisfies Definition 2.1.1, i.e., that $\mathcal{L}$ is marginally stable. $\hfill\square$

2.1.3 Critical parameters for the GKGS-model

Before we can study the critical parameters at which the (irreversible) Turing-Hopf instability occurs for $C \neq 0$, we first need to determine the (critical) scaling of C, that is, the critical value of the exponent ν (1.1). If C is too small (i.e., ν too large), it will only have a higher order impact on the analysis of the previous section. If C is very large, it will have a major impact on the linear stability. The critical scaling of C is determined by the value of ν at which the influence of C becomes of leading order in the linear stability analysis (this ν is a 'significant degeneration', cf. [29]). Therefore, we use the scalings obtained in Proposition 1 in $\mathcal{M}(a, c, ik)$. Write $k = \delta^{\frac{1}{2}(\gamma+1)\alpha - \gamma\beta} \hat{k}$ (so that $\hat{k}_c = \mathcal{O}(1)$). The scalings for A, B and C in (1.1) imply that we have, to leading order in δ,

$$\mathcal{M}(a, c, ik) = \begin{pmatrix} \delta^{2\alpha-2\beta} \left[-\Gamma\tilde{k}^2 - \frac{a^2}{b^2} + ic\delta^{\nu-\frac{1}{2}(3-\gamma)\alpha-(\gamma-2)\beta}\tilde{k} \right] & \delta^\beta[-2b] \\ \delta^{2\alpha-2\beta} \left[\frac{a^2}{b^2} \right] & \delta^\beta[-\tilde{k}^2 + b] \end{pmatrix},$$
(1.17)

where we have introduced $\Gamma = \Gamma(\gamma, a) := \gamma \left(\frac{b^2}{a} \right)^{\gamma-1}$. Hence, it follows that the critical scaling of ν is given by

$$\nu = \frac{1}{2}(3 - \gamma)\alpha + (\gamma - 2)\beta.$$
(1.18)

For this ν, the dispersion relation is determined by

$$\det \begin{pmatrix} \delta^{2\alpha-2\beta} \left[-\Gamma\hat{k}^2 - \frac{a^2}{b^2} + ic\hat{k} - \delta^{3\beta-2\alpha}\hat{\lambda} \right] & \delta^\beta[-2b] \\ \delta^{2\alpha-2\beta} \left[\frac{a^2}{b^2} \right] & \delta^\beta[-\hat{k}^2 + b - \hat{\lambda}] \end{pmatrix} = 0,$$
(1.19)

where we have introduced $\hat{\lambda}$ by $\lambda = \delta^\beta \hat{\lambda}$.

It follows from (1.10) that the term with $\hat{\lambda}$ in the upper left entry of (1.19) is not of leading order. Hence, we conclude that at leading order in δ, and by dropping hats on $\hat{k}$ and $\hat{\lambda}$, the appearance of the Turing-Hopf instability is governed by the simplified dispersion relation

$$\det \mathcal{M}_\lambda(a, c, \mathrm{i}k) = 0, \tag{1.20}$$

with $\mathcal{M}_\lambda(a, c, \mathrm{i}k)$ defined as follows

$$\mathcal{M}_\lambda(a, c, \mathrm{i}k) := \begin{pmatrix} -\Gamma k^2 - \frac{a^2}{b^2} + \mathrm{i}ck & -2b \\ \frac{a^2}{b^2} & -k^2 + b - \lambda \end{pmatrix}. \tag{1.21}$$

If we define

$$F(k) := \Gamma k^2 + \frac{a^2}{b^2} \quad \text{and} \quad G(k) := k^2 - b, \tag{1.22}$$

it follows from (1.21) that the dispersion relation of the GKGS-system (0.5) is, to leading order in δ,

$$\begin{aligned} d(\lambda, \mathrm{i}k) &:= \lambda[F - \mathrm{i}ck] + \det \mathcal{M}_0(a, c, \mathrm{i}k) \\ &\equiv \lambda[F - \mathrm{i}ck] + \det \mathcal{M}_0(a, 0, \mathrm{i}k) - \mathrm{i}ckG \quad = \quad 0. \end{aligned} \tag{1.23}$$

Recall that (1.7) determines two necessary conditions for marginal stability. Substituting the first relation of (1.7) in (1.23) gives, to leading order in δ,

$$\begin{aligned} \omega ck &+ \det \mathcal{M}_0(a, 0, \mathrm{i}k) &= 0 \\ \omega F &- ckG &= 0, \end{aligned} \tag{1.24}$$

where $\omega = \omega_*$ is the critical frequency defined by $\lambda(k)|_{k=k_*} = \mathrm{i}\omega_*$ (see Definition 2.1.1). Differentiation of (1.23) with respect to k yields, after substitution of the conditions in (1.7),

$$\begin{aligned} \frac{\partial \omega}{\partial k}ck &+ \omega c &+ \partial_k \det \mathcal{M}_0(a, 0, \mathrm{i}k) &= 0 \\ \frac{\partial \omega}{\partial k}F &+ \omega F' &- cG - ckG' &= 0. \end{aligned} \tag{1.25}$$

From the second equations in (1.24) and (1.25) it now follows that

$$\omega = \frac{ckG}{F} \quad \text{and} \quad \frac{\partial \omega}{\partial k} = \frac{c}{F^2}[F(G + kG') - kGF']. \tag{1.26}$$

Note that unlike in the case $c = 0$, here it holds that $\lambda(k)|_{k=k_*} = \mathrm{i}\omega_* \neq 0$. Thus the destabilization that sets in at marginal stability indeed is of Turing-Hopf type if $c \neq 0$. The right equation in (1.26) gives the *group velocity* $c_{\mathrm{g}} := -\frac{\partial \omega}{\partial k}\big|_{k=k_*}$, that may be interpreted as the velocity with which wave packets with Fourier spectrum centered around the frequency k_* evolve.

The equations in (1.24) and (1.25) give

$$\begin{array}{rcl} \det \mathcal{M}_0(a,0,ik) & = & -\frac{c^2 k^2 G}{F} \\ \partial_k \det \mathcal{M}_0(a,0,ik) & = & -\frac{kc^2}{F^2}[F(2G + kG') - kGF']. \end{array} \qquad (1.27)$$

These equations determine a_* and k_* of Definition 2.1.1.

Proposition 2 *Let $0 < \delta \ll 1$, $\tilde{k} = \delta^{-\frac{1}{2}(\gamma+1)\alpha+\beta\gamma}k$ and drop the tilde on $\tilde{k}$, and let $C = c\delta^{\frac{1}{2}(3-\gamma)\alpha+(\gamma-2)\beta} \neq 0$. Let, as before, $g = 3 - 2\sqrt{2}$. The stationary state (U_+, V_+) undergoes a Turing-Hopf instability at a uniquely defined critical parameter $a = a_*$ and critical wavenumber $k = k_*$ that satisfy*

$$a_*^{\gamma+1} \geq g\gamma b^{2\gamma+1} \quad and \quad k_*^2 < b. \qquad (1.28)$$

If $c = \frac{2}{3}b\Gamma$, the Turing-Hopf instability takes place at the explicit parameter values, to leading order in δ,

$$a_*^{\gamma+1} = \frac{1}{3}\gamma b^{2\gamma+1} \quad and \quad k_*^2 = \frac{1}{3}b.$$

Moreover, for $c \gg 1$, we have, to leading order in c and δ,

$$a_*^{\gamma+3}(c) = \frac{g}{\gamma}b^{2\gamma+3}c^2 + \mathcal{O}(c) \quad and \quad k_*^2(c) = \frac{1}{2}(1 - g)b + \mathcal{O}(1/c). \qquad (1.29)$$

Proof. First we show that a Turing-Hopf instability occurs. We rewrite equations (1.27) by

$$K = k^2 \quad and \quad E = \frac{a^2}{b^2} \qquad (1.30)$$

to obtain

$$\begin{array}{rcl} (K^2 + K(\frac{E}{\Gamma} - b) + \frac{E}{\Gamma}b)(K + \frac{E}{\Gamma}) & = & -\left(\frac{c}{\Gamma}\right)^2 K(K - b) \\ (2K + \frac{E}{\Gamma} - b)(K + \frac{E}{\Gamma})^2 & = & -\left(\frac{c}{\Gamma}\right)^2 (K^2 + 2\frac{E}{\Gamma}K - \frac{E}{\Gamma}b), \end{array}$$

and we further introduce X, ρ and η by

$$K = bX, \quad \frac{E}{\Gamma} = b\rho \quad and \quad \frac{c^2}{\Gamma^2} = b\eta. \qquad (1.31)$$

Then the equations simplify to

$$\begin{array}{rcl} (X^2 + X(\rho - 1) + \rho)(X + \rho) & = & -\eta X(X - 1) \\ [(X + \rho)(2X + (\rho - 1))](X + \rho) & = & -\eta(X^2 + 2\rho X - \rho). \end{array} \qquad (1.32)$$

As a shorthand we introduce polynomials f, g, h, j and write (1.32) in the obvious way as

$$\begin{array}{rcl} f(X,\rho)(X + \rho) & = & -\eta g(X) \\ h(X,\rho)(X + \rho) & = & -\eta j(X,\rho). \end{array} \qquad (1.33)$$

We view these as functions of X and sometimes suppress the dependence on ρ. With the above rescalings of a and k, the problem of finding a parameter $a = a_* > 0$ with

wavenumber $k = k_*$ such that (1.27) holds, has been reduced to the problem of finding a $\rho > 0$ and an $X \geq 0$ such that (1.33) holds. We may assume $\eta \neq 0$ (since the case $c = 0$ is dealt with in Proposition 1. From this and from (1.33) it follows that we search for $X \geq 0$ such that

$$j(X)f(X) = g(X)h(X). \tag{1.34}$$

We notice the following:

$$j(0) \cdot f(0) = -\rho \cdot \rho = -\rho^2 < 0 \quad \text{and} \quad j(1) \cdot f(1) = (1 + \rho) \cdot 2\rho > 0$$

while

$$g(0)h(0) = g(1)h(1) = 0.$$

Hence it follows that for each $\rho \in \mathbb{R}$, there is a $X = X_*(\rho) \in (0,1)$ such that (1.34) holds.

If $g(X_*) \neq 0$, we can define

$$\eta(\rho) := -\frac{f(X_*(\rho), \rho)}{g(X_*(\rho))}(X_*(\rho) + \rho). \tag{1.35}$$

The triplet $\rho, X_*(\rho), \eta(\rho)$ is a solution for (1.33).

We need to consider the case $g(X_*) = 0$ or $j(X_*) = 0$ separately. It holds that $g(X) = 0$ if and only if $X = 0$ or $X = 1$. However, if $X = 0$ or $X = 1$, the first equation of (1.32) contradicts the assumption that $\rho > 0$, so we find that the condition $g(X_*) \neq 0$ is never violated. On the other hand, if $j(X_*) = 0$ then, by $(1.33)_2$, it must hold that $X_* = \frac{1}{2}(1 - \rho)$. Solving $j(\frac{1}{2}(1 - \rho)) = 0$ gives $\rho = \frac{1}{3}$ and so $X_* = \frac{1}{3}$. Substituting these values for X and ρ in $(1.33)_1$, gives $\eta = \frac{2}{3}$. Hence, by rewriting to original parameters, we obtain the special case for which

$$a_*^{\gamma+1} = \frac{1}{3}\gamma b^{2\gamma+1}, \quad k_*^2 = \frac{1}{3}b \quad \text{and} \quad c = \frac{2}{3}b\Gamma.$$

We have now proven that for each $\rho > 0$, there is a pair $X_*(\rho), \eta(\rho)$ that solves (1.33). In order to complete the proof it remains to show that for each $\eta > 0$ (and thus for each $c \in \mathbb{R}$), there is a unique pair $X_*(\eta)$, $\rho(\eta)$ (or k_*, a_*) that solves (1.33). This can be proved by showing that $\eta(\rho)$ as defined in (1.35), attains each value in $[0, \infty)$ and is an invertible map.

By (1.32) it is easy to see that $\eta(\rho) = 0$ if $\rho = g$. On the other hand, as we will prove below, η is unbounded as a function of ρ: $\eta \to \infty$ if $\rho \to \infty$ (which by (1.31) is $c \to \infty$). Also, the function $\eta(\rho)$ has no (vertical) asymptotes since we saw that $g(X_*) \neq 0$. Hence, $\eta(\rho)$ attains each value in $[0, \infty)$. It now suffices to show that $\eta = \eta(\rho)$ is injective. This can be derived by a tedious analysis of the polynomials in (1.32): for all η there is at most one pair (X, ρ) such that (1.32) holds. We omit the details.

Next we derive the estimates in (1.28). The estimate in $(1.28)_2$ follows from the

fact that $0 < X_* < 1$ and (1.30) and (1.31). We prove the estimate in $(1.28)_1$. From (1.31) it is clear that η does not allow for negative values. That is, by (1.35), and since $g(X) < 0$ for all $X \in (0,1)$, we can only allow for those ρ for which $\mathrm{sign}(f) > 0$. It is straightforward to show that $f(X) > 0$ for all $X \in (0,1)$ if $\rho > g$, and $f(X) < 0$ for all $X \in (0,1)$ if $\rho < g$. Hence, if we rewrite the condition $\rho > g$ to original parameters, we obtain $(1.28)_1$:

$$a_*^{\gamma+1} \geq g\gamma b^{2\gamma+1}.$$

Finally, we analyze the case for asymptotically large values of η (or equivalently, asymptotically large values for c and derive equations (1.29)). Consider equation (1.32). Since X_* is bounded ($|X_*| < 1$), we must rescale ρ and obtain

$$\mathcal{O}(\rho^2) = \mathcal{O}(\eta).$$

We therefore set $\eta = \tilde{\eta}\rho^2$, with $\rho \gg 1$, and expand (1.32):

$$\begin{aligned} X + 1 &= -\tilde{\eta}X(X-1) + \mathcal{O}(1/\rho) \\ 1 &= -\tilde{\eta}(2X-1) + \mathcal{O}(1/\rho). \end{aligned}$$

Solving this gives, to leading order,

$$X_* = \frac{1}{2}(1-g) + \mathcal{O}(1/\rho) \quad \text{and} \quad \tilde{\eta}_* = 3 + 2\sqrt{2} + \mathcal{O}(1/\rho).$$

Rescaling X_* back to k_* and $\tilde{\eta}_*$ back to a_* and c gives (1.29),

$$k_*^2 = \frac{1}{2}(1-g)b + \mathcal{O}(1/c) \quad \text{and} \quad a_*^{\gamma+3}(c) = \frac{g}{\gamma}b^{2\gamma+3}c^2 + \mathcal{O}(c).$$

$\square$

2.1.4 Modulation equations for the rising patterns

At the Turing instability of the stationary state (U_+, V_+) (that takes place if $c = 0$) or Turing-Hopf instability ($c \neq 0$), the homogeneous equilibrium becomes unstable with respect to periodic perturbations for $a < a_*$. If the instability is supercritical, one expects a small band of stable patterns, the so-called Eckhaus-band for $|a - a_*| = \mathcal{O}(\varepsilon^2)$ and $0 < \varepsilon \ll 1$.

In this section we will derive and analyze the associated Ginzburg-Landau equations for the GKGS-model in each of the four classes of Figure 1.1 and for the special cases of Proposition 2. The Ginzburg-Landau equation (GLE) governs the behaviour of the amplitude of the pattern near criticality. Solutions to this equation are slow modulations of the amplitude of the underlying 'most unstable' Fourier mode $\sim e^{\mathrm{i}(k_* x + \omega_* t)}$ (see [1, 55] and the references therein).

In the case of the Gray-Scott system it is shown in [56] that the Turing instability is supercritical, meaning that stable small amplitude periodic solutions exist in

the region where the underlying homogeneous pattern is unstable. In §2.1.5 we derive that for $\gamma > \gamma_* \approx 13$ and $c = 0$, the Turing instability of the stationary state (U_+, V_+) of the GKGS-model becomes subcritical (however, we do not see a relevant ecological interpretation of these values for γ). We also find that the Turing-Hopf instability that occurs for $c \neq 0$ is supercritical for all values of c and either $\gamma = 1$ or $\gamma = 2$.

In §2.1.6 it is shown that, near criticality, the Klausmeier system can be derived as a limit case of the GKGS-system for $c \to \infty$ (in particular, $0 < 1/\sqrt{c} \ll \varepsilon^2 \ll 1$). It is explained that the GLE for the Klausmeier model is the same as the limiting GLE for the GKGS-system for large c and asymptotically small $|\varepsilon| \ll 1$ (that is, we assume $0 < \varepsilon^2 \ll 1/\sqrt{c} \ll 1$). This is surprising: a priori, it is not at all clear that it is possible to interchange the limits $\varepsilon \to \infty$ and $c \to \infty$. In particular, the Turing-Hopf instability of the background state (U_+, V_+) of the Klausmeier system inherits the supercriticality from the Turing-Hopf instability of the background state of the GKGS-model.

Let $0 < \varepsilon \ll 1$ and assume that the stationary state (U_+, V_+) is almost marginally unstable ($a = a_* - r\varepsilon^2$, $r > 0$). Patterns close to the stationary state (U_+, V_+) can be described by

$$
\begin{aligned}
U &= \delta^{2\beta-\alpha}(\hat{U}_+ + \varepsilon\hat{U}(x,t)) \\
V &= \delta^{\alpha-\beta}(\hat{V}_+ + \varepsilon\hat{V}(x,t)).
\end{aligned}
\tag{1.36}
$$

By substitution of these expressions in (0.5) and recalling the previous scaling for ν in (1.18) and the previous scalings for $\tilde{k}$ and $\tilde{\lambda}$ that induce the spatial and temporal scalings

$$
\tilde{x} = x\delta^{\frac{1}{2}\alpha - \frac{1}{2}(2\beta-\alpha)\gamma} \quad \text{and} \quad \tilde{t} = t\delta^\beta,
\tag{1.37}
$$

we deduce the following leading order system for the GKGS-system,

$$
\begin{aligned}
\delta^{3\beta-2\alpha}U_t &= \gamma\left(\frac{b^2}{a_*}\right)^{\gamma-1}U_{xx} + cU_x - [\frac{a_*^2}{b^2}U + 2bV] \\
&\quad + \varepsilon\left[\gamma(\gamma-1)\left(\frac{b^2}{a_*}\right)^{\gamma-2}[U_{xx}U + (U_x)^2] - \frac{b^2}{a_*}V^2 - 2\frac{a_*}{b}UV\right] \\
&\quad + \varepsilon^2\left[\gamma(\gamma-1)(\gamma-2)\left(\frac{b^2}{a_*}\right)^{\gamma-3}[U(U_x)^2 + \frac{1}{2}U^2U_{xx}]\right. \\
&\quad\quad \left. + \gamma(\gamma-1)\frac{1}{a_*}\left(\frac{b^2}{a_*}\right)^{\gamma-1}U_{xx} + 2r\frac{a_*}{b^2}U - UV^2\right] \\
V_t &= V_{xx} + \left[\frac{a_*^2}{b^2}U + bV\right] + \varepsilon\left[\frac{b^2}{a_*}V^2 + 2\frac{a_*}{b}UV\right] - \varepsilon^2\left[2r\frac{a_*}{b^2}U - UV^2\right],
\end{aligned}
\tag{1.38}
$$

where we have dropped all hats and tildes and have implicitly assumed $\delta \ll \varepsilon$. Remark that after application to the linearly 'most unstable' Fourier mode $\sim e^{i(k_*x+\omega_*t)}$, the leading order part of (1.38) indeed corresponds to $\mathcal{M}_{i\omega_*}(a_*, c, ik_*)$ (see (1.21)). The kernel of $\mathcal{M}_{i\omega_*}(a_*, c, ik_*)$ is given by

$$\ker \mathcal{M}_{\mathrm{i}\omega_*}(a_*, c, \mathrm{i}k_*) = \begin{pmatrix} 2b \\ \eta_{\gamma,c} \end{pmatrix}, \tag{1.39}$$

with

$$\eta_{\gamma,c} := -\Gamma k_*^2 - \left(\frac{a_*}{b}\right)^2 + \mathrm{i}k_* c, \tag{1.40}$$

and the range of $\mathcal{M}_{\mathrm{i}\omega_*}(a_*, c, \mathrm{i}k_*)$ is given by

$$\mathrm{Rg}\,\mathcal{M}_{\mathrm{i}\omega_*}(a_*, c, \mathrm{i}k_*) = \begin{pmatrix} -2b \\ -k_*^2 + b - \mathrm{i}\omega_* \end{pmatrix}. \tag{1.41}$$

Thus, $\mathcal{M}_{\mathrm{i}\omega_*}(a_*, c, \mathrm{i}k_*)\mathbf{x} = \mathbf{y}$ has a solution if and only if $\mathbf{y} \in \mathrm{Rg}\,\mathcal{M}_{\mathrm{i}\omega_*}(a_*, c, \mathrm{i}k_*)$, that is, if and only if

$$2by_2 - (k_*^2 + i\omega_* - b)y_1 = 0, \tag{1.42}$$

where $\mathbf{y} = (y_1, y_2)^T$. We will need this in our derivation of the GLE and refer to it as the *solvability condition*.

The modulation Ansatz for the derivation of the Ginzburg-Landau Equation is that solutions of the system behave as slow spatio-temporal modulations of the solution for the linear first order problem, i.e., they are of the form:

$$\begin{pmatrix} U \\ V \end{pmatrix} = \mathcal{A}(\xi, \tau) \begin{pmatrix} 2b \\ \eta_{\gamma,c} \end{pmatrix} e^{\mathrm{i}(k_* x + \omega_* t)} + \mathrm{c.c.} + \mathrm{h.o.t.}, \tag{1.43}$$

with $\xi = \varepsilon x$ and $\tau = \varepsilon^2(x - c_g t)$ and c_g the group velocity defined by (1.26) [1, 55].

In [56] the GLE for periodic patterns near the Turing instability of the background state (U_+, V_+) for the Gray-Scott system was computed. Using a result of Schneider [81], the diffusive stability of the Turing patterns described by the Gray-Scott system could be derived from the spectral stability of periodic solutions of this GLE. However, to our knowledge there does not exist a similar result in the literature that can be applied to the present system, i.e., a quasilinear reaction-diffusion system with nonlinear diffusion. In fact, we are not aware of any (even formal) GLE analysis in a system with nonlinear diffusion. Still, we expect that a result similar to that of [81] must hold – although a proof is beyond the scope of this paper. The reason for this is that the nonlinear diffusion term in (0.5) can be controlled if U remains bounded away from 0, i.e., if $U(x,t) \geq d_0 > 0$ uniformly in x and t. By the nature of the method, the GLE analysis is applied to solutions $(U(x,t), V(x,t))$ of (0.5) that are asymptotically close to the background state (U_+, V_+) of (0.5), as is made explicit by 'Ansatz' (1.36). Since clearly $U_+ > 0$ (see also (1.2)), the GLE approach indeed only considers patterns in (0.5) for which $U(x,t) \geq d_0 > 0$ uniformly in x and t on the time scales associated to this approach. In this region the equation is still parabolic and existence theory is essentially similar to the semilinear case [?, ?].

In §2.1.5 we derive a Ginzburg-Landau equation for the slowly varying amplitude $\mathcal{A}(\xi, \tau)$. The Ginzburg-Landau equation is first derived without inserting explicit values of a_* and k_*. The coefficients of the GLE are functions of b, c and γ, as it is proven in Proposition 2 that the critical values of a_* and k_* depend on b, c and γ. In Proposition 2 however, we also deduced explicit values for a_* and k_* for a number of special parameter values for b, c and γ. In each of these cases, we will present an explicit GLE.

2.1.5 Ginzburg-Landau equation for the GKGS-model

Proposition 3 *Assume $|a - a^*| = r\varepsilon^2$. Then solutions of the form (1.43) to the GKGS-model (0.5) are described by the governing Ginzburg-Landau equation*

$$\mathcal{A}_\tau = (a_1 + \mathrm{i}a_2)\mathcal{A}_{\xi\xi} + (b_1 + \mathrm{i}b_2)\mathcal{A} + (L_1 + \mathrm{i}L_2)|\mathcal{A}|^2\mathcal{A}. \tag{1.44}$$

with coefficients given by

$$
\begin{aligned}
a_1 + \mathrm{i}a_2 &= \tfrac{1}{2b\eta_{\gamma,c}}\left[2b(\mathrm{c_g}y_{12} + \eta_{\gamma,c} + 2ik_*y_{12}) - (k_*^2 + i\omega_* - b)(cx_{12} + 2b\Gamma + 2ik_*\Gamma x_{12})\right] \\
b_1 + \mathrm{i}b_2 &= \tfrac{-1}{2b\eta_{\gamma,c}}\left[4\tfrac{a_c}{b}(k_*^2 + i\omega_* + b) + L_{\mathcal{A},\mathrm{NLD}}(k_*^2 + i\omega_* - b)\right] \\
L_1 + \mathrm{i}L_2 &= \tfrac{1}{2b\eta_{\gamma,c}}\left[\left(k_*^2 + i\omega_* + b\right)L_{\mathrm{tot}} - \left(k_*^2 + i\omega_* - b\right)L_{\mathrm{NLD}}\right].
\end{aligned}
\tag{1.45}
$$

We refer to Appendix 6 for the detailed derivation of the GLE as well as the full expressions for L_{tot}, L_{NLD} and $L_{\mathcal{A},\mathrm{NLD}}$ and x_{ij}, y_{ij}, $ij = 02, 12, 13$. Here we remark that if $c = 0$, then $\omega_* = 0$ and $\mathrm{c_g} = 0$ by (1.26) and $L_{\mathrm{NLD}} = 0$ and $L_{\mathcal{A},\mathrm{NLD}} = 0$ if $\gamma = 0$, i.e., these coefficients originate from the nonlinear diffusion.

In the GLE (1.44), the coefficient $L_1 + \mathrm{i}L_2$ is called the Landau-coefficient. The Turing-Hopf instability of the stationary state (U_+, V_+) is supercritical if and only if its real part satisfies $L_1 < 0$. It is subcritical if $L_1 > 0$.

If the Turing-Hopf bifurcation is supercritical, it is straightforward to show [54] that there exists a band of stable spatially periodic patterns if and only if

$$1 + \frac{a_2 L_2}{a_1 L_1} > 0. \tag{1.46}$$

This inequality is usually called the *Benjamin-Feir-Newell criterion* [1]. The patterns that satisfy condition (1.46) form a parabolically shaped region of stable periodic patterns near the Turing(-Hopf) instability at $a = a_*$ that lies within a larger parabolically shaped region of periodic patterns [54, 55]. See Figure 2.3 for a schematic picture. For $a \approx a_* - r\varepsilon^2$, the region of stable patterns is called the *Eckhaus region*, after its boundary which is called the Eckhaus instability [55]. In Figure 2.3 the Eckhaus region is depicted as a part of the larger Busse balloon (the concept of the Busse balloon will be discussed in more depth in §**??**).

(a) (b)
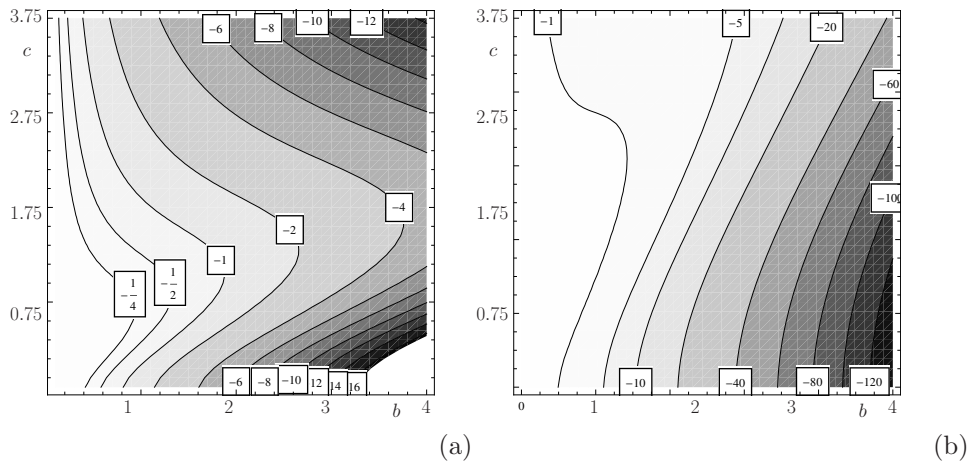
Figure 2.2: Contourplots of the real part of the Landau-coefficient for (a) the GKGS-model with linear diffusion ($\gamma = 1$) and for (b) the GKGS-model with nonlinear diffusion ($\gamma = 2$), drawn on a grid of points at $(b, c) = (0.1, 0.0) + 0.1(k, l)$, $k, l = 0, \ldots, 40$. In both pictures, the non-advection case ($c = 0$) is depicted by the horizontal axis. Notice that the origin in the pictures is at $(b, c) = (0.1, 0.0)$, since the case $b = 0$ has no ecological meaning.
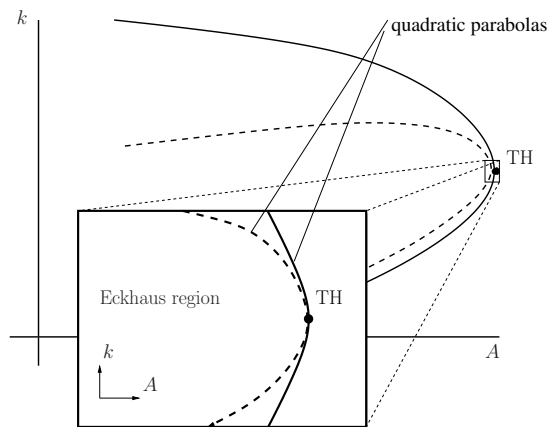
Figure 2.3: An impression of the stable Eckhaus region as part of a Busse balloon. Compare Figure 1.5. Inset: the Eckhaus region of stable patterns (boundary depicted by a dashed line) lies within the larger locally parabolic region of (not necessarily stable) patterns.

As explained in the introduction, the ecologically relevant parameter values for γ are $\gamma = 1$ or $\gamma = 2$. With the help of MATHEMATICA we evaluated the Landau coefficient of the GLE for the GKGS-model with $\gamma = 1$ and $\gamma = 2$. This way, we have obtained sufficient evidence to claim:

Claim 1 *For the GKGS-model (0.5) with $\gamma \in \{1, 2\}$, the real part of the Landau coefficient L_1 of (1.44) is negative for all values of b and c up to $c \sim 10^6$ and $b \sim 10^2$. Therefore we claim that the Turing-Hopf bifurcation at $a = a_*$ of the stationary state (U_+, V_+) of the GKGS-model with $c > 0$ and $\gamma = 1, 2$ is supercritical.*

As an illustration, we have depicted in Figure 2.2 a set of contourlines of the real part of the Landau-coefficient L_1 for $\gamma = 1$ and $\gamma = 2$ and values of (b, c) on a grid spanned by $(b, c) = (0.1, 0.0) + 0.1(k, l)$, $k, l = 0, \ldots, 40$.

By computing the Benjamin-Feir-Newell criterion (1.46), we checked that this inequality holds for the Ginzburg-Landau equation for the GKGS-model for all b and c up to $c \sim 10^6$ and $b \sim 10^2$ and $\gamma \in \{1, 2\}$. Hence we claim

Claim 2 *For (0.5) with $c > 0$ and $\gamma = 1, 2$, there exists a stable band of periodic patterns that appears at the Turing-Hopf instability.*

Next, we present four explicit Ginzburg-Landau equations for which we have explicit values for the critical parameter value a_* and wavenumber k_* at hand. The parameter choices for the three Ginzburg-Landau equations are drawn from three different cases of the GKGS-model as depicted in Figure 1.1. Of course, the sign of the real part of the Landau coefficient confirms the evaluations presented in Figure 2.2 in all three cases.

2.1.5.1 The GKGS-model with $c = 0$ and $\gamma = 1$. Clearly, the GKGS-model with $\gamma = 1$ and $c = 0$ reduces to the Gray-Scott system. By recalling from Proposition 1 (or from [56]), $a_*^2 = (3 - 2\sqrt{2})b^3$ and $k_*^2 = (\sqrt{2} - 1)b^3$, the above equation simplifies to

$$\mathcal{A}_\tau = 2\sqrt{2}\,\mathcal{A}_{\xi\xi} + \frac{2}{\sqrt{b}}\mathcal{A} - \frac{2}{9}(10\sqrt{2} - 7)b^2|\mathcal{A}|^2\mathcal{A}. \tag{1.47}$$

Since the real part of the Landau coefficient is negative, the Turing-bifurcation is supercritical. Note that this equation corresponds to (3.27) derived in [56].[1]

2.1.5.2 The GKGS-model with $c = 0$. In the case of $c = 0$ and $\gamma \geq 1$, we have derived explicit expressions for the critical parameter a_* and wavenumber k_* in Proposition 1, namely

$$a_*^{\gamma+1} = g\gamma b^{2\gamma+1} \quad \text{and} \quad k_*^2 = \frac{1}{2}(1 - g)b. \tag{1.48}$$

with $g = 3 - 2\sqrt{2}$ (notice we rescaled k_* in §2.1.3). Due to the reflexion symmetry of the GKGS-system at $c = 0$, all coefficients of the GLE are real. In this case, the GLE (1.45) has the form

---

[1]Notice however the extra b^2 in the coefficient in front of the nonlinear term. In [56], b is scaled out of the matrix $\mathcal{M}_c$ in formula (3.24). That is, the matrix $b\mathcal{M}_c$ in [56] plays the role of our matrix $\mathcal{M}_{i\omega_c}(a_c, 0, ik_c)$. This is equivalent to scaling $\mathcal{A} \to b\mathcal{A}$ in (1.47).

$$\mathcal{A}_\tau \;=\; 2\sqrt{2}\,\mathcal{A}_{\xi\xi} + b_1(\gamma)\mathcal{A} + L_1(\gamma)|\mathcal{A}|^2\mathcal{A} \tag{1.49}$$

with

$$
\begin{aligned}
b_1(\gamma) &= [-39 + 27\sqrt{2} + (41 - 29\sqrt{2})\gamma]\left(\frac{g\gamma}{b}\right)^{\frac{-1}{1+\gamma}}\frac{1}{b}\\
L_1(\gamma) &= -\frac{1}{9}(2-\sqrt{2})\left[18(3+2\sqrt{2}) + 12(2+\sqrt{2})\gamma + (-8+3\sqrt{2})\gamma^2\right]\left(\frac{g\gamma}{b}\right)^{\frac{2}{\gamma+1}}b^3
\end{aligned}
$$

One can check that $b_1(\gamma) > 0$ for $\gamma > 0$ as it – of course – should be. Moreover, the Ginzburg-Landau equation for the GKGS-system for general γ (1.49) reduces to the Ginzburg-Landau equation for the Gray-Scott system (1.47) if $\gamma = 1$.

However we notice that the real part of the Landau coefficient $L_1(\gamma)$ becomes positive for large γ and equals zero for

$$\gamma_{ss} \approx 13.0446. \tag{1.50}$$

Therefore we have the following result.

Proposition 4 *The Turing bifurcation for the GKGS-model (0.2) with $c = 0$ is supercritical for $\gamma < \gamma_{ss}$ and subcritical for $\gamma > \gamma_{ss}$.*

2.1.5.3 The Ginzburg-Landau equation for the GKGS-model with $\gamma = 1$ and $c = \sqrt{\frac{2}{3}}b$.

In this case, the critical parameters for the Turing-Hopf instability can be drawn from the 'special case' in Proposition 2:

$$k_*^2 = \frac{1}{3}b, \quad a_*^2 = \frac{1}{3}b^3, \quad \omega_* = \frac{1}{3}b\sqrt{2} \quad \text{and} \quad \mathrm{c_g} = \sqrt{\frac{2}{3}}b.$$

The GKGS-model for $\gamma = 1$ is not reflexion symmetric. Therefore, traveling spatially periodic patterns appear in a Turing-Hopf bifurcation. The associated GLE is a complex GLE (cGLE),

$$\mathcal{A}_\tau = \frac{1}{3}(8 + \mathrm{i}\sqrt{2})\mathcal{A}_{\xi\xi} + \frac{2}{9}\sqrt{\frac{3}{b}}(5 + \mathrm{i}\sqrt{2})\mathcal{A} - \frac{2}{33}(5 - 2\mathrm{i}\sqrt{2})b^2|\mathcal{A}|^2\mathcal{A}. \tag{1.51}$$

Since $\mathrm{Re}\left(-\frac{2}{33}(5 - 2i\sqrt{2})b^2\right) < 0$, the bifurcation is supercritical. We refer to Appendix 6.0.1 for a complete derivation. We remark that it is possible to derive a special case GLE for general γ (see Proposition 2). However, this gives no additional insight.
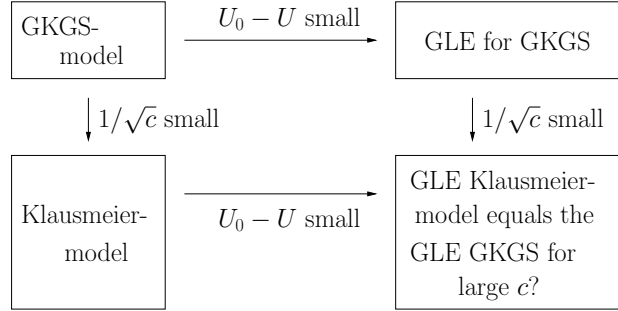
Figure 2.4: Diagram for the GLE for the GKGS for large c and the GLE for the Klausmeier-model. A priori, it is unclear whether this diagram commutes.

2.1.6   Ginzburg-Landau equation for the case $c \gg 1$: the Klausmeier model and the GKGS model for $c \gg 1$

In the Gray-Scott scaling introduced in (0.5), the original Klausmeier system reads[2]

$$\begin{cases} U_t & = & U_x & + & A(1-U) & - & UV^2 \\ V_t & = & \delta^{2\sigma}V_{xx} & - & BV & + & UV^2. \end{cases} \qquad (1.53)$$

Of course, the stationary states for the Klausmeier system are the same as the stationary states for the GKGS-model: we have the 'desert' state (U_0, V_0) and the stationary states $(U_\pm, V_\pm)$ given in (0.6).

A priori, equation (1.53) cannot be considered as a natural limit of the GKGS-system (0.5) since the diffusion coefficient d_u in front of U has been scaled to $d_u = 1$ in (0.5) (so d_u cannot be set to 0). In fact, from the point of view of mathematical modelling the original Klausmeier system is somewhat inconsistent: the (linear or nonlinear) diffusion of water U is neglected since it is dominated by the advection term, while the diffusion of vegetation V, which is in fact much smaller than that of U, is retained in (1.53).

In this subsection we justify this for $C \gg 1$ in (0.5) or $c \gg 1$ in (1.38) and discuss the relation between the GKGS model with $c \gg 1$, i.e., the case in which advection dominates diffusion in the U-equation, with the original Klausmeier model. We will do so in the context of the 'rise of patterns' and handle the problem in terms of the GLE associated to the Turing-Hopf bifurcations. As shown in the diagram of Figure 2.4, there are two paths to obtain a GLE for the case $c \gg 1$. Based on the previous sections, the most direct way is to consider the case $c \gg 1$ in the general GLE with

---

[2]Notice that this rescaling of the Klausmeier system can be acquired from Klausmeier's original nondimensional system (see [46]),

$$\begin{cases} u_T & = & \nu u_X & + & a - u & - & uv^2; \\ v_T & = & \delta^{2\sigma}v_{XX} & - & mv & + & uv^2, \end{cases} \qquad (1.52)$$

by rescaling with $x = \frac{a^2}{\nu}X$, $t = a^2T$, $v = aV$, $u = aU$, $A = \frac{1}{a^2}$, $B = \frac{m}{a^2}$ and by further introducing $0 < \delta^\sigma := \frac{a}{\nu} \ll 1$. (From the estimates for a and ν in [46], it can be deduced that indeed $0 < \frac{a}{\nu} \ll 1$.)

coefficients given by (1.45) by introducing a new small parameter $1/\sqrt{c}$. This choice implies that it is implicitly assumed that $0 < \varepsilon \ll 1/\sqrt{c} \ll 1$ (recall that ε is the distance from criticality introduced in §2.1.3).

However, we will first start out with a path that is closer to the original motivation behind the Klausmeier model: before we embark upon the weakly nonlinear GLE analysis, we first consider the limit $c \gg 1$ in (0.5). In other words, we take the other path in Figure 2.4 and assume that $0 < 1/\sqrt{c} \ll \varepsilon \ll 1$. We show that under this assumption the GKGS equation indeed agrees exactly with the Klausmeier model (at leading order). Nevertheless, this limit is significantly different from the limit associated to the other path in the diagram of Figure 2.4 and there is a priori no reason for the diagram in 2.4 to commute. The somewhat surprising outcome to our analysis is that the two resulting GLEs are identical. Before we consider asymptotically large $c \gg 1$, we introduce the scalings

$$U = \frac{\tilde{U}b^{3/4}}{\sqrt{c}}; \quad V = b^{1/4}\sqrt{c}\tilde{V}; \quad a_* = \tilde{a}_*b^{5/4}\sqrt{c};$$
$$x = b^{-1/2}\tilde{x}; \quad t = b^{-1/4}\tilde{t}; \quad r = \tilde{r}b^{5/4}\sqrt{c}. \tag{1.54}$$

These rescalings appear a little abrupt. We remark however that it follows from Proposition 2 that a_* grows with $\sqrt{c}$ as $c \gg 1$ and that the rescalings in terms of c are 'balanced' such that the terms resulting from the nonlinear diffusion in the U-component of the GKGS-system for $\gamma \geq 1$ are of higher order in $1/\sqrt{c}$ and such that all other terms are of the same, lowest order. The rescalings with b are balanced such that all terms in the GKGS-model that are of lowest order in $1/\sqrt{c}$ are also of the same order in b. We refer to appendix 6.0.3 for a more elaborate account on the derivation of these rescalings.

Now, starting from the GKGS model we employ the following scalings. As before, we rescale $\tilde{x}$ and $\tilde{t}$ in the GKGS-model (0.5) as given by (1.37). In §2.1.4, we have seen that patterns close to the stationary state given by (1.36) are described by the leading order form (1.38) with respect to ε. We adopt the rescalings as given in (1.54) and obtain, by disregarding all terms that are of higher order in $1/\sqrt{c}$,

$$\begin{aligned} 0 &= \tilde{U}_{\tilde{x}} - [\tilde{a}_*^2\tilde{U} + 2\tilde{V}] \\ &\quad -\varepsilon\left[\frac{1}{\tilde{a}_*}\tilde{V}^2 + 2\tilde{a}_*\tilde{U}\tilde{V}\right] + \varepsilon^2\left[2\tilde{r}\tilde{a}_*\tilde{U} - \tilde{U}\tilde{V}^2\right], \\ \tilde{V}_{\tilde{t}} &= \tilde{V}_{\tilde{x}\tilde{x}} + [\tilde{a}_*^2\tilde{U} + \tilde{V}] \\ &\quad +\varepsilon\left[\frac{1}{\tilde{a}_*}\tilde{V}^2 + 2\tilde{a}_*\tilde{U}\tilde{V}\right] - \varepsilon^2\left[2\tilde{r}\tilde{a}_*\tilde{U} - \tilde{U}\tilde{V}^2\right]. \end{aligned} \tag{1.55}$$

Note that the leading order formulation of the GKGS-system for large c presented in (1.55) does not include any terms that result from the nonlinear diffusion in the U-component. In ecological terms this confirms the (natural) observation that the character of the diffusion is irrelevant in a strongly sloped – and thus advection dominated – setting.

It is easy to verify that the leading order system (1.55) is identical to the one that could be derived from the Klausmeier system (1.52), had we adopted the rescalings given in (1.54) with $c = 1$ (as is the case in (1.53)). Thus, the system (1.55) also

describes the dynamics of the Klausmeier system near the Turing-Hopf instability of (U_+, V_+). Therefore, we indeed have deduced that the Klausmeier model coincides with the GKGS model (at leading order) if we assume that $0 < 1/\sqrt{c} \ll \varepsilon \ll 1$.

Now we turn to the GLE analysis. In Appendix 6.0.3, it is shown that the associated GLE is given by

$$
\begin{aligned}
\mathcal{A}_\tau &= \tfrac{1}{41}\left[(66 - 56\sqrt{2}) - \mathrm{i}(63 - 23\sqrt{2})\sqrt{\sqrt{2}-1}\right]\mathcal{A}_{\xi\xi} \\
&+ \tilde{r}\left[4\sqrt{\sqrt{2}-1} + i(4 - 2\sqrt{2})\right]\mathcal{A} \\
&+ \tfrac{4}{69}\left[-807 + 534\sqrt{2} + \mathrm{i}(418 - 286\sqrt{2})\sqrt{\sqrt{2}-1}\right]|\mathcal{A}|^2\mathcal{A}
\end{aligned}
\tag{1.56}
$$

Numerically, the Landau-coefficient in front of the $|\mathcal{A}|^2\mathcal{A}$-term is given by

$$
L_{|\mathcal{A}|^2\mathcal{A}} \approx -1.50174 + 0.252493\,\mathrm{i}
$$

We see that the real part of the Landau-coefficient is negative. This once more confirms that the Turing-Hopf bifurcation of the equilibrium (U_+, V_+) in the Klausmeier-model is supercritical. We note that this establishes the supercriticality of the Turing-Hopf instability of the background state (U_+, V_+) that was suggested in [87].

Next, we consider the alternative path in the diagram given in Figure 2.4 and assume $0 < \varepsilon \ll 1$. In order to obtain an end result that can be compared to the other path, we scale (1.38) with (1.54) for $c \neq 0$ (i.e., not necessarily $c \gg 1$) and obtain

$$
\begin{aligned}
\delta^{3\beta - 2\alpha} & b^{1/2} c^{-1/2}\tilde{U}_{\tilde{t}} \\
&= \gamma\tilde{a}_*^{1-\gamma} b^{\frac{3}{4}\gamma - \frac{1}{4}} c^{-\frac{1}{2}\gamma}\tilde{U}_{\tilde{x}\tilde{x}} + c^{1/2}\tilde{U}_{\tilde{x}} - c^{1/2}[a_*^2\tilde{U} + 2\tilde{V}] \\
&\quad + \varepsilon\left[\gamma(\gamma-1)\tilde{a}_*^{2-\gamma} b^{\frac{3}{4}\gamma - \frac{1}{4}} c^{-\frac{1}{2}\gamma}[\tilde{U}_{\tilde{x}\tilde{x}}U + (\tilde{U}_{\tilde{x}})^2] - c^{1/2}[\tfrac{1}{\tilde{a}_*}V^2 + 2\tilde{a}_*\tilde{U}\tilde{V}]\right] \\
&\quad + \varepsilon^2\left[\gamma(\gamma-1)(\gamma-2)\tilde{a}_*^{3-\gamma} b^{\frac{3}{4}\gamma - \frac{1}{4}} c^{-\frac{1}{2}\gamma}[\tilde{U}(\tilde{U}_{\tilde{x}})^2 + \tfrac{1}{2}\tilde{U}^2\tilde{U}_{\tilde{x}\tilde{x}}]\right. \\
&\qquad\qquad \left. + \gamma(\gamma-1)\tilde{a}_*^{-\gamma} b^{\frac{3}{4}\gamma - \frac{3}{2}} c^{-\frac{1}{2}\gamma - \frac{1}{2}}\tilde{U}_{\tilde{x}\tilde{x}} + 2r\tilde{a}_* c^{1/2}\tilde{U} - c^{1/2}\tilde{U}\tilde{V}^2\right]; \\
\tilde{V}_{\tilde{t}} &= \tilde{V}_{\tilde{x}\tilde{x}} + \left[\tilde{a}_*^2\tilde{U} + \tilde{V}\right] + \varepsilon\left[\tfrac{1}{a_*}\tilde{V}^2 + 2a_*\tilde{U}\tilde{V}\right] - \varepsilon^2\left[2r\tilde{a}_*\tilde{U} - \tilde{U}\tilde{V}^2\right].
\end{aligned}
\tag{1.57}
$$

In Appendix 6.0.3 we derive that the GLE for this system equals the GLE for the Klausmeier system (0.33). Therefore, patterns near the Turing-Hopf point of the GKGS-system for large c are, to first order, described by the Klausmeier system. Ecologically, one may put this by saying that ecosystems for which the slope along which the water flows downhill has a relatively steep gradient, are, to first order, described by the Klausmeier model.

Chapter 3

Busse balloons for the GKGS-system

The Ginzburg-Landau analysis of the last chapter is weakly nonlinear in the sense that it is valid only given the necessary assumption that the parameter a is close to its critical value a_* at which the Turing(-Hopf) bifurcation takes place, that is, $|a - a_*| = \mathcal{O}(\varepsilon^2)$ for a small parameter $0 < \varepsilon \ll 1$. Naturally, we are interested in the existence of stable patterns if a is not asymptotically close to a_*. In this chapter, by using novel techniques implemented in the continuation software package AUTO [10], we will present a complete picture of all the instabilities that spatially periodic patterns can undergo for different values of a and fixed values for b, c and γ. This complete picture will be called the Busse balloon, after the physicist F. Busse who introduced the concept in [4]. Later, mostly partial presentations of Busse balloons for reaction-diffusion systems have been presented, see [6, 30, 56] and the references therein. To our knowledge, the first complete Busse balloon has been described in [21]. In this chapter, we will give a description of a series of Busse balloons for the GKGS-model. See also Figure 2.3, in which we have depicted the Eckhaus region as part of the larger Busse balloon.

To be more precise, let us consider the GKGS-system (0.5) for some fixed B, C and γ and let, as before, κ be the nonlinear wavenumber.[1] A *Busse balloon* for the GKGS-system (0.5) for B, C and γ is a (not necessarily connected) set $\mathcal{B}$ in (A, κ)-space with the following property: a point (A, κ) lies in $\mathcal{B}$ if equations (0.5) with parameter A allow for at least one stable periodic solution (U_p, V_p) with wavenumber κ. Periodic patterns on the boundary of a Busse balloon $\partial\mathcal{B}$ are marginally stable.

The Busse balloon is part of the larger realm of existing (i.e., not necessarily stable) patterns. Let us give a proper definition for the convenience of terminology.

---

[1]Remark that we silently switched back to the original parameters A, B and C in (0.5). We will comment on the relation between A, B and C on the one hand and a, b and c on the other hand in §4.3.2.

The *existence region* or *existence balloon* is a (not necessarily connected) set $\mathcal{E}$ in (A, κ)-space with the following property: a point (A, κ) lies in $\mathcal{E}$ if equations (0.5) with parameter A allow for at least one periodic solution (U_p, V_p) with wavenumber κ. Typically, this means that the set has nonempty interior [71].

In this chapter, we present a series of Busse balloons for a number of choices for the values of B, C and γ (we will explain our choices for the values of these parameters later). First, we briefly present some facts from the stability theory of wave trains. Then, we consider the instabilities that will appear in the construction of the Busse balloons. Thirdly, we explain the numerical continuation method.

Stability of wave trains.　The GKGS-system (0.5) can be recast in a moving frame of reference, with respect to the variables $(\xi, t) = (x - st, t)$ (and with a slight abuse of notation),

$$\begin{cases} U_t & = & (U^\gamma)_{\xi\xi} & + & (s + C)U_\xi & + & A(1 - U) & - & UV^2 \\ V_t & = & DV_{\xi\xi} & + & sU_\xi & & & - & BV & + & UV^2 \end{cases} \quad (0.1)$$

The basic advantage here is that generic wave trains $u_{\mathrm{per}}(\xi) = (U_{\mathrm{per}}(\xi), V_{\mathrm{per}}(\xi))$ with $\xi = \kappa x + \Omega t$ and $u_{\mathrm{per}}(\xi) = u_{\mathrm{per}}(\xi + 2\pi)$ then become stationary L-periodic solutions for $s = \Omega/\kappa$ (and with $L = 2\pi/\kappa$),

$$\begin{cases} 0 & = & (U_{\mathrm{per}}^\gamma)_{\xi\xi} & + & (s + C)U_{\mathrm{per},\xi} & + & A(1 - U_{\mathrm{per}}) & - & U_{\mathrm{per}}V_{\mathrm{per}}^2 \\ 0 & = & DV_{\mathrm{per},\xi\xi} & + & sU_{\mathrm{per},\xi} & & & - & BV_{\mathrm{per}} & + & U_{\mathrm{per}}V_{\mathrm{per}}^2 \end{cases} \quad (0.2)$$

To establish spectral stability, we linearize (0.1) about $u_{\mathrm{per}} = (U_{\mathrm{per}}, V_{\mathrm{per}})$ by perturbing the wave train with $u(\xi)e^{\lambda t}$. We obtain the linear problem (write $u = (U, V)$),

$$\begin{cases} \lambda U & = & \gamma U_{\mathrm{per}}^{\gamma-1} U_{\xi\xi} & + & D_1 U_\xi & - & D_2 U & - & 2U_{\mathrm{per}}V_{\mathrm{per}}V \\ \lambda V & = & DV_{\xi\xi} & + & sV_\xi & + & V_{\mathrm{per}}^2 U & - & (B - 2U_{\mathrm{per}}V_{\mathrm{per}})V \end{cases} \quad (0.3)$$

with $D_1 = D_1[U_{\mathrm{per}}, \gamma, s, C] := \gamma(\gamma - 1)U_{\mathrm{per}}U_{\mathrm{per},\xi\xi}^{\gamma-2} + \gamma(\gamma - 1)(\gamma - 2)U_{\mathrm{per}}^2 U_{\mathrm{per},\xi\xi}^{\gamma-3} + s + C$ and $D_2 = D_2[U_{\mathrm{per}}, U_{\mathrm{per}}, \gamma, A,] := 2\gamma(\gamma - 1)U_{\mathrm{per}}U_{\mathrm{per},\xi\xi}^{\gamma-2} + A + V_{\mathrm{per}}^2$. Written as a first-order ODE, (0.3) defines a four-component system

$$\phi_\xi = \mathcal{A}_\lambda(u_{\mathrm{per}}(\xi))\phi \quad (0.4)$$

with

$$\mathcal{A}_\lambda(u_{\mathrm{per}}(\xi)) = \begin{pmatrix} 0 & 1 & 0 & 0 \\ \frac{\lambda + D_2}{\gamma U_{\mathrm{per}}^{\gamma-1}} & -\frac{D_1}{\gamma U_{\mathrm{per}}^{\gamma-1}} & \frac{2U_{\mathrm{per}}V_{\mathrm{per}}}{\gamma U_{\mathrm{per}}^{\gamma-1}} & 0 \\ 0 & 0 & 0 & 1 \\ -\frac{V_{\mathrm{per}}^2}{D} & 0 & \frac{\lambda + B - 2U_{\mathrm{per}}V_{\mathrm{per}}}{D} & -\frac{s}{D} \end{pmatrix}, \quad (0.5)$$

The matrix $\mathcal{A}_\lambda(u_{\mathrm{per}}(\xi))$ is L-periodic. Hence, by Floquet theory, there exists an L-periodic matrix $\mathcal{B}_\lambda(\xi)$ and a constant matrix $\mathcal{R}_\lambda$ such that the fundamental solution to the above first-order system is given by

$$\Phi_\lambda(\xi) = \mathcal{B}_\lambda(\xi) e^{\mathcal{R}_\lambda \xi}.$$

Since we only allow for bounded perturbations, it follows that the Floquet exponents ν of Φ_λ are purely imaginary, $\nu = \mathrm{i}k$. That is, the dispersion relation

$$d(\lambda, \mathrm{i}k) := \det(\Phi_\lambda(L) - e^{\mathrm{i}k}LI) = 0 \quad \text{for some} \quad k \tag{0.6}$$

holds. This is equivalent to the boundary value problem (see [70])

$$
\begin{aligned}
\lambda u &= \mathcal{L}_{\mathrm{i}k} u \\
u(0) &= u(L) \\
u_\xi(0) &= u_\xi(L)
\end{aligned}
\tag{0.7}
$$

with $\mathcal{L}_{\mathrm{i}k} : H^1_{\mathrm{per}}(0, L) \oplus H^1_{\mathrm{per}}(0, L) \to L^2_{\mathrm{per}}(0, L) \oplus L^2_{\mathrm{per}}(0, L)$ defined by

$$\mathcal{L}_{\mathrm{i}k} := \begin{pmatrix} \gamma U_{\mathrm{per}}^{\gamma-1}\partial^2 + D_1 \cdot \partial - D_2 & -2U_{\mathrm{per}}V_{\mathrm{per}} \\ V_{\mathrm{per}}^2 & D\partial^2 + s\partial - [B - 2U_{\mathrm{per}}V_{\mathrm{per}}] \end{pmatrix}, \tag{0.8}$$

where $\partial := \partial_\xi + \mathrm{i}k$. We will occasionally refer to (0.7) as the dispersion relation for the linearization about u_{per}.

The operator $\mathcal{L}_{\mathrm{i}k}$ has compact resolvent for each k, so its spectrum consists of countably many isolated eigenvalues [**?**]. Since each of these eigenvalues is a root of the complex analytic dispersion relation $d(\lambda, \mathrm{i}k)$, one can continue the eigenvalues $\lambda_j(k), j \in \mathbb{N}$ globally in k. By periodicity, each homotopy along $\lambda_j(k) \to \lambda_j(k + 2\pi)$ will map the set of eigenvalues $\lambda_j(k), j \in \mathbb{N}$ onto itself (notice however that it will generally not be the case that each eigenvalue λ_j is mapped onto itself by the homotopy!). Therefore, the essential spectrum of the wave train u_{per} will generally consist of (at most) countably many connected components. One of these components is connected to the translational eigenvalue at the origin.

A spatially periodic pattern is *marginally stable* if its associated operator $\mathcal{L}_{\mathrm{i}k}$ and the dispersion relation $d(\lambda, \nu)$ (0.7) satisfy the conditions in Definition 2.1.1.

Each of the destabilization mechanisms through which a periodic pattern $(U_{\mathrm{per}}, V_{\mathrm{per}})$ may destabilize, is characterized by a specific configuration of the essential spectrum. The GKGS-model with $C \neq 0$ breaks the spatial symmetry that allows for Turing patterns. This is a crucial observation, since the robust codimension-one destabilization mechanisms for generic wave trains are in principle different from the destabilization mechanisms for Turing patterns [71]. We only discuss the robust codimension-one instability mechanisms that we have encountered for wave trains in our construction of Busse balloons for the GKGS-model; these are: Turing-Hopf instability[2], fold and sideband instability. Note that Hopf instabilities and sideband instabilities are robust destabilization mechanisms for all wave trains, while a fold is not a robust instability

---

[2]With slight abuse of terminology, in the context of perturbations of periodic patterns we abbreviate the Turing-Hopf instability to 'Hopf instability' in the rest of this paper.
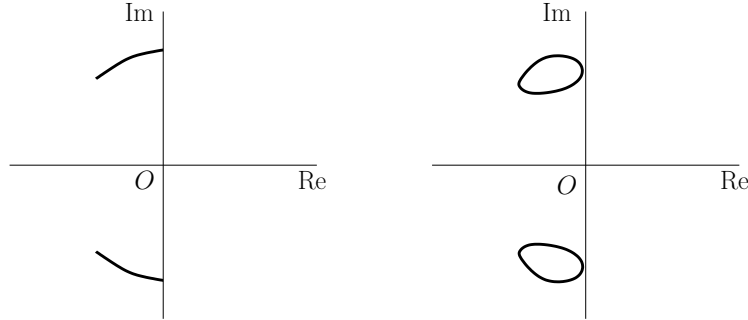
Figure 3.1: Sketches of spectra at Hopf instabilities with $\lambda \in \mathbb{C}$. Left: Spectral branches for $C = 0$. Due to the reversibility, the spectral branches have collapsed to curved line segments (see [21]). Right: Spectral branches for $C \neq 0$.

mechanism for generic spatially periodic patterns (with $\Omega \neq 0$ and $\kappa \neq 0$) though it is robust for Turing patterns ($\Omega = 0$) (see [71]).

A spatially periodic pattern u_{per} undergoes a Hopf instability at $A = A_*$ if the operator $\mathcal{L}_{\text{i}k}$ in (0.8) is at marginal stability with $k_* \neq 0$ at critical eigenvalue $\lambda = \text{i}\omega_*$ with $\omega_* \neq 0$. See Figure 3.1. A fold and a sideband instability are both characterized as instabilities for which $k_* = 0$ at critical eigenvalue $\lambda = \text{i}\omega_* = 0$. A sideband instability satisfies the additional condition that

$$\text{Re} \left. \frac{\partial^2 \lambda}{\partial k^2} \right|_{k=k_*} = 0. \tag{0.9}$$

We have depicted the difference between the fold (in the reversible case) and the sideband instability schematically in Figure 3.2. Note that the dispersion relation in the reversible case possesses the symmetry $d(\lambda, \nu) = d(\lambda, -\nu)$ and is thus of the form

$$d(\lambda, \text{i}k) = a_1 \lambda + a_2 \lambda^2 + a_3 k^2 + a_4 \lambda k^2 + a_5 k^4 + \mathcal{O}(\lambda^3 + k^6), \tag{0.10}$$

where $a_j \in \mathbb{R}$. See also [71]. A fold occurs at $a_1 = 0$ and the sketches in the top row of Figure 3.2 correspond to $a_1 < 0, a_1 = 0, a_1 > 0$ (and $a_j > 0$ for $j > 1$).

Methods and implementation notes.   For the construction of the Busse balloons, we have made use of the continuation and bifurcation software package AUTO (see [10]). The methods we have used to construct the Busse balloons are based upon [70]. In this section, we describe these methods.

Using (0.2), a wave train solution (U, V) of the GKGS-model can be written as a first order system,
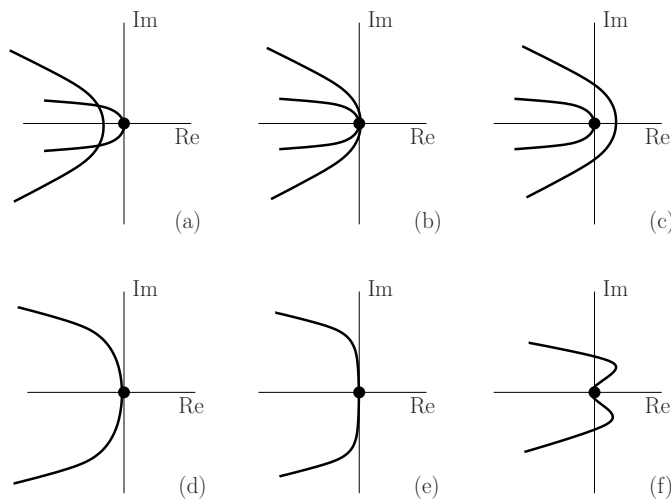
Figure 3.2: Sketches of spectral configurations we encounter for wave trains close to marginal stability, when a system parameter is crossing a critical value. Top row: reversible fold for $C = 0$. Bottom row: sideband instability for general C.

$$
\begin{aligned}
U_\xi &= P \\
P_\xi &= -\frac{1}{\gamma U^{\gamma-1}} \left[\gamma(\gamma-1)U^{\gamma-2}P^2 + A(1-U) - UV^2 + (s+C)P \right] \\
V_\xi &= Q \\
Q_\xi &= -D^{-1} \left[sQ - BV + UV^2 \right]
\end{aligned}
\tag{0.11}
$$

We denote the vectorfield at the right hand of (0.11) by $F = F(U, P, V, Q) : \mathbb{R}^4 \to \mathbb{R}^4$ and write $\psi = (U, P, V, Q)^T$. If we normalize the period L to unity, then (0.11) together with the boundary condition from (0.7) can be written as

$$
\begin{aligned}
\psi_\xi &= LF(\psi) \\
\psi(0) &= \psi(1)
\end{aligned}
\tag{0.12}
$$

In AUTO, the nonlinear equation for the wave train (0.12) is solved together with the dispersion relation (0.7). By a translation of the independent variable via $\partial_\zeta = \partial_\xi + \mathrm{i}k$, the dispersion relation (0.7) can also be conveniently cast as a first order system. Translating back and normalizing the period L to unity again, one obtains

$$
\begin{aligned}
\phi_\xi &= L[\mathcal{A}_\lambda(u_{\mathrm{per}}(\xi)) - \mathrm{i}k]\phi \\
\phi(0) &= \phi(1)
\end{aligned}
\tag{0.13}
$$

with $\mathcal{A}_\lambda(u_{\mathrm{per}}(\xi))$ as in (0.4). Hence, we consider the boundary value problem

$$
\begin{aligned}
\psi_\xi &= LF(\psi) \\
\phi_\xi &= L[\mathcal{A}_\lambda(u_{\mathrm{per}}(\xi)) - \nu]\phi \\
\phi(0) &= \phi(1) \\
\psi(0) &= \psi(1)
\end{aligned}
\tag{0.14}
$$

In AUTO, we consider the boundary value problem (0.14) for general ν, as this allows us to switch between connected components of the essential spectrum [70]. The essential spectrum is characterized by solutions to (0.14) such that $\nu = \mathrm{i}k$. We also impose the normalization conditions

$$
\int_0^1 \langle \psi_\xi, \psi_{\mathrm{old}} - \psi \rangle \, d\xi = 0; \qquad \int_0^1 \langle \phi_{\mathrm{old}} - \phi \rangle \, d\xi = 1,
\tag{0.15}
$$

where the solutions ψ_{old} and ϕ_{old} are solutions from a previous continuation step or an initial solution [70].

Remark that $\psi \in \mathbb{R}^4$ and $\phi \in \mathbb{C}^4 \simeq \mathbb{R}^8$. Hence, we have $8 + 4 = 12$ real unknowns. On the other hand, we have 12 boundary conditions plus 3 real integral conditions, so we need $3 + 1 = 4$ parameters for continuation. We have at our disposal the system parameters A, B, C and D, as well as $\mathrm{Re}\lambda$, $\mathrm{Im}\lambda$, the linear wavenumber $k = \mathrm{Re}\,\nu$, the imaginary part $\mathrm{Im}\,\nu$, the comoving frame speed s and the spatial period L (that is related to the (nonlinear) wavenumber via $\kappa = \frac{2\pi}{L}$).

The sideband can be continued by defining the curvature

$$
\lambda_{||} := \left. \frac{\partial^2 \mathrm{Re}\lambda_0}{\partial k^2} \right|_{k=k_*}
$$

where $\lambda_0(k)$ is the curve through the origin, and k_* the wavenumber associated to $\lambda_0(k_*) = 0$ at the origin (cf. (0.9)). We refer to [70] for an exact account on the implementation.

Hopf instabilities are continued in a similar way. Hopf instabilities generically occur when a connected component of the essential spectrum crosses the imaginary axis, see Figure 3.1(b). A sufficient condition in order to fix the spectral component at marginal stability when a system parameter is changed, is:

$$
\mathrm{Re}\lambda|_{k=k_*} = 0 \quad \text{and} \quad \left. \frac{\partial \mathrm{Re}\lambda}{\partial k} \right|_{k=k_*} = 0.
\tag{0.16}
$$

This condition makes sure that the connected component of the essential spectrum extends into the left half-plane when continued from $\lambda(k_*) = \mathrm{i}\omega_*$. In AUTO, one therefore defines the tangency

$$
\lambda_| := \frac{\partial \mathrm{Re}\lambda}{\partial k}
$$

and keeps it zero during a continuation of Hopf instabilities, along with Reλ. The implementation can be derived in the same way as for the sideband instability by differentiating the dispersion relation. (Note that some terms do not vanish for $\lambda \neq 0$.)

The above considerations are purely local in the spectrum. The determination of (marginal) stability requires more effort. We refer to [70] for the algorithms.. In addition, we checked the stability of the spectrum within the Busse balloon by explicit numerical evaluations on a grid.

3.0.7 The existence balloon

From §2.1.3 we know that the stationary state u_+ undergoes a Turing-Hopf instability at some $A = A_*$ with critical eigenmode e^{ik_*} and critical frequency $\lambda = i\omega_*$. Hence, at $A = A_*$ the dispersion relation of the stationary state u_+ (1.6) satisfies

$$d(i\omega_*, ik_*) = 0.$$

In §2.1.4 we deduced by our Ginzburg-Landau approach (see also Figure 2.3), that for $A < A_{\mathrm{TH}}$ sufficiently close to the Turing-Hopf instability of the background state $u_+ = (U_+, V_+)$, there exists a parabolically shaped region of periodic patterns. More precisely, for $A < A_{\mathrm{TH}}$ sufficiently close to A_{TH}, there exists an interval $I_A = (\kappa_-(A), \kappa_+(A))$ such that for each $\kappa \in I_A$ there is a spatially periodic pattern with wavenumber κ and these form a continuous family. For each A, the endpoints $\kappa_\pm = \kappa_\pm(A)$ of the interval I_A are characterized by the dispersion relation of u_+ at A,

$$d(i\Omega_\pm, i\kappa_\pm) = 0. \tag{0.17}$$

We remark that this characterization for the endpoints $\kappa_\pm$ of I_A holds for a full range of $A < A_{\mathrm{TH}}$ not necessarily close to A_{TH}. An equivalent formulation to (0.17) can be given by means of the first order ODE formulation of the linearisation about u_+ (see (0.4)),

$$\phi_\xi = \mathcal{A}_\lambda(u_+)\phi. \tag{0.18}$$

(notice that $\mathcal{A}_\lambda(u_+)$ is a constant matrix here). The dispersion relation (1.6) satisfies (0.17) for some Ω_* and κ_* if and only if there exists an Ω_* such that there is a solution to (0.18) for $\lambda = i\Omega_*$ that has purely imaginary eigenvalues $\nu = i\kappa_*$.

More generally, $\lambda \in \mathbb{C}$ is in the essential spectrum of u_+ if and only if there is a solution to (0.17) for some $\nu = i\kappa$. Since the wavenumbers ν from the dispersion relation of the stationary state u_+ (1.6) appear as eigenvalues to the spatial ODE (0.18), they are also referred to as spatial eigenvalues. With AUTO, we have traced out a curve of boundary points $\kappa_\pm = \kappa_\pm(A)$ that mark the boundary of the existence balloon in (A, κ)-space. By construction, this provides an extension of the existence of the band of periodic patterns near the Turing-Hopf instability that is predicted by the GLE.

We digress a little on the characterization of the boundary of the existence balloon. Let $C \neq 0$, and consider fixed A and $\kappa_+ = \kappa_+(A)$, so that there exists a $\lambda = i\Omega$

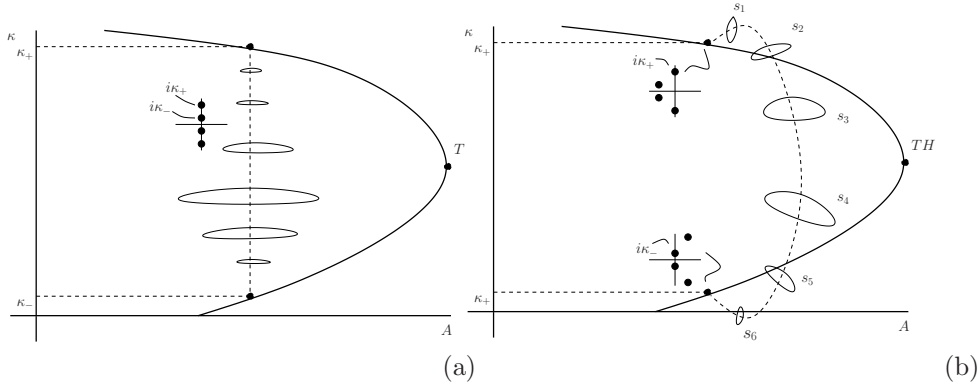(a)   (b)

Figure 3.3: The boundary of the existence region near the Turing and Turing-Hopf bifurcations. Closed curves are sketches of some periodic patterns *for fixed A*, illustrating the amplitude variations. Compare with Figure 2.3. Insets show the configurations of spatial eigenvalues of u_+ at the boundary of the existence balloon at this value of A. (a) the reversibly symmetric case $C = 0$ with $s \equiv 0$; spatial eigenvalues are two pairs of purely imaginary values. (b) Asymmetric case $C, s \neq 0$, where spatial eigenvalues change with s; note that at each end of the dotted curve, a different (single) pair of eigen valueslies on the imaginary axis.

such that (0.18) has purely imaginary spatial eigenvalue κ_+ and therefore a pair of complex conjugated spatial eigenvalues $\pm \kappa_+$. Hence, for fixed A, and by changing the speed s of the comoving frame, typically two spatial eigenvalues $\pm i\kappa_+$ cross the imaginary axis so that a Hopf bifurcation occurs. Therefore, locally there exists a one-parameter family of periodic orbits parametrized by the speed s.

Likewise, there exists a one-parameter family of periodic orbits when the other pair of eigenvalues $\pm\kappa_-$ crosses the imaginary axis. By a continuation of the two families of periodic patterns with Auto, we have found that they are connected. See Figure 3.3(b). This extends the band of periodic patterns that is described by the GLE close to the Turing-Hopf bifurcation for $A = A_{\mathrm{TH}}$.

If $C = 0$, the reversible symmetry forces the spatial spectrum to be symmetric with respect to the real axis and the imaginary axis. At the Turing bifurcation of the stationary state u_+, the spatial spectrum shows a 1:1 reversible Hopf bifurcation: there are two identical pairs of complex conjugate purely imaginary spatial eigenvalues $\pm k_*$. By the reversible symmetry, for $A < A_{TH}$, two pairs of spatial eigenvalues will move along the imaginary axis. Then one can apply the reversible Lyapunov center theorem [9]: for (non-resonant) κ_- as well as for (non-resonant) κ_+, there is a one-parameter family of periodic orbits with limiting wavenumber $\kappa_\pm$ as the orbits approach the background state u_+. (At resonances additional bifurcations occur, which are not relevant here.) Again, by continuation, we find that the family that emerges from κ_-
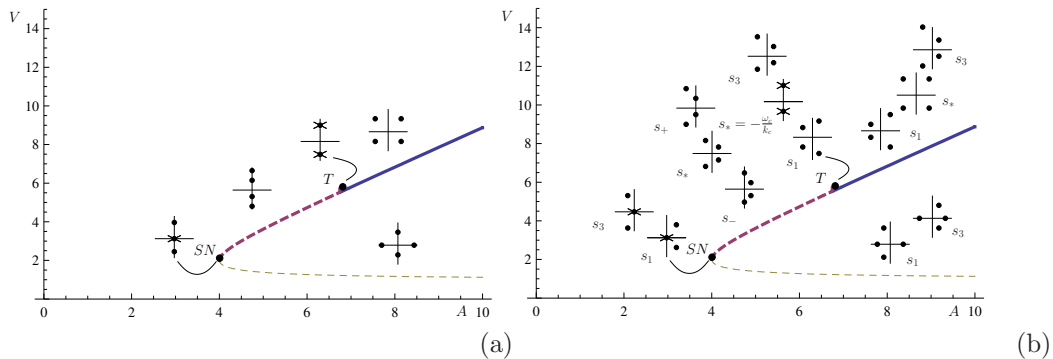
Figure 3.4: The $V_\pm$-component of the stationary states $u_\pm$ against A, with $B = 1$. (a) reflection symmetric case $C = 0$. (b) the nonsymmetric case $C \neq 0$. The insets show the typical configuration of the spatial spectrum of the stationary state u_+. In the nonsymmetric case, the spatial spectrum depends on s – the speed of the pattern – and thus various distinct configurations have been plotted. Compare to Figure 3.3.

is connected to the family that emerges from κ_+, which in turn extends the connected band of periodic solutions close to the Turing-Hopf bifurcation that we know from the Ginzburg-Landau analysis. See Figure 3.3(a).

The spectral stability of a stationary state is partly characterized by its spatial spectrum. In Figure 3.4 we have plotted the spatial spectrum of the stationary states u_+ and u_- for different values of either A and the comoving frame speed s. We briefly comment on Figure 3.4(b) here. First, we check that the speed of the critical pattern that appears at the Turing-Hopf instability equals $s_* = -\frac{\omega_*}{k_*}$. If we write the (stationary) dispersion relation $d_s(\lambda, \nu)$ in (1.6) with respect to a comoving coordinate $\xi = x - st$, it holds that $d_s(\lambda, \nu) = d_0(\lambda - s\nu, \nu)$. In particular, if $k_* \neq 0$ we see

$$d_{\omega_*/k_*}(0, \mathrm{i}k_*) = d_0(\mathrm{i}\omega_*, \mathrm{i}k_*) = 0.$$

Secondly, the spatial spectrum of the fold of the stationary states u_- and u_+ is characterized by a complex conjugated pair of purely imaginary eigenvalues that come together in the origin and move on to the real axis. Thirdly, we remark that for fixed $A_{\mathrm{SN}} < A < A_{\mathrm{TH}}$ for any relevant value of s and $\kappa_-(A) < \kappa < \kappa_+(A)$, the spatial spectrum of the stationary state u_+ has no intersection with the imaginary axis. In Figure 3.4(b), s_+ is the critical frame speed when κ_+ crosses the imaginary axis and s_- is the critical frame speed when κ_- crosses the imaginary axis. In the pictures of spatial spectra for the different s_i, $i = 1, 2, 3$ it is understood that the comoving frame speed s varies but differs from either s_-, s_+ or s_*.

3.0.8 Busse balloons for the GKGS-model

In this section we present a series of Busse balloons for a number of parameter sets, that we have constructed using AUTO (by methods discussed above).
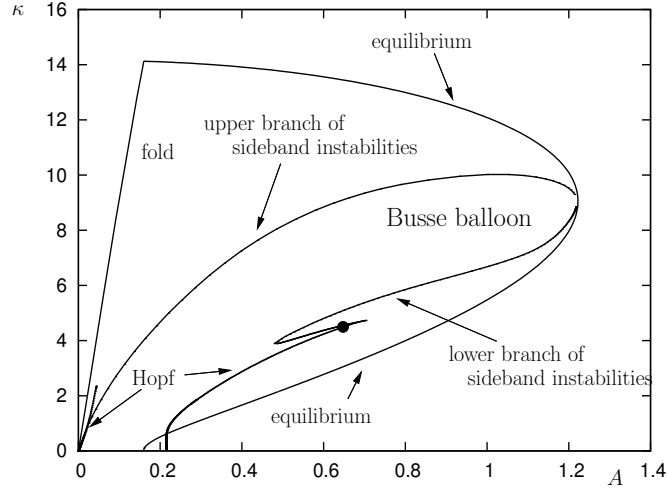
Figure 3.5: Busse balloon and existence balloon for $B = 0.2$, $C = 0.4$, $\gamma = 1$. Here, periodic patterns become unstable by either sideband or Hopf instability. Compare Figure 1.5.

In [46] the parameters of the Klausmeier model have been estimated. In our scaling of the GKGS-model, it is estimated that $A_{\text{tree}} \in [18.9, 169]$, $B_{\text{tree}} \in [5.7 \cdot 10^{-3}, 5.1 \cdot 10^{-2}]$ and $D_{\text{tree}} \in [4.2 \cdot 10^{-4}, 1.2 \cdot 10^{-2}]$ and that $A_{\text{grass}} \in [0.127, 1.13]$, $B_{\text{grass}} \in [5.7 \cdot 10^{-2}, 5.1 \cdot 10^{-1}]$ and $D_{\text{grass}} \in [5.2 \cdot 10^{-3}, 1.5 \cdot 10^{-2}]$. The advection term that measures the slope of the surface has been put to $C = 182.5$. We therefore set $B = B_{\text{grass}} = 0.2$ and $D = 1.0 \cdot 10^{-3}$. In the results we are about to present, we found interesting behaviour for C satisfying $0 < C < 1$, which is relatively small compared to the estimate of C in [46]. There seem to be no significant changes in the characteristics of the Busse balloon for $C > 1$. Therefore, we focus on Busse balloons with these parameter values for C rather than on Busse balloons with $C \approx 182.5$. This means that we focus on a presentation of Busse balloons that describe periodic patterns for ecosystems with a weaker slope than in [46]. The power γ in the nonlinear diffusion term is either set to $\gamma = 1$ or $\gamma = 2$.

We have checked that the Turing-Hopf bifurcation indeed takes place at the parameter values predicted by the analysis in §2.1.2 and 2.1.3. Consider for instance Figure 3.5. There, $B = 0.2$, $C = 0.4$, $D = 0.001$, $\gamma = 1$ and further $A_{\text{TH}} \approx 1.24$ and $k_* \approx 9.1$. The estimates for a_* and k_* from Proposition 2 are satisfied given that $(2\gamma + 1)\beta - (\gamma + 1)\alpha = 2\sigma$. Further, it must hold that ν satisfies its critical scaling (1.18): $\nu = \frac{1}{2}(3 - \gamma)\alpha + (\gamma - 2)\beta$. For $\alpha = \frac{1}{2}$, $\beta = 1$, $\gamma = 1$, $\nu = -\frac{1}{2}$ and $\sigma = 1$ (so that $D = 0.001$ gives $\delta = \sqrt{0.001}$) these conditions are satisfied. The rescaling for k introduced in §2.1.3 is then: $k_* = \delta^{\frac{1}{2}(\gamma+1)\alpha - \gamma\beta}\tilde{k}_* = 1.62$ since $\tilde{k} \approx 9.0$. Fur-

ther, we compute $a_* = A\delta^{-\alpha} = 1.24 \cdot \delta^{-1/2} = 7.0$, $b = B\delta^{-\beta} = 0.2 \cdot \delta^{-1} = 6.3$ and $c = C\delta^{-\nu} = 0.4 \cdot \delta^{1/2} = 0.07$. Hence, the estimates of Proposition 2 are easily verified: $k_*^2 = 1.62^2 < 6.3 = b$ and $a_*^2 = 7.0^2 > 42.9 \approx (3 - 2\sqrt{2}) \cdot 6.3^3$.

Both branches of sideband instabilities extend far into the region that is not asymptotically close to A_{TH}. More precisely, there exists an interval $I_{\mathrm{sb}} = (A_{\mathrm{sb}}, A_{\mathrm{TH}})$ such that for each $A \in I_{\mathrm{sb}}$ there is an interval $(\kappa_{\mathrm{sb}-}(A), \kappa_{\mathrm{sb}+}(A))$ of stable patterns that destabilize by sideband instabilities at $\kappa_{\mathrm{sb}-}(A)$ and $\kappa_{\mathrm{sb}+}(A)$. Notice that this is analogous to the existence of the Eckhaus region of stable patterns near A_{TH} (see Figure 2.3).

3.0.8.1 Hopf instabilities In Figure 3.5 both branches of sideband instabilities are crossed by a branch of Hopf instabilities. The nature of these Hopf instabilities can be better understood if we first deal with the situation for $C = 0$, so we first discuss the Hopf instabilities for $C = 0$ and refer to the more elaborate account on this topic in [21] when necessary.
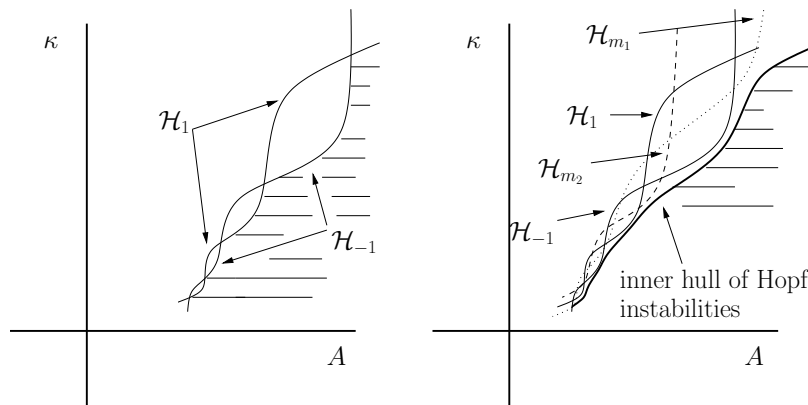
Figure 3.6: Left: sketch of a Hopf dance for the GKGS-model with $C = 0$. Right: four Hopf curves, each associated to a different Floquet multiplier m. For each $m \in \mathbb{S}^1$ there exists a Hopf curve $\mathcal{H}_m$. At the right, the inner hull of Hopf instabilities forms the boundary of the Busse balloon. It is assumed that $m_1 \neq m_2$ and $m_1, m_2 \neq \pm 1$. The horizontal lines indicate the stable region.

For $C = 0$, the branch of Hopf instabilities decouples in two intertwining curves of Hopf bifurcations (see [21]). As is shown in [21], the reversibility induces a symmetry of the essential spectrum Σ_{ess}. See, for example, Figure 3.1. Each connected component that has the structure of a closed loop for $C > 0$, collapses to a (slightly) bended line-segment in the limit $C = 0$. Due to an additional effect (called the 'Belly-dance', see [21]), a Hopf instability occurs only if one of the end points of the destabilizing line segment crosses the imaginary axis (see Figure 3.1(b)). It is shown that the end

points are associated with Floquet multipliers $m = e^{ik \cdot \frac{2\pi}{L}}$ that satisfy $m = -1$ or $m = 1$. Hence, the Hopf bifurcation for $C = 0$ occurs either with respect to a Fourier mode that is in phase ($m = 1$) with the destabilizing periodic pattern or with respect to a Fourier mode that is exactly out of phase ($m = -1$) with the destabilizing pattern. Each of these instabilities traces out a different curve in (A, κ)-space. As a consequence, in the reversible case the boundary of the Busse balloon associated to a Hopf bifurcation, typically has a (nonsmooth) fine structure of two intersecting curves, one associated to $m = 1$ and the other to $m = -1$, separated by co-dimension two points; the intersections of these $m = \pm 1$ curves.

For $C > 0$, the reversible symmetry is broken. Therefore, the essential spectrum consists of at most countably many open or closed loops. Each loop is parametrized by Floquet exponents k, $k \in [0, L]$, or equivalently, by Floquet multipliers $m \in \mathbb{S}^1$. A Hopf instability occurs when a loop crosses the imaginary axis. In Figure 3.1(a) one can see a closed loop of essential spectrum crossing the imaginary axis. The destabilizing Fourier mode is characterized by its Floquet multiplier $m \in \mathbb{S}^1$. The difference between the reversible case and the irreversible case is that in the irreversible case the destabilizing modes exhaust all Floquet multipliers $m \in \mathbb{S}^1$, while in the reversible case the destabilizing Floquet multiplier is either $m = -1$ or $m = 1$. For each Floquet multiplier $m \in \mathbb{S}^1$ there exists a curve of Hopf instabilities that is associated to m. The multitude of these curves defines an inner hull of Hopf instabilities that is the boundary of the Busse balloon. See Figure 3.6 for a schematic picture.

3.0.8.2   The homoclinic fall of patterns   An intriguing characteristic of all Busse balloons we have constructed for the GKGS-equation is that the homoclinic pattern, i.e., a localized vegetated 'oasis' state with wavenumber $\kappa = 0$, is the last pattern to become unstable if we change A and keep all other parameters fixed. On the one hand, this is not atypical for reaction-diffusion models; in the context of Gierer-Meinhardt type equations it is called Ni's conjecture (see [60] and [21] for a deeper discussion). On the other hand, it is certainly not well understood why this 'homoclinic fall of patterns' turns up naturally in reaction-diffusion equations.

The homoclinic fall of (stable) patterns is strongly associated to the appearance of the 'Hopf-dance' at the boundary of the Busse balloon near the homoclinic tip that we described in §3.0.8.1. In fact, the Hopf-dance phenomenon has been discovered in the context of our research of the GKGS model and led to [21] as 'spin-off'. In this paper it is shown for a class of reversible model problems that the intertwining $m = \pm 1$ Hopf curves described above (§3.0.8.1) accumulate on the homoclinic tip of the Busse balloon as A approaches its minimal value (for which stable periodic patterns exist). Thus, the curves have countably many intersections that accumulate on the homoclinic tip of the Busse balloon – see Figure 3.6(a) for a schematic sketch. The GKGS-model is not of this class (certainly not for $\gamma = 2$) but we found that all Busse balloons for the GKGS model with $C = 0$ do exhibit this 'Hopf-dance' near the homoclinic tip. Of course, this fine structure and its associated co-dimension two points immediately disappear as C becomes unequal to zero and gives rise to a simple

smooth oscillating curve of Hopf instabilities. See Figure 3.6.

3.0.8.3 Upper branch of sideband instabilities An intriguing phenomenon is the fact that this branch of Hopf instabilities crosses the upper branch of sideband instabilities, moves out of the Busse balloon for increasing C. See Figure 3.7 for a series of (zoomed in) Busse balloons and a schematic sketch from which the 'dynamics' of the Hopf bifurcation curve are more clear. More precisely, there exists a $C_{T_1} > 0$ such that the branch of Hopf instabilities is tangent to the branch of sideband instabilities. For C slightly larger than C_{T_1}, two connected components of the boundary of the Busse balloon consist of Hopf instabilities. At $C = C_H > C_{T_1}$ the branch of Hopf instabilities gets connected to the origin. For C slightly larger than C_H, locally there is only one connected component of the boundary of the Busse balloon that consists of Hopf instabilities. If one increases C even further, it passes a second value C_{T_2} at which there is a tangency between the branch of Hopf instabilities and the branch of sideband instabilities. For $C > C_{T_2}$ the sideband is the only destabilization mechanism for long wavelength patterns.

If $C = 0$, the sideband reaches the A-axis at $A \neq 0$. However, the intersection of the upper branch of sideband instabilities with the A-axis rapidly moves to $A = 0$ as C is increased. This is certainly not fully understood.

3.0.8.4 Lower branch of sideband instabilities We recall that the lower branch of sideband instabilities is intersected by a branch of Hopf instabilities as well. See Figure 3.8, where we have magnified the intersection between the lower branch of sideband instabilities and the right branch of Hopf instabilities. It is visible as a strikingly sharp cusp. In Figure 3.8 we have also depicted the spectrum associated to the stability of a solution at the sideband instability close to the crossing point, denoted by ①, the spectrum associated to the solution at the crossing point, denoted by ②, and the spectrum associated to a solution close to the crossing point undergoing a Hopf instability, denoted by ③. The crossing point ② is a codimension-two point at the boundary of the Busse balloon: the solution at the crossing point simultaneously undergoes a sideband instability and Hopf instability, as is visible in the plot of the spectrum of solution 2.
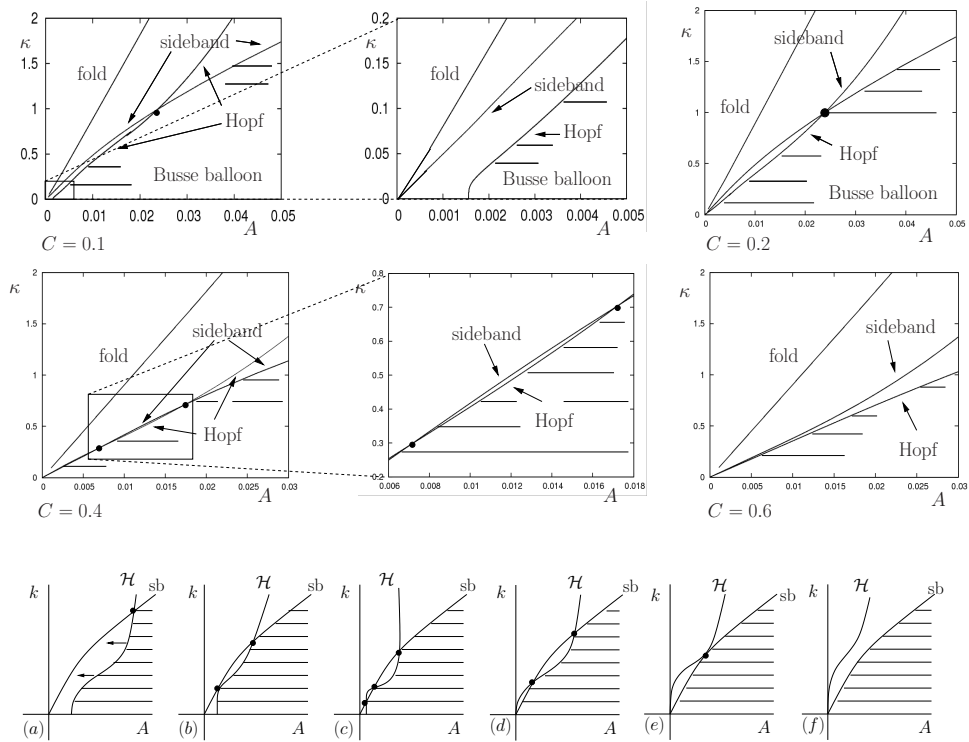
Figure 3.7: *Upper panels:* The left Hopf curve moving out of the Busse balloon for increasing C. The horizontal lines indicate the stable region. Center panel magnify the box in left panels. The fold curve in the upper left panel has not been plotted in the other panels for readability. *Lower panels:* A schematic sketch of the same process (sb=sideband). (a) The curve of Hopf instabilities has one intersection with the upper branch of sideband instabilities. (b) At $C = C_{T_1}$, there is a tangency between the two curves. (c) For $C_{T_1} < C < C_H$ there are two connected components of the boundary of the Busse balloon formed by Hopf instabilities. (d) At $C = C_H$, the curve of Hopf instabilities is connected to the origin: only one connected component of the boundary that consists of Hopf instabilities. (e) At $C = C_{T_2}$, there is a second tangency between the two curves remains. (f) For $C > C_{T_2}$, the sideband remains as the only destabilization mechanism in the homoclinic tip (see §3.0.8.2).
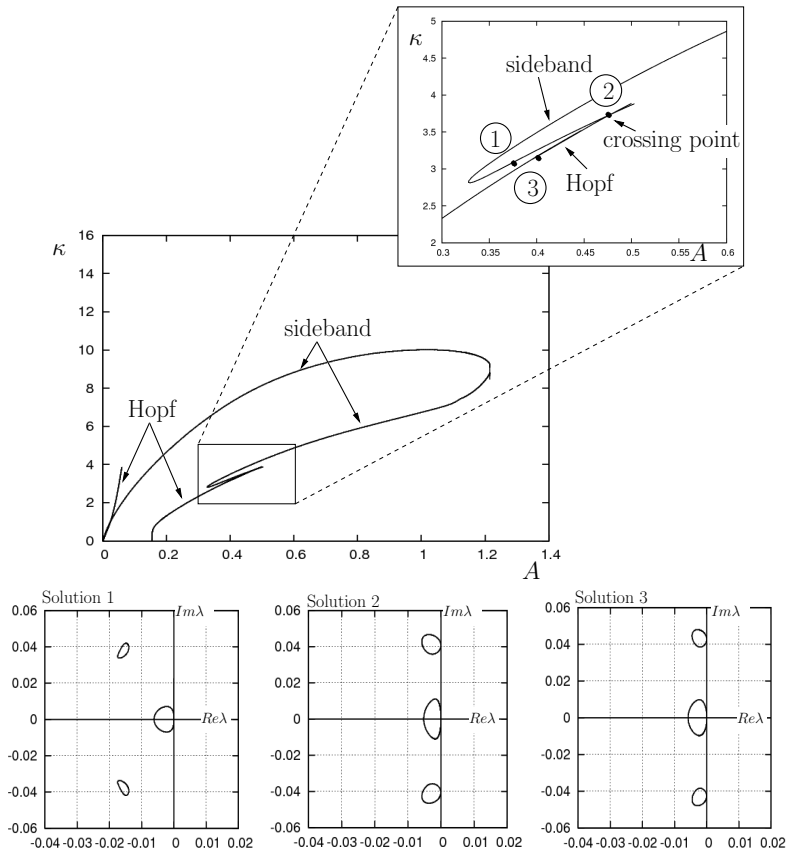
Figure 3.8: Close-up of the crossing point between the right curve of Hopf instabilities and the lower branch of sideband instabilities. Here, $C = 0.2$ and $B = 0.2$. The spectra near the origin for the solutions 1, 2 and 3 indicated in the magnification are plotted in the three figures at the bottom.
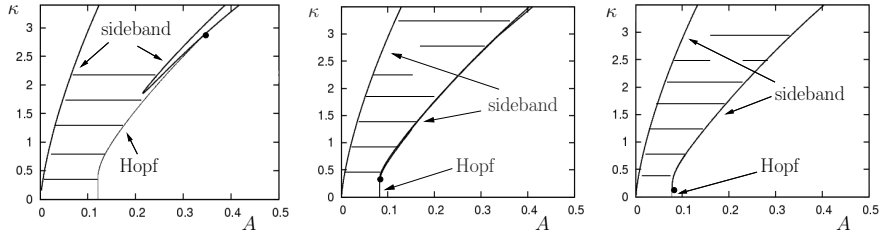
Figure 3.9: The right branch of Hopf instabilities disappears into the A-axis when $C \downarrow 0$. At the left, we see a part of the Busse balloon for $C = 0.1$. In the middle, $C = 0.01$. At the right, $C = 0.001$. The fold curve plotted in the left panel has moved very close to the Hopf and sideband curves in the other panels so that it cannot be visually distinguished.

When C approaches zero, the lower branch of sideband instabilities stretches out towards the A-axis and thereby decreases the size of the branch of Hopf instabilities. The Hopf instabilities disappear at $C = 0$ where also the sideband curve merges with the very nearby fold curve (see [21]). The fact that reversible folds yield sideband instabilities upon symmetry breaking can be readily seen by perturbing (0.10). See also Figure 3.2. In Figures 3.9 we have plotted three close-ups of the Busse balloons for $C = 0.1$, $C = 0.01$ and $C = 0.001$.

A second intriguing phenomenon is the irregular 'jazzy' behaviour of the lower branch of sideband instabilities for relatively small C ($C = 0$ to approximately $C = 0.8$). See Figure 3.10. This fine structure of the lower branch of sideband instabilities is in sharp contrast with the regular, parabolically shaped Eckhaus region for A near A_{TH}. Even a closed curve of sideband instabilities occurs (see Figure 3.10(b)). For increasing C, the fine structure gradually disappears.

While the fine structure of sideband instabilities lies in the unstable region, we digress a little on its structure and location within the existence region. To the right of the fine structure lies the fold curve mentioned above (see Figure 3.9, left), which we refer to as the *right fold*. For the C values considered in Figure 3.10, the right fold curve (see the discussion in §4.4.1) terminates on the equilibrium curve at some $(A_{\mathrm{fe}}, \kappa_{\mathrm{fe}})$ near $(0.8, 4)$. Hence, for $A < A_{\mathrm{fe}}$ there is a second co-existing 'sheet' of (unstable) spatially periodic patterns.

In the lower panel of Figure 3.11(a) we plot (for a different C) the L^2-norm for fixed κ to illustrate the different sheets of solutions. Here the co-existence region is rather small. See top right panel. continuation of periodic patterns for constant wavenumber κ. Comparison with Figures 3.9 and 3.10 shows how the fine structure of sideband instabilities is to the left of the right fold, thus lying on the same "sheet" of solutions as the stable periodic patterns of the Busse balloon.

An additional phenomenon of the existence region is shown by the region near $A = 0.3$:
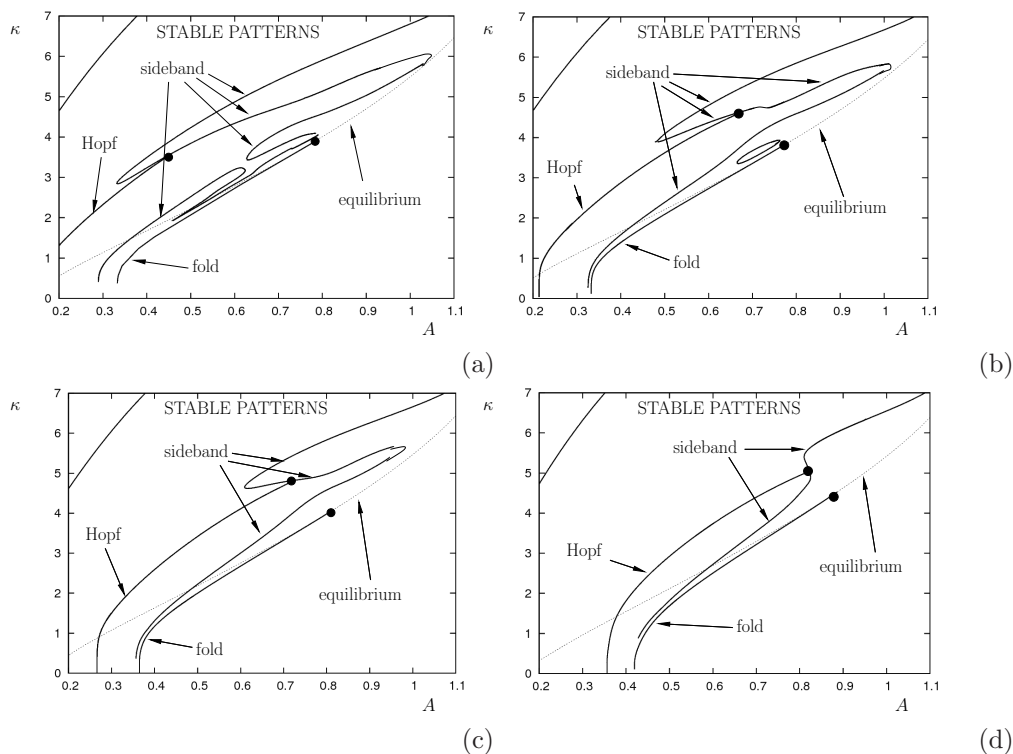
Figure 3.10: (a-d) The fine structure of the lower branch of sideband instabilities for $B = 0.2$ and (a) $C = 0.2$, (b) $C = 0.4$, (c) $C = 0.6$, (d) $C = 1.0$. The equilibrium continues through the fold and reaches a second sheet of (unstable) patterns; therefore it is plotted with a dashed curve. The intersection point of the Hopf instabilities with the sideband is indicated with a black circle. Also, the intersection point of the fold with the equilibrium is indicated with a black circle. Note that some pieces of the curve of sideband instabilities are missing; here the continuation of the sideband with AUTO becomes extremely difficult since the norm of one of the eigenvectors in (0.15) rapidly increases.

there are two more folds which emerged through a cusp bifurcation when decreasing C from $C = 0.2$. lower branch, thereby giving rise to a cusp. We notice that this behaviour of the unstable sheet of solutions close to the Busse balloon is highly nongeneric. Indeed, the existence region has a much richer structure than what we encounter within the Busse balloon. Finding out the precise geometrical mechanism that triggers the formation of this cusp is beyond the scope of the present paper. However, this will be the subject of future research.
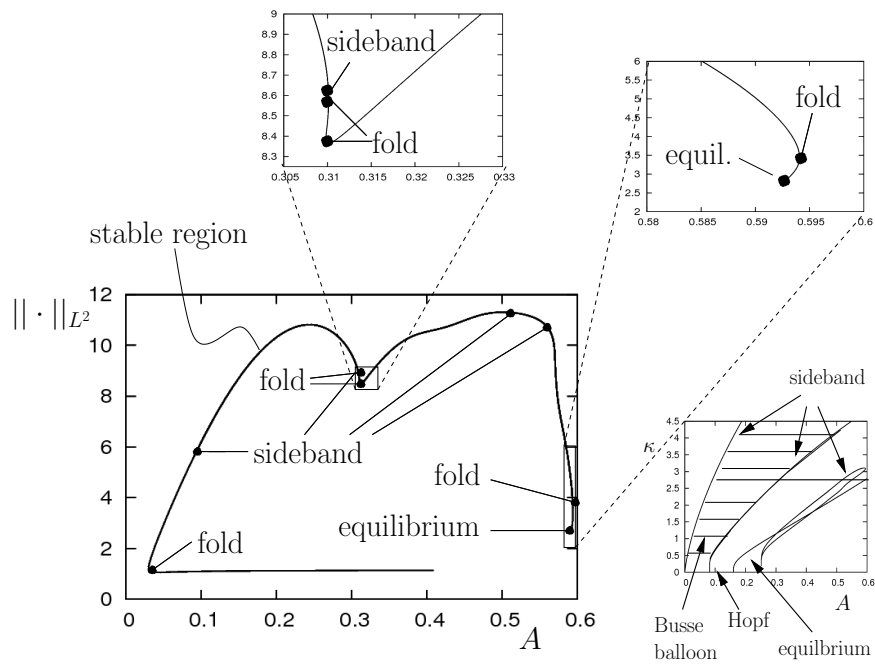
Figure 3.11: Computations for $B = 0.2$, $C = 0.01$. (a) Plot for continuation in A with constant wavenumber $\kappa = 2.78$. Top panels magnify the indicated regions. (b) Part of the existence balloon. The thick line indicates the value of κ used in (a).

3.0.9 Busse balloons for $C > 0$ and $\gamma = 2$

We are not aware of any (even partial) representations of a Busse balloon for a system with nonlinear diffusion in the literature. Nevertheless, the approach with AUTO developed here can also be directly applied to the GKGS model (0.5) with $\gamma > 1$. In Figure 3.12 an existence and a Busse balloon for periodic patterns of the GKGS-model with $\gamma = 2$ and $B = C = 0.2$ are shown. One can see that the structure of the Busse balloon of the existence region closely resembles the structure of the Busse balloon and existence region of the GKGS-model for $\gamma = 1$ (see for instance Figure 3.5).

As before for $\gamma = 1$, we check that the Turing-Hopf bifurcation indeed takes place at the parameter values predicted by the analysis in §2.1.2 and §2.1.3. We therefore check whether $k_*^2 < b$ and $a_*^3 = a_*^{\gamma+1} > g\gamma b^{2\gamma+1} = 2gb^5$ with $k = k_*$ scaled as in §2.1.3 and Figure 3.12. There, $B = 0.2$, $D = 0.001$, $\gamma = 2$ and further $A_{\mathrm{TH}} \approx 0.525$ and $k_* \approx 8.9$. If $\gamma = 2$, the estimates for a_* and k_* from Proposition 2 are satisfied given that $5\beta - 3\alpha = 2\sigma$. Since $D = \delta^{2\sigma} = 0.001$ we choose $\sigma = 1$ and $\delta = \sqrt{0.001}$ and $\alpha = \beta = \sigma = 1$. The rescaling for k introduced in §2.1.3 is then: $\tilde{k}_* = \delta^{-\frac{1}{2}(\gamma+1)\alpha+\gamma\beta}k_* = \delta^{1/2}k_* = (0.001)^{1/4} \cdot 8.9 \approx 1.58$. Further, we compute $a = A\delta^{-\alpha} = 0.525 \cdot \sqrt{1000} \approx 16.6$ and $b = B\delta^{-\beta} = 0.2 \cdot \sqrt{1000} \approx 6.3$. Hence, the estimates of Proposition 2 are verified by $k_*^2 = 1.58^2 < 6.3 = b$ and $a_*^3 = 16.6^3 \approx 4.75 \cdot 10^3 > 3.47 \cdot 10^3 \approx 2gb^5$.

A priori, the GKGS-model for $\gamma = 2$ can of course not be interpreted as a 'perturbation' of the GKGS-model for $\gamma = 1$. Quantitatively the structure between the Busse balloon for $\gamma = 2$ and the Busse balloons for $\gamma = 1$ is quite different. This is already apparent in the simple verification of the parameter estimates for a, b and c above. Nevertheless, qualitatively the structure of the Busse balloon for $\gamma = 2$ is remarkable akin to the structure of the Busse balloons for $\gamma = 1$. All main features of the (behavior of the) Busse balloon for various C as studied in the previous section for $\gamma = 1$ and described in the Introduction, also appear for $\gamma = 2$. Figure 3.12 shows that the sideband instabilities make most of the boundary of the Busse balloon, until the upper and lower branches of sideband instabilities are crossed transversally by Hopf instabilities for decreasing wavenumbers k. Also, for relatively small $C > 0$ there is a 'Hopf dance' (if $C = 0$) in the homoclinic tip of the upper branch of sideband instabilities. In the Figure, where $C = 0.2$, there is a Hopf curve crossing the upper branch of sideband instabilities. Just as in the case for $\gamma = 1$, the left curve of Hopf instabilities disappears into the unstable region for bigger values of C. These are not new phenomena and are known from the previous numerical analysis of the GKGS-model for $\gamma = 1$.
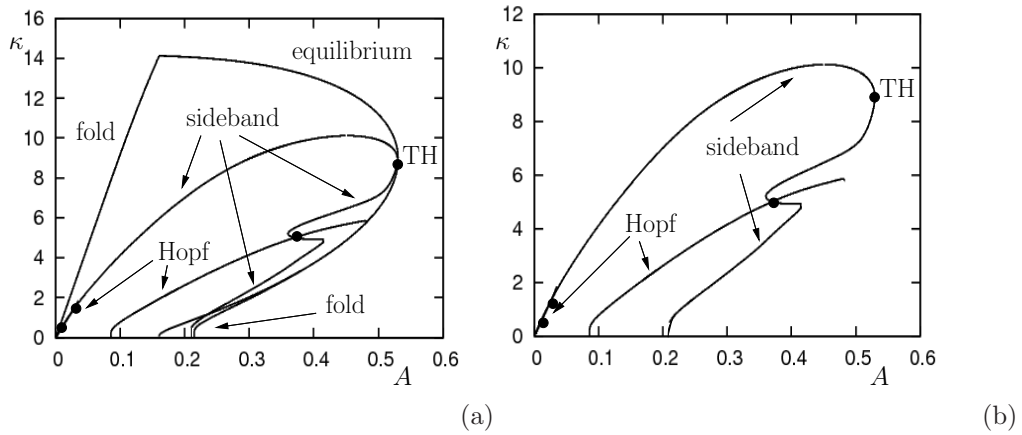
Figure 3.12: An existence balloon (left) and a Busse balloon (right) for the GKGS-model with $\gamma = 2$. B and C are $B = C = 0.2$. The intersection points of the Hopf instabilities with the upper and lower curves of sideband instabilities are indicated with a black circle.

Chapter 4

Hopf dances near the tips of Busse balloons

4.1 Introduction

The (complex) Ginzburg-Landau equation exhibits bands of stable periodic patterns that are generically destabilized by the sideband (or Eckhaus, or Benjamin-Feir) instability mechanism. Moreover, the boundary of a Busse balloon near onset is generically given by a parabola – the Eckhaus parabola – of sideband destabilizations, see chapter 2. Ginzburg-Landau theory is a general and very powerful theory, however, it only applies to the asymptotically small part of a Busse balloon near onset.

Of course, one can in general not hope to obtain a full analytical control over an entire Busse balloon. As for the Ginzburg-Landau theory one should only expect to be able to capture small, but essential, parts of the Busse balloon by analytical means (see however Remark 1.1). Moreover, it is at present too ambitious to propose to develop a theory for 'far-from-equilibrium-patterns' that is as general as Ginzburg-Landau theory. Based on recent developments in the (mathematical) theory, we nevertheless claim it is possible to consider the above question in the setting of a well-specified class of problems: the stability and destabilization of nearly localized, spatially periodic patterns in reaction-diffusion equations, see Figure 4.1. This class of problems is especially interesting, since there are quite a number of results in the literature that indicate that these (singular) long wavelength periodic multi-pulse/front/spike patterns appear as the 'most stable' – i.e the last periodic patterns to destabilize – spatially periodic patterns [17, 44, 48, 49, 56, 58, 60, 68, 97]. This is also confirmed by the Busse balloon for the Gray-Scott system (1.1) presented in Figure 4.2(a): for decreasing A, stable patterns appear at a Ginzburg-Landau/Turing bifurcation and eventually disappear at a 'tip' at which the wavenumber k approaches zero (i.e. at which the wavelength of the patterns becomes large). Thus, these singular patterns may indeed represent an essential (but small) part of the Busse balloon. Complemen-
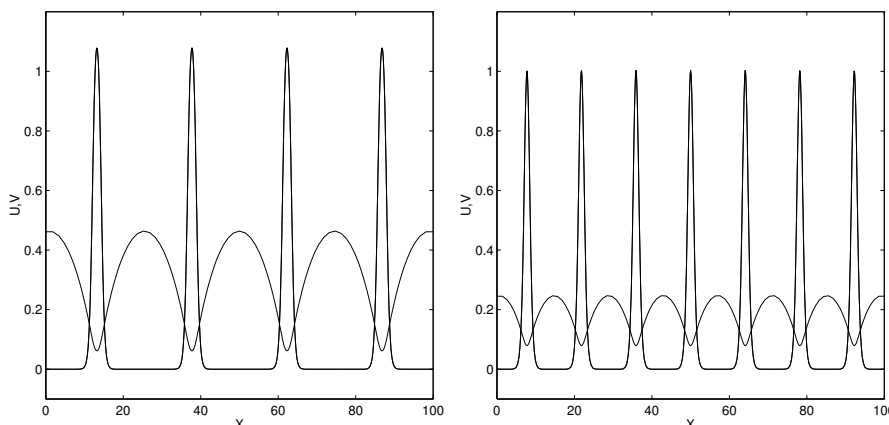
Figure 4.1: Two typical stationary, nearly localized, reversible spatially periodic patterns with different wavelengths L/wavenumbers k. These patterns coexist as stable solutions of the Gray-Scott model (1.1) with $A = \varepsilon^4 = 0.01$ and $B = 0.060$ [16].

tary to the small amplitude Ginzburg-Landau patterns that indicate the 'bottom' of the Busse balloon at which patterns appear, the nearly localized patterns may form the 'tip' of the Busse balloon at which the stable periodic patterns disappear.

Therefore, we focus in this chapter on the study of Busse balloons associated to periodic patterns in reaction-diffusion systems in one spatial dimension. In the numerical (first) part of the chapter, we do consider a 'full' Busse balloon, but only in the context of a very explicit, singularly perturbed two component model, the well-studied Gray-Scott equation,

$$\begin{cases} U_t &=& U_{xx} &+& A(1-U) &-& UV^2 \\ V_t &=& \varepsilon^4 V_{xx} &-& & BV &+& UV^2 \end{cases} , \qquad (1.1)$$

in which $A, B > 0$ and $\varepsilon > 0$ are parameters (and $0 < \varepsilon \ll 1$ in the singularly perturbed setting). In the analytic part of this chapter, we restrict ourselves to the nearly-localized tip of the Busse balloon, in the context of a certain (sub)class of problems that a priori includes the patterns considered in the Gray-Scott model (see sections §4.1.2 and §4.3.5): the stability and destabilization of nearly localized reversible patterns in singularly perturbed two component reaction-diffusion equations.

The specific choice to restrict the analysis to singularly perturbed systems is motivated by the state-of-the-art of the mathematical theory for the existence and stability of nearly localized periodic patterns. There is a well-developed qualitative mathematical theory for (one-dimensional) localized structures, such as (homoclinic) pulses/spikes and (heteroclinic) fronts, in reaction-diffusion equations – see [76] and the references therein. By the methods developed in [35, 36, 78], it is possible to extend this theory

to nearly-localized spatially periodic patterns. However, at this point, the general theory does not provide the amount of quantitative information necessary to study the nearly homoclinic ($k = 0$) tip of Busse balloons in full detail. Such a more quantitative theory has been developed in the context of singularly perturbed reaction-diffusion equations, both for the localized patterns [17], as well as for the nearly-localized spatially periodic patterns [68]. We refer to section §4.6 for a discussion of the extension of our main results to non-singularly perturbed systems.

The generic mechanism proposed here – the *'Hopf dance near the tip of Busse balloons'* – is graphically presented in Figure 4.2. Figure 4.2(a) is the outcome of a comprehensive numerical study of the stability and existence boundaries in (parameter,wavenumber)-space of spatially periodic patterns of the Gray-Scott model, by means of continuation techniques (see especially [70]). Although the Gray-Scott system is one of the most thoroughly studied reaction-diffusion systems in the recent literature, see e.g. [16, 18, 23, 48, 49, 56, 57, 58, 62, 63, 66, 67, 73, 98], we are not aware of a comparable comprehensive (numerical) study of periodic patterns in the Gray-Scott model (a rough approximation of this Busse balloon, obtained by direct simulation the Gray-Scott model, has been presented in [56]; in [89] the same continuation approach has been used to study the stability of periodic patterns in lambda-omega systems, where it can be reduced to the much more simple case of constant coefficients). The *'Hopf dance'* is performed by two intertwined snaking curves of Hopf instabilities, denoted by $\mathcal{H}_{\pm 1}$ in Figure 4.2, that terminate in the limit $k = 0$ at the Hopf bifurcation of the limiting homoclinic pulse. Figure 4.2(b) gives a schematic sketch of the Hopf dance destabilization mechanism. The curve $\mathcal{H}_{+1}$, represents a Hopf destabilization in which all extrema of the pattern start to oscillate exactly in phase at the bifurcation; at $\mathcal{H}_{-1}$ the maxima (or minima) of the patterns that are one period away from each other begin to oscillate exactly out of phase. The Hopf dance gives the boundary of the Busse balloon a fine structure of alternating pieces of the curves $\mathcal{H}_{+1}$ and $\mathcal{H}_{-1}$, representing different types of destabilizations, separated by an infinite sequence of corners, or co-dimension 2 points.

The $\mathcal{H}_{\pm 1}$ Hopf instabilities stem from the intersections with the imaginary axis of the endpoints of a bounded curve of the spectrum associated to the linearized stability of the periodic pattern (see section §4.2). To leading order, this spectral curve is a straight line segment that, as a function of decreasing wavenumber k, rotates around its center while shrinking exponentially in length. At second order, the spectral curve is bent, and it is striking to note that its overall curvature oscillates with twice the frequency of the rotation, so that the most unstable point of the spectral curve cannot be an interior point, but must always be one of the two $\mathcal{H}_{\pm 1}$ endpoints. In this chapter, we refer to this oscillation as the *'belly dance'*.

A priori, the Hopf (and belly) dance performed by the (spectrum associated to the) periodic patterns in the Gray-Scott model may seem very special, and thus non-generic, behavior. However, this is not the case. In the second part of this chapter, §4.4–§4.5, we prove that both the Hopf and the belly dances occur in a class of two component, singularly perturbed reaction-diffusion systems that includes the gener-

(a)   (b)
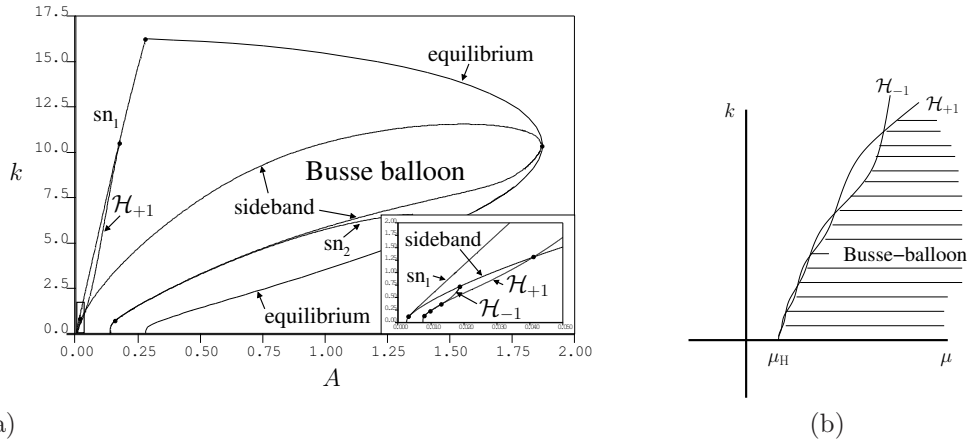
Figure 4.2: (a) A Busse balloon associated to the Gray-Scott equation, (1.1) with
$B = 0.26$ and $\varepsilon^4 = 0.001$, embedded in the associated existence balloon, i.e. the
region in (parameter, wavenumber)-space in which spatially periodic patterns exist
(but are not necessarily stable). For decreasing A, the Busse balloon is initiated by a
Turing/Ginzburg-Landau bifurcation; it ends at a 'homoclinic tip' at A of the order
of ε^4. The boundary segments are labeled according to their type: for existence these
are curves of folds (sn$_1$, sn$_2$) and of vanishing amplitude at equilibria; for stability
these are curves of Hopf instabilities, sideband instabilities and also folds – the exact
meaning and interpretation of these labels are discussed in detail in section §4.3.
Bullets mark corners (co-dimension 2 points). The inset enlarges the rectangular
region near the homoclinic ($k = 0$) limit at which the Hopf dance of the curves $\mathcal{H}_{\pm 1}$
occurs. Note that only the first three intersections of the curves $\mathcal{H}_{\pm 1}$ have been
plotted. (b) A schematic sketch of the Hopf dance at the homoclinic tip of a Busse
balloon; μ is a parameter and μ_{H} indicates the Hopf bifurcation value associated to
the homoclinic pulse pattern that appears as $k \downarrow 0$.

alized Gierer-Meinhardt model [17]. Based on the Evans function analysis of [68], we
give explicit formulas for the leading and next order geometry of the spectral curves
associated to the stability of the nearly localized spatially periodic patterns in this
class of systems. In particular, our formulas give explicit expressions (in terms of
exponentially small quantities in ε) for the local (fine) structure of the boundary of
the Busse balloon. Moreover, we identify the quantity that determines whether the
limiting homoclinic $k = 0$ pulse is the last periodic pattern to become unstable as the
parameter varies (called Ni's conjecture [60], see Remark 5.4). Similarly, we identify
the quantity that determines the orientation of the belly dance, that is, whether the
$\mathcal{H}_{\pm 1}$ endpoints of the spectral curves are always the most unstable or not. In the
latter case, the actual stability boundary will be a smoothed out version of that ob-
tained from considering the endpoints alone, see Figure 4.10 and section §4.6.

We conclude this chapter by a discussion of the robustness of the Hopf dance destabilization mechanism within larger classes of systems (section §4.6).

Remark 1.1 An important class of equations with a rich, and relatively easy to study, class of periodic patterns (or wave trains) is the widely studied complex Ginzburg-Landau equation. In the most simple case, the real Ginzburg-Landau equation, the boundary of the Busse balloon is in its entirety given by the (unbounded) Eckhaus parabola of sideband instabilities. For the general (complex) cubic Ginzburg-Landau equation, the Busse balloon may be non-existent, or its boundary may consist of certain Hopf bifurcations [54]. The structure of the Busse balloon becomes less simple, and for instance includes co-dimension 2 corners, for (extended) cubic-quintic Ginzburg-Landau equations that occur near the transition of super- to subcritical bifurcations [14, 30, 83, 84]. In fact, the analysis in [30] indicates that there may even be bounded Busse balloons in this case.

Remark 1.2 Some aspects of the Hopf dance destabilization mechanism were already found analytically in [68] for the special case of the classical Gierer-Meinhardt model. However, it was not yet recognized in [68] as a generic phenomenon, and not analyzed in detail.

4.1.1 The setting

In their most general form, two component reaction-diffusion equations in one spatial dimension are given by,

$$\begin{cases} U_t & = & U_{xx} & + & F(U,V;\vec{\mu}) \\ V_t & = & D^2 V_{xx} & + & G(U,V;\vec{\mu}) \end{cases} \tag{1.2}$$

The reaction is described by the vector fields $F, G : \mathbb{R}^2 \to \mathbb{R}^2$ that depend on the parameter(s) $\vec{\mu} \in \mathbb{R}^m$ ($m \geq 1$) in the problem. The system is considered on the unbounded real line, i.e. $x \in \mathbb{R}$, and x is scaled such that the diffusion coefficient associated to U is 1; V diffuses with coefficient $D^2 > 0$.

The stationary problem associated to (1.2) consists of two purely second order ordinary differential equations in the time-like space variable x. Such equations always possess a reversible symmetry induced by spatial reflection $x \to -x$. Solutions that are reflection symmetric in x are called *reversible*, which is the case for all solutions that are relevant for our purposes. Reflection symmetric periodic patterns, or standing wave trains, of (1.1) are reversible periodic orbits and typically persist as periodic orbits under perturbation with an adjusted period L (or wavenumber k), e.g., [25, 71]. Hence, we can expect open regions of existence in the $(\vec{\mu}, k)$-parameter space.

Let $(U_{\mathrm{p}}(x;k), V_{\mathrm{p}}(x;k))$ be such a family of stationary spatially periodic patterns with associated periodic solutions $\gamma_{\mathrm{p}}(x;k)$ of the 4-dimensional (spatial) dynamical system for stationary solutions of (1.2). Existence regions then come as (maximal) connected regions $I_{\mathrm{e}}(\vec{\mu}) \subset \mathbb{R}$ in k for which $(U_{\mathrm{p}}(x;k), V_{\mathrm{p}}(x;k))$ exist. Note that for a given $\vec{\mu}$,

$I_e(\vec{\mu})$ may only be one of several disjoint existence regions. The physically most relevant patterns are the solutions of (1.2) that are dynamically stable. In this chapter we are only concerned with spectral stability. We define $\sigma = \sigma(U_p, V_p)$ as the spectrum associated to the linearization about a pattern $(U_p(x; k), V_p(x; k))$ (1.2) and call a pattern spectrally *stable* if $\sigma \cap \{\mathrm{Re}(\lambda) \geq 0\} = \{0\}$, and if the curve of σ through the origin has quadratic tangency, see e.g, [71]. Stable periodic patterns form a subset of $I_e(\vec{\mu})$. Let $I_s(\vec{\mu}) \subset I_e(\vec{\mu})$ be a connected component of this subset in the sense that $(U_p(x; k), V_p(x; k))$ destabilizes as k approaches the boundary of $I_s(\vec{\mu})$. A Busse balloon B_B of (1.2) is defined as a connected component of the $(\vec{\mu}, k)$-parameters of stable periodic patterns, that is,

$$B_B = \bigcup_{\vec{\mu} \in \mathbb{R}^m} (\vec{\mu}, I_s(\vec{\mu})) \subset \mathbb{R}^{m+1}, \tag{1.3}$$

see also Remark 1.3. For practical reasons, one often fixes $(m-1)$-components of $\vec{\mu}$ and only plots a two-dimensional cross-section of B_B in (μ_j, k)-space – see Figure 4.2.

The reversible symmetry has consequences for the (stability) boundary of the Busse balloon. According to [71], the following types of instabilities can generically occur along curves of the boundary. Where noted, this is with respect to a destabilizing mode $e^{i(\alpha t - \eta x)}$ (and its complex conjugate).

'Sideband'	curvature of the curve of σ at the origin changes sign through the instability (also called Benjamin-Feir or Eckhaus instability)
'Hopf'	$\alpha \neq 0$, $\eta \neq 0$ (also called Turing-Hopf)
'Turing'	$\alpha = 0$, $\eta \neq 0$
'Period doubling'	as Turing, but with $\eta = k/2$,
'Pure Hopf'	as Hopf but with $\eta = 0$,
'Fold'	the pattern undergoes a saddle-node bifurcation.

In all cases $\sigma \cap \{\mathrm{Re}(\lambda) \geq 0\} = \{0, i\alpha, -i\alpha\}$, where $\alpha = 0$ for sideband, fold and Turing.

Inspired by the Hopf dance observed in the Gray-Scott model, we focus in the analytic part of this chapter on the 'normal form model' for large amplitude pulse patterns to singularly perturbed equations given by

$$\begin{cases} \varepsilon^2 U_t &= U_{xx} - \varepsilon^2 \mu U + U^{\alpha_1} V^{\beta_1} \\ V_t &= \varepsilon^2 V_{xx} - V + U^{\alpha_2} V^{\beta_2}, \end{cases} \tag{1.4}$$

in which $0 < \varepsilon \ll 1$. This model is known as the generalized Gierer-Meinhardt equation [17, 43, 44, 60, 97, 99]; $U(x,t), V(x,t)$ are scaled versions of their counterparts in (1.2) and are by construction $\mathcal{O}(1)$ w.r.t. ε. This equation was originally derived as leading order normal form model for large amplitude pulse patterns to singularly perturbed two component reaction-diffusion equations in [17]. It is derived from equations of the type (1.2) by imposing a couple of assumptions:

(A-i)   the system has a stable 'background state' $(U(x,t), V(x,t)) \equiv (0,0)$;
(A-ii)   the equations decouple at the linear level (i.e. as $\|(U,V)\|$ becomes small);
(A-iii)   the nonlinearities grow algebraically and are 'separable' in a sense explained in §4.1.2.

We refer to section §4.1.2 for a sketch the derivation of (1.4) and the conditions on its parameters. As for the Gray-Scott model, there are many indications in the literature that tip of the Busse balloon associated to (1.4), i.e. the last region in which stable periodic patterns exist, is also formed by nearly homoclinic, nearly localized, spatially periodic patterns [17, 44, 60, 68, 97]. More specifically, the limiting homoclinic $k = 0$ pattern generally appears as 'the last pattern to become unstable' – see §4.5 and particularly Remark 5.4 on Ni's conjecture. In section §4.4, (part of) the existing literature on the existence and stability of stationary singular spatially periodic patterns to (1.4) is summarized.

Remark 1.3 Reaction-diffusion equations naturally also exhibit traveling spatially periodic patterns, or wave trains, i.e. non-stationary solutions that are periodic in space and in time. For these patterns, one can also define the concept of a Busse balloon (in a completely equivalent fashion). However, in this chapter we only consider stationary periodic patterns.

4.1.2   The normal form model

In this section we give a brief derivation of (1.4) as normal form model for large amplitude pulses in the general class of singularly perturbed (two component) reaction-diffusion models (1.2). First, we bring the equation into a singularly perturbed form that satisfies the first two assumptions (*(A-i)* and *(A-ii)*),

$$\begin{cases} U_t = U_{xx} - \mu U + H_1(U, V; \varepsilon, \vec{\mu}) \\ V_t = \varepsilon^4 V_{xx} - V + H_2(U, V; \varepsilon, \vec{\mu}), \end{cases} \tag{1.5}$$

where $H_1(U, 0) = H_2(U, 0) \equiv 0$. Note that the parameter μ controls the (relative) decay rates of U and V (i.e. $\mu > 0$). Singular equations of this type generally exhibit localized patterns that are singular in various ways: *(E-i)* the 'fast' V-components are spatially localized in regions in which the 'slow' component U remains at leading order constant; *(E-ii)* the U-components vary slowly in regions in which V is exponentially small; *(E-iii)* the amplitude of both U- and V-components scale with a negative power of ε – i.e. they are asymptotically large. Therefore, it is natural to scale out the asymptotic magnitudes of U and V,

$$\tilde{U}(x,t) = \varepsilon^r U(x,t), r \geq 0, \; \tilde{V}(x,t) = \varepsilon^s V(x,t), s \geq 0,$$

so that $\tilde{U}(x,t)$ and $\tilde{V}(x,t)$ are $\mathcal{O}(1)$ w.r.t. ε; the magnitudes r and s are a priori unknown. The following assumption on the asymptotic behavior of the nonlinearities $H_{1,2}(U, V)$, which is the technical version of assumption *(A-iii)*, is crucial to the derivation of (1.4),

$$H_i(U, V) = H_i(\frac{\tilde{U}}{\varepsilon^r}, \frac{\tilde{V}}{\varepsilon^s}) = \tilde{U}^{\alpha_i} \tilde{V}^{\beta_i} \varepsilon^{-(r\alpha_i + s\beta_i)} \left[h_i + \hat{\varepsilon} \tilde{H}(\tilde{U}, \tilde{V}; \varepsilon) \right], \tag{1.6}$$

in which $\hat{\varepsilon}$ is some positive power of ε and $\tilde{H}_i = \mathcal{O}(1)$ w.r.t. ε. Hence, it is assumed that the growth of nonlinear terms $H_i(U,V)$ for U, V large is dominated by the algebraic expression $U^{\alpha_i} V^{\beta_i}$. Note that this part of assumption *(A-iii)* is quite natural, as are assumptions *(A-i)* and *(A-ii)* – see Remark 1.4. However, there is an additional part to assumption *(A-iii)* that is more restrictive: the asymptotic decomposition (1.6) is also assumed to be separable, in the sense that the leading order terms (for U, V large) can be factored out of $H_i(U,V)$. Note that this assumption implies that the leading order behavior for large solutions also dominates as these solutions are no longer large. See §4.6 and Remark 1.4 for a discussion of this issue and its relation to the (conjectured) genericity of the Hopf dance. The magnitudes r and s of U and V can now be determined in terms of $\alpha_1, \alpha_2, \beta_1, \beta_2$ by the assumption that (large, singular) pulse type patterns can indeed exist as solutions of (1.5),

$$r = \frac{\beta_2 - 1}{d} > 0, \ s = -\frac{\alpha_2}{d} > 0, \ \text{with} \ d \stackrel{\text{def}}{=} (\alpha_1 - 1)(\beta_2 - 1) - \alpha_2 \beta_1 > 0, \qquad (1.7)$$

see [17]. This analysis also yields that $h_j > 0$, for $j = 1, 2$, and that the parameter(s) $\vec{\mu} = (\mu, \alpha_1, \alpha_2, \beta_1, \beta_2)$ in (1.4) must satisfy the following conditions,

$$\mu > 0, \ d > 0, \ \alpha_2 < 0, \ \beta_1 > 1, \ \beta_2 > 1. \qquad (1.8)$$

By introducing the spatial scale $\tilde{x} = x/\varepsilon$ and neglecting all tildes, equation (1.5) can now at leading order be brought into the 'normal form' (1.4).

Remark 1.4 A more general model that satisfies *(A-i)* and *(A-ii)* and that generalizes *(A-iii)* to non-separable nonlinearities is,

$$\begin{cases} \varepsilon^2 U_t &= \quad U_{xx} \quad - \quad \varepsilon^2[\mu U - F_1(U; \varepsilon)] \quad + \quad F_2(U, V; \varepsilon), \\ V_t &= \varepsilon^2 V_{xx} \quad - \quad V \quad + \quad G(U, V; \varepsilon). \end{cases} \qquad (1.9)$$

Note that especially the fact that there is a spatial nonlinearity $F_1(U; \varepsilon) \neq 0$ distinguishes this model from the Gray-Scott/Gierer-Meinhardt types models in the literature [13]. We will come back to this generalized model in the discussion of the (non-)generic effect of the 'belly dance' in section §4.6.

4.2 Preliminaries I: The stability of periodic patterns

In this section, we sketch several aspects of the literature on the stability of periodic patterns in reaction-diffusion equations. The presentation is largely based on [35, 36, 68, 70, 71, 78]. For simplicity, we restrict ourselves to the two components setting of (1.2). However, the ideas presented here can be readily extended to N-component systems. Moreover, (1.2) includes all other, more specific, models considered in this chapter.

4.2.1 The structure of the spectrum

The spectral stability problem associated to a stationary, spatially periodic solution $(U_{\mathrm{p}}(x;k), V_{\mathrm{p}}(x;k))$ of (1.2) with respect to perturbations (for instance) in $BC_{\mathrm{unif}}(\mathbb{R}, \mathbb{R}^2)$, i.e. the space of bounded and uniformly continuous functions, is obtained by substitution of

$$U(x,t) = U_{\mathrm{p}}(x;k) + u(x)e^{\lambda t}, \quad V(x,t) = V_{\mathrm{p}}(x;k) + v(x)e^{\lambda t},$$

into (1.4), followed by linearization. This yields the system,

$$\begin{cases} \lambda u = u_{xx} + \partial_U F(U_{\mathrm{p}}(x), V_{\mathrm{p}}(x))u + \partial_V F(U_{\mathrm{p}}(x), V_{\mathrm{p}}(x))v \\ \lambda v = D^2 v_{xx} + \partial_U G(U_{\mathrm{p}}(x), V_{\mathrm{p}}(x))u + \partial_V G(U_{\mathrm{p}}(x), V_{\mathrm{p}}(x))v \end{cases} \tag{2.1}$$

Since $x \in \mathbb{R}$, (2.1) can be written in the form of a 4-dimensional (linear) system,

$$\dot{\phi}(\xi) = \mathcal{A}_{\mathrm{p}}(\xi; \lambda, L, \varepsilon)\phi(\xi), \tag{2.2}$$

where $\phi = (u, p = Du_\xi, v, q = v_\xi)^t$ in the scaled spatial variable $\xi = x/D$ and the dot denotes differentiation with respect to ξ. Note that ξ is introduced in anticipation of the singularly perturbed setting in which ξ represents the 'fast' spatial scale. For the same reason, we introduce L as half of the wavelength of the periodic pattern $(U_{\mathrm{p}}, V_{\mathrm{p}})$, i.e., with a slight abuse of notation, $(U_{\mathrm{p}}(x;k), V_{\mathrm{p}}(x;k)) = (U_{\mathrm{p}}(\xi;L), V_{\mathrm{p}}(\xi;L))$ with $L = \pi/kD$. Therefore, the periodic matrix $\mathcal{A}_{\mathrm{p}}(\xi; \lambda, k)$ in (2.2) is given by,

$$\mathcal{A}_{\mathrm{p}}(\xi; \lambda, L) = \begin{pmatrix} 0 & D & 0 & 0 \\ D(\lambda - \partial_U F(U_{\mathrm{p}}(\xi; L), V_{\mathrm{p}}(\xi; L))) & 0 & -D\partial_V F(U_{\mathrm{p}}(\xi; L), V_{\mathrm{p}}(\xi; L)) & 0 \\ 0 & 0 & 0 & 1 \\ -\partial_U G(U_{\mathrm{p}}(\xi; L), V_{\mathrm{p}}(\xi; L)) & 0 & (\lambda - \partial_V G(U_{\mathrm{p}}(\xi; L), V_{\mathrm{p}}(\xi; L))) & 0 \end{pmatrix}. \tag{2.3}$$

Since $\mathcal{A}_{\mathrm{p}}(\xi; \lambda, L)$ is $2L$ periodic, solutions to (2.2) can (by Floquet theory) be assumed to be of the form

$$\phi(\xi) = \psi(\xi)e^{c\xi} \text{ for some } c \in \mathbb{C} \text{ and } \psi(\xi) \ 2L-\text{periodic.}$$

However, the perturbations $\phi(\xi; \lambda)$ must be in $BC(\mathbb{R}, \mathbb{C}^4)$, so that $c = i\tilde{c} \in i\mathbb{R}$. Hence,

$$\phi(\xi + 2L; \lambda) = \gamma\, \phi(\xi; \lambda) \text{ for a } \gamma \in \mathbb{S}^1, \tag{2.4}$$

since $\gamma = e^{2i\tilde{c}L} \in \mathbb{C}$ with $|\gamma| = 1$. Note that if $\phi(\xi; \lambda)$ satisfies condition (2.4) in one particular point ξ, it satisfies (2.4) everywhere. Since bounded solutions of (2.2) can be decomposed into a combination of functions $\phi(\xi; \lambda)$ that satisfy (2.4) for some $\gamma \in \mathbb{S}^1$, it follows that the spectrum $\sigma((U_{\mathrm{p}}, V_{\mathrm{p}}))$ of the stability problem associated to the periodic pattern $(U_{\mathrm{p}}(\xi; L), V_{\mathrm{p}}(\xi; L))$ entirely consists of γ-eigenvalues [35], i.e. $\lambda(\gamma) \in \mathbb{C}$ such that there is a solution $\phi(\xi)$ of (2.2) that satisfies (2.4) for some $\gamma \in \mathbb{S}^1$. Thus, by varying γ over $\mathbb{S}^1$, we may conclude that $\sigma((U_{\mathrm{p}}, V_{\mathrm{p}}))$ is the union of – a priori countably many – bounded curves $\Lambda(L; \vec{\mu})$ with

$$\Lambda(L; \vec{\mu}) = \{\lambda \in \mathbb{C} : \lambda(\gamma) \text{ is a } \gamma-\text{eigenvalue}, \gamma \in \mathbb{S}^1\} \tag{2.5}$$

(see [35, 70, 78]). In general, these curves can either be a smooth image of $\mathbb{S}^1$ or have a more degenerate structure. In particular, they often form closed loops that are isolated connected components of the spectrum.

4.2.2   Reversibility: the collapse of $\Lambda(L; \vec{\mu})$

Due to the reversibility symmetry in both the equation (1.2) and the patterns $(U_{\mathrm{p}}(\xi; L), V_{\mathrm{p}}(\xi; L))$, the spectral loops $\Lambda(L; \vec{\mu})$ (2.5) collapse to branches with well-defined endpoints $\partial_{\pm}\Lambda(L; \vec{\mu})$. To see this, we need to be more explicit about nature of these symmetries. First, we may define $\xi = 0$ as a reflection point for the pattern $(U_{\mathrm{p}}(\xi; L), V_{\mathrm{p}}(\xi; L))$, i.e. we may assume that $(U_{\mathrm{p}}(-\xi; L), V_{\mathrm{p}}(-\xi; L)) = (U_{\mathrm{p}}(\xi; L), V_{\mathrm{p}}(\xi; L))$ for all ξ. Note that,

$$(U_{\mathrm{p}}(L + \xi), V_{\mathrm{p}}(L + \xi; L)) = (U_{\mathrm{p}}(\xi - L), V_{\mathrm{p}}(\xi - L)) = (U_{\mathrm{p}}(L - \xi), V_{\mathrm{p}}(L - \xi))$$

by the $2L$-periodicity of $(U_{\mathrm{p}}(\xi; L), V_{\mathrm{p}}(\xi; L))$. Hence, $(U_{\mathrm{p}}(\xi; L), V_{\mathrm{p}}(\xi; L))$, and thus $\mathcal{A}_{\mathrm{p}}(\xi; L)$ (2.3), is reflection symmetric with respect to all points $\xi = kL$, $k \in \mathbb{Z}$. Thus, system (2.2) is also reversible, that is, if $\phi(\xi)$ is a solution, then so is,

$$\hat{\phi}(\xi) = R\phi(-\xi) = (u(-\xi), -p(-\xi), v(-\xi), -q(-\xi))$$

(with involution $R : \mathbb{R}^4 \to \mathbb{R}^4$). Now, if λ is a γ-eigenvalue, and $\phi(\xi)$ its associated γ-eigenfunction, then (by (2.4)),

$$\hat{\phi}(\xi + 2L) = R\phi(-\xi - 2L) = \frac{1}{\gamma} R\phi(-\xi) = \overline{\gamma}\hat{\phi}(\xi),$$

since $\gamma \in \mathbb{S}^1$. In other words, $\hat{\phi}(\xi)$ is a $\overline{\gamma}$-eigenfunction (2.4), which implies that λ is both a γ- and a $\overline{\gamma}$-eigenvalue. Hence, as γ is varied over $\mathbb{S}^1$, every point $\lambda(\gamma) \in \Lambda(L; \vec{\mu})$ is visited twice, except for the points $\lambda(\pm 1)$ since $\gamma = \overline{\gamma}$ for $\gamma = \pm 1$: the loop $\Lambda(L; \vec{\mu})$ collapses to a branch with endpoints $\partial_{\pm}\Lambda(L; \vec{\mu}) = \lambda(\pm 1)$

If a branch $\Lambda(L; \vec{\mu})$ crosses through the imaginary axis as a function of $\vec{\mu}$, it is very likely that one of the endpoints $\partial_{\pm}\Lambda(L; \vec{\mu})$ is the first point of $\Lambda(L; \vec{\mu})$ to make contact with the imaginary axis. Indeed, if this occurs, it is robust under perturbations. However, note that this is not necessary: $\Lambda(L; \vec{\mu}) \subset \mathbb{C}$ is in general curved, so $\Lambda(L; \vec{\mu})$ may be tangent to the imaginary axis at its point $\lambda(\gamma)$ of first contact, i.e. $\lambda(\gamma)$ may certainly be an interior point with $\gamma \neq \pm 1$. Even when $\Lambda(L; \vec{\mu}) \subset \mathbb{R}$, the possibility that $\Lambda(L; \vec{\mu})$ is folded cannot be excluded, so that the first point of contact of $\Lambda(L; \vec{\mu})$ with the imaginary axis is not necessarily an endpoint $\partial_{\pm}\Lambda(L; \vec{\mu})$, but possibly an interior point at the fold. Nevertheless, it can be expected that the ± 1-eigenvalues do play a dominant role in the stability and bifurcation analysis of reversible periodic patterns $(U_{\mathrm{p}}(\xi; L), V_{\mathrm{p}}(\xi; L))$. And thus, the bifurcations associated to these eigenvalues can be expected to turn up abundantly in the study of Busse balloons B_B.

We therefore define $\mu_{\pm}$ as the following critical value of μ, where μ represents one of the m components of $\vec{\mu}$: $\mathrm{Re}[\sigma(U_{\mathrm{p}}, V_{\mathrm{p}})] < 0$ for $\mu < \mu_{\pm}$, $\mathrm{Re}[\sigma(U_{\mathrm{p}}, V_{\mathrm{p}})] = 0$ only for a $\partial_{\pm}\Lambda(L; \vec{\mu}) \in \sigma(U_{\mathrm{p}}, V_{\mathrm{p}})$ at $\mu = \mu_{\pm}$ and $\mathrm{Re}[\partial_{\pm}\Lambda(L; \vec{\mu})] > 0$ for $\mu > \mu_{\pm}$ (this situation occurs in the Gray-Scott system, §4.3, and in the normal form model (1.4), §4.5). A priori, we need to distinguish between two cases: $\mathrm{Im}[\partial_{\pm}\Lambda(L; \mu = \mu_{\pm})] = 0$ and $\mathrm{Im}[\partial_{\pm}\Lambda(L; \mu = \mu_{\pm})] \neq 0$. However, in this chapter we focus on the latter case. We

refer to [68] for an example at which $\partial_-\Lambda(L; \mu_j = \mu_\pm) \in \mathbb{R}$ initiates a saddle node bifurcation.

The $+1$-eigenfunction $\phi(\xi; \lambda(+1))$ associated to $\partial_+\Lambda(L; \mu = \mu_+)$ is $2L$-periodic (by (2.4)). Since $\partial_+\Lambda(L; \mu = \mu_+)$ induces a Hopf instability if $\text{Im}[\partial_+\Lambda(L; \mu = \mu_+)] \neq 0$ [71], this means that the destabilization at $\mu = \mu_+$ initiates an oscillation at which all extrema of the pattern $(U_\text{p}(\xi; L), V_\text{p}(\xi; L))$ move in phase. Note that description is only based on linear data, without further analysis it is not possible to extract information about the nonlinear, long-time, behavior beyond the bifurcation. Nevertheless, this linear prediction agrees with the (subcritical) Hopf bifurcation destabilization of $+1$-type most commonly encountered in simulations of the Gray-Scott and (classical) Gierer-Meinhardt equations, see [16, 43, 44, 48, 49, 56, 58, 68, 97].

If $\gamma = -1$, i.e. if $\partial_-\Lambda(L; \mu = \mu_-) \notin \mathbb{R}$ initiates the bifurcation, the linear dynamics are driven by a -1-eigenfunction $\phi(\xi; \lambda(-1))$ that is periodic with a doubled period $4L$,

$$\phi(\xi + 4L; \lambda(-1)) = -\phi(\xi + 2L; \lambda(-1)) = \phi(\xi; \lambda(-1))$$

(2.4). Thus, the Hopf instability driven by $\partial_-\Lambda(L; \mu = \mu_-) \notin \mathbb{R}$ induces an out of phase oscillation when the pattern $(U_\text{p}(\xi; L), V_\text{p}(\xi; L))$ destabilizes: the initial (linear) dynamics of (1.2) on an interval $(\xi_0, \xi_0 + 2L)$ are opposite to those on the neighboring intervals $(\xi_0 - 2L, \xi_0)$ and $(\xi_0 + 2L, \xi_0 + 4L)$, and identical to the dynamics on the intervals that are at a distance of $4Lk$, $k \in \mathbb{Z}$. We are not aware of any simulations in the literature on Gray-Scott or Gierer-Meinhardt type models that exhibit this type of behavior near a Hopf bifurcation, see however sections §4.3 and §4.5.

In this chapter, we will denote the locus if instability induced by $\partial_\pm\Lambda(L; \mu = \mu_\pm) \notin \mathbb{R}$ by the manifolds $\mathcal{H}_{\pm 1} \subset \partial B_B$ in the $(\vec{\mu}, k)$-space.

4.2.3 An Evans function approach

It is well-known that the spectrum associated to spatially periodic patterns can be studied by an Evans function [32, 35, 36, 64, 68]. Here we sketch the construction of such an Evans function based on [35, 36]. First, we consider a fundamental (matrix) solution $\Phi(\xi; \lambda)$ of (2.2) and define its associated monodromy matrix $\mathcal{M}_L(\lambda)$ by

$$\Phi(\xi + 2L; \lambda) = \Phi(\xi; \lambda)\mathcal{M}_L(\lambda). \tag{2.6}$$

Note that the existence of the (constant coefficients) matrix $\mathcal{M}_L(\lambda)$ follows from the fact $\mathcal{A}_\text{p}(\xi; \lambda, L)$ is $2L$-periodic (2.3), so that $\Phi(\xi + 2L; \lambda)$ also is a fundamental matrix solution of (2.2). Now, let $\vec{v} \in \mathbb{C}^4$ be an eigenvector of $\mathcal{M}_L(\lambda)$ with eigenvalue $\rho \in \mathbb{C}$, and define the solution $\phi(\xi)$ of (2.2) by $\phi(\xi; \lambda) = \Phi(\xi; \lambda)\vec{v}$, then

$$\phi(\xi + 2L) = \Phi(\xi + 2L)\vec{v} = \Phi(\xi)\mathcal{M}_L\vec{v} = \Phi(\xi)\rho\vec{v} = \rho\Phi(\xi)\vec{v} = \rho\phi(\xi).$$

Thus, $\phi(\xi)$ is a ρ-eigenfunction (2.4), and it follows that λ is a γ-eigenvalue if and only if $\mathcal{M}_L(\lambda)$ has an eigenvalue $\rho = \gamma \in \mathbb{S}^1$. Therefore, we define the Evans function

$\mathcal{D}(\lambda, \gamma; L)$ associated to the stability problem (2.2) by

$$\mathcal{D}(\lambda, \gamma; L) = \ \det\left[\mathcal{M}_L(\lambda) - \gamma \operatorname{Id}\right], \ \lambda \in \mathbb{C}, \gamma \in \mathbb{S}^1. \tag{2.7}$$

Hence, $\lambda(\gamma)$-eigenvalues correspond to zeroes of $\mathcal{D}(\lambda, \gamma)$. It is straightforward to check that these zeroes do not depend on the choice of the fundamental matrix solution $\Phi(\xi; \lambda)$. Nevertheless, the precise choice of $\Phi(\xi; \lambda)$ can be crucial: in the case of singularly perturbed systems, it is possible to construct a $\Phi(\xi; \lambda)$ so that the zeroes of $\mathcal{D}(\lambda, \gamma; L)$ can be determined analytically – see [32, 68] and §4.4.2.

4.3   A Busse balloon for the Gray-Scott model

In this section we discuss details of the (construction of the) Busse balloon, and the larger existences balloon, for the Gray-Scott model (1.1) as presented in Figure 4.2(a). The Busse balloon consists of stationary spatially periodic solutions of the 4-dimensional (spatial) dynamical system associated to (1.1). These spatial patterns correspond to periodic solutions of this 4-dimensional system with period, or wavelength, L ($k = 2\pi/L$ with $k =$ the wavenumber of the patterns). In all numerical computations we used the software AUTO [10] and fixed B at 0.26, ε^4 at 0.001, which means $\varepsilon \approx 0.18$, and varied A and L or equivalently k. In §4.3.5 we will bring equation (1.1) into a form that's comparable to the normal form model (1.4) and discuss the similarities/differences between the models.

4.3.1   Existence region

Before describing the Busse balloon, we discuss several aspects of the existence region in which the Busse balloon is embedded. As a consequence of the reversible symmetry discussed in §4.2.2, the 4-dimensional ODE reduction of (1.1) is also reversible and we can thus apply the 'reversible Lyapunov center theorem' [9]. This theorem guarantees the existence of reversible periodic orbits, or: spatially periodic patterns, in the vicinity of an equilibrium, i.e. of a homogeneous background state $(U, V) \equiv (\bar{U}, \bar{V})$ of (1.1). To apply the theorem, we first define ν_j, $j = 1, ..., 4$, as the eigenvalues associated to the linearization around an equilibrium – note that this linearization corresponds to (2.1) with $\lambda = 0$ and $(U_{\mathrm{p}}, V_{\mathrm{p}}) \equiv (\bar{U}, \bar{V})$. By the symmetry, the set of eigenvalues ν_j is reflection symmetric about the real *and* imaginary axes – see Figure 4.3. The center theorem can be applied if $\nu_j = i\eta$, $\eta > 0$, for some j – see Remark 3.1 – and if all such modes are non-resonant. It states that there exists, within the 4-dimensional phase space, a two-dimensional manifold containing the equilibrium which is fibered by periodic orbits whose wavenumbers converges to η as one approaches the equilibrium. Since $i\eta$ is a purely imaginary spatial eigenvalue, η corresponds to a wave number k, we therefore refer to η as a linear wavenumber.

By the Lyapunov center theorem, a natural starting point for finding symmetric stationary spatially patterns is an unstable (Remark 3.1) background state. The
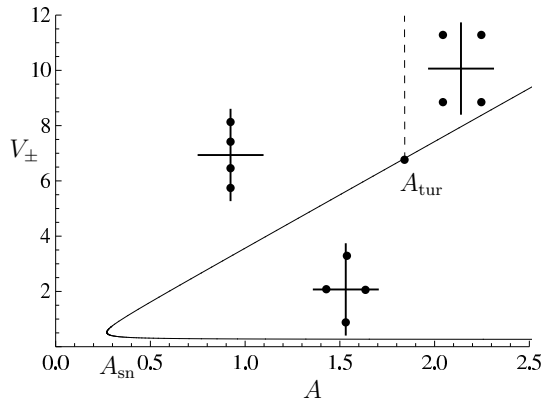
Figure 4.3: The branches $V_\pm$ as function of A of the background states $(U_\pm, V_\pm)$ of (1.1). The insets are sketches of the three qualitatively different distributions of the associated eigenvalues $\nu_j \in \mathbb{C}$, $j = 1, \ldots, 4$, one for the lower branch V_-, and two for the upper branch V_+ (one to the left and one to the right of the Turing instability).

background states of (1.1) are

$$U_0 = 1, V_0 = 0, \quad U_\pm = \frac{1}{2A}\left(A \mp \sqrt{A^2 - 4AB^2}\right), V_\pm = \frac{1}{2B}\left(A \pm \sqrt{A^2 - 4AB^2}\right),$$

where the conjugate pair $(U_\pm, V_\pm)$ undergoes a fold, or saddle node, bifurcation at A_{sn} determined by the condition $A = 4B^2$ (i.e. $A_{\mathrm{sn}} = 0.2704$ here). Thus, three real solutions exist for $A > A_{\mathrm{sn}}$. It can be checked that (U_0, U_0) is stable for all parameter values, that (U_-, U_-) is always unstable, and that (U_+, V_+) becomes stable through a Turing bifurcation for increasing A at A_{tur} (≈ 1.87 for the parameter values chosen here). We refer to [56] for more (analytical and computational) details on the Turing/Ginzburg-Landau bifurcation in the Gray-Scott model. Within the 4-dimensional ODE reduction, the Turing bifurcation corresponds to the 1 : 1 reversible Hopf bifurcation, see Figure 4.3.

Thus, by the Lyapunov center theorem, and by Figure 4.3, two one-parameter families of small amplitude periodic patterns emerge near the equilibrium (U_+, V_+) for each $A \in (A_{\mathrm{sn}}, A_{\mathrm{tur}})$, one for each (non-resonant) pair of linear wavenumbers η. We denote the positive linear wavenumbers by $\eta_\pm(A)$ ordered so that $\eta_+ > \eta_-$. At the fold point $A = A_{\mathrm{sn}}$, we have $\eta_- = 0$ and the corresponding eigenvalue becomes real when continuing along the (U_-, V_-)-branch. At the Turing bifurcation, $\eta_- = \eta_+$, and the eigenvalues move off the imaginary axis when increasing A. A single one-parameter family emerges near (U_-, V_-), but these turn out to be of no interest to us.

In the (A, k)-parameter plane, the curves $\eta_\pm(A)$ provide part of the boundary of the existence region of periodic patterns. We denote these curves in Figure 4.2(a) by

'equilibrium'. The aforementioned two one-parameter families of periodic patterns bifurcate off $\eta_\pm(A)$, respectively, so that periodic patterns exist for $k < \eta_+$ and $k > \eta_-$. In fact, numerically we find that the two families are connected so that the patterns exist for $k \in (\eta_-, \eta_+)$ and $A \in (A_{sn}, A_{tur})$. Near the Turing bifurcation this is the well-known parabola shaped 'Ginzburg-Landau existence region' – see section §4.3.2 and [56].

At $A = A_{sn}$ and $k = \eta_+(A_{sn})$, the boundary has a corner and continues as a curve of folds, or saddle node bifurcations, of periodic orbits, denoted by 'sn$_1$'. While it is entirely expected that the fold of the underlying equilibrium induces a fold of the periodic solutions, we are not aware of any reference for a rigorous proof in the literature. The relevant existence boundary emerging from η_- when decreasing A from A_{tur} is slightly more involved. Between A_{tur} and $A \approx 1.3$, it involves period doubling bifurcations, but we omit details of this here as it lies outside the stability region (i.e. the Busse balloon). For smaller values of A, the relevant boundary is the fold curve 'sn$_2$'.

Remark 3.1 The assumption that $\nu_j(0) \in i\mathbb{R}$ implies that $\lambda = 0$ lies in the spectrum associated to the background state $(\bar{U}, \bar{V})$ as solution of the PDE (1.2) – see section §4.2.1. Perturbing the real part of λ away from zero, typically implies that such purely imaginary solutions persist with an adjusted linear wavenumber. Conversely, we locally find a curve $\lambda(\eta)$ transversely crossing the imaginary axis. It thus follows that under the conditions of the Lyapunov center theorem, the underlying equilibrium is typically *unstable* as a solution of the PDE.

4.3.2   The Busse balloon

We continue the discussion of Figure 4.2(a), now looking at the stability boundaries, i.e. at the Busse balloon. Near the Turing instability we find the expected parabola shaped Eckhaus stability region bounded by sideband instabilities. Note that the existence and (side band) type of these boundaries has been proved rigorously near the Turing bifurcation by the Ginzburg-Landau analysis presented in [56]. Here, we extended these curves beyond the (asymptotically small) Ginzburg-Landau region, using the method described in [70]. A priori these sideband curves are only sufficient for establishes instability, since other instabilities could occur beyond the Ginzburg-Landau setting. However, we checked that this does not happen by finite difference approximations of the spectrum at regular intervals along the curves. In addition, there may in principle be an isolated region of unstable periodic patterns in the interior of the Busse balloon, but this is not the case, at least on the grid where we checked.

For decreasing values of k, the lower branch of sideband instabilities hugs very close to the fold curve 'sn$_2$', until it appears to merge with it. It should be noted that it is in this region in parameter space, and in particular for parameters that cross the curve 'sn$_2$' beyond the point where it has merged with the sideband curve, that the PDE dynamics exhibit the well-known and well-studied (but still largely not understood)
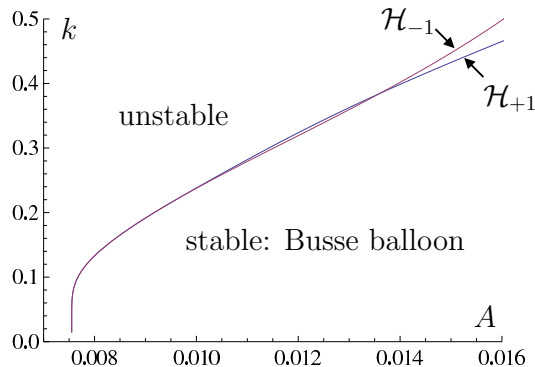
Figure 4.4: The $\mathcal{H}_\pm$ Hopf instabilities near the long wavelength limit of the Busse balloon; compare to Figure 4.2(a).

phenomenon of self-replicating pulses, see [23, 48, 57, 62, 66, 67, 73].

The upper branch of sideband instabilities similarly merges with the fold curve 'sn$_1$', however the sideband curve is no longer the stability boundary here. Instead, at $A \approx 0.041$, a curve $\mathcal{H}_{+1}$ of Hopf instabilities crosses the sideband curve – which generates a co-dimension 2 corner – and becomes the stability boundary. Following this curve for decreasing values of A we find another corner when a second curve, $\mathcal{H}_{-1}$, of Hopf instabilities crosses the first and takes over the stability boundary. These two curves repeatedly intersect and generate a sequence of corners in the stability boundary, see Figure 4.4. This is the generic Hopf dance destabilization mechanism that is the central theme of this manuscript. We discuss more details in the next subsection.

We continued the Hopf curves numerically up to $k = 0.01$ and observe a near vertical tangency, so that we predict the limiting value to be $A \approx 0.00755$. Since $\varepsilon \approx 0.18$ is not very small, this compares reasonably well to the predicted value for $\varepsilon \to 0$ of $A \approx 0.0049$ which we compute (analytically) from the results in [16, 18].

4.3.3 The Hopf dance and the rotation of the spectrum

The $\mathcal{H}_{\pm 1}$ curves can locally be seen as graphs of functions $A_\pm(k)$ over the k-axis (Figure 4.4). In Figure 4.5(a), we plot the difference $A_+(k) - A_-(k)$ over the first two crossings of $\mathcal{H}_{\pm 1}$. We plot this same difference for a larger interval of k values in Figure 4.5(b), where we have also blown up the difference by an ad hoc guess for an exponential decay factor (and where we have switched to $L = 2\pi/k$ for convenience). The result is a sinusoidal curve and we conjecture that this is the first part of an infinite 'Hopf dance' as L increases. Note that this sinusoidal shape and exponential decay of the parameter as function of the wavelength L is confirmed by the analysis of the normal form model in section §4.5.1 (see especially Corollary 5.5).
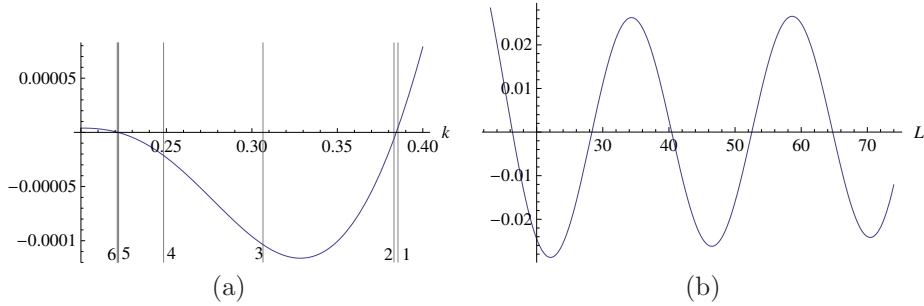
Figure 4.5: (a) The difference $A_+(k) - A_-(k)$ for k values including the first two crossing points of the curves $\mathcal{H}_{\pm 1}$. The vertical lines and their labels correspond to the k-values and the labels of the curves plotted in Figure 4.6. (b) The blown up difference $(A_+(L) - A_-(L)) \exp(0.27L)$ over more intersections of $\mathcal{H}_\pm$.

Each point $(A_\pm(k), k)$ corresponds to a critical intersection of the spectrum $\sigma(U_\mathrm{p}, V_\mathrm{p})$ associated to a spatially periodic pattern $(U_\mathrm{p}, V_\mathrm{p})$ with the imaginary axis. As discussed in §4.2.1, this means that there are γ-eigenvalues $\lambda(\gamma_\pm) \in i\mathbb{R}$ such that $\mathrm{Re}(\partial_\gamma \lambda(\gamma_\pm)) = 0$. It turns out that both spectral curves stem from the continuation of the same curve $\Lambda(L)$ and that this is the spectral curve, denoted by $\Lambda_\mathrm{h}(L)$, that shrinks to the (discrete) eigenvalue $\lambda_h \in \mathbb{C}$ associated to the homoclinic pulse that appears in the limit $L \to \infty$ (or $k \downarrow 0$); $\Lambda_\mathrm{h}(L)$ is – by definition – parametrized by $\lambda_\mathrm{Ho}(\gamma; A, k$ or $L)$ (see (2.5)). Moreover, we find that $\gamma_+ \equiv +1$ and $\gamma_- \equiv -1$ for all k, which at least locally is not surprising, since $\gamma = +1$ and $\gamma = -1$ represent the endpoints of the bounded curve $\Lambda_\mathrm{h}(L)$ (section §4.2.2), see Figure 4.6. However, the fact that $\gamma_\pm$ are globally constant is a more subtle issue that is related to the periodicity of the curvature of $\Lambda_\mathrm{h}(L; \mu)$, i.e. to the 'belly dance'.

In Figure 4.6 we plot the spectral curves $\Lambda_\mathrm{h}(L) = \{\lambda_\mathrm{Ho}(\gamma, k) : \gamma \in \mathbb{S}^1\}$ for the six values of k marked by the vertical lines in Figure 4.5(a). We also indicate the '+1' endpoints, i.e, $\lambda_\mathrm{Ho}(+1, k)$. Curve 1 of Figure 4.6 touches the imaginary axis at $\gamma = +1$ for the k value slightly above the first crossing of the two Hopf curves. Curve 2 is slightly below this value of k and here the '+1' end lies in the open left half plane while $\lambda_\mathrm{Ho}^+(-1, k)$ touches the imaginary axis. Comparing curves 1 and 2 we notice an overall counter-clockwise rotation. This rotation continues as k is decreased further, and at the same time the curve of spectrum straightens while decreasing in length, see curves 3 and 4. Curves 5 and 6 are already very small, and hence magnified in the inset. Note that curve 6 is similar to curve 1 only the linear wavenumbers $\gamma = \pm 1$ of the endpoints are interchanged. Up to this change, the picture for the next two intersections is qualitatively the same. In particular, the curvature of $\lambda_\mathrm{Ho}^+(\gamma, k)$ changes sign so that most unstable point of this part of the spectrum is either $\lambda_\mathrm{Ho}^+(+1, k)$ or $\lambda_\mathrm{Ho}^+(-1, k)$. We corroborated this by computing the curve in the (A, k)-parameter plane for which $\lambda_\mathrm{Ho}(i, A, k) \in i\mathbb{R}$, that is, where a representative point inside the
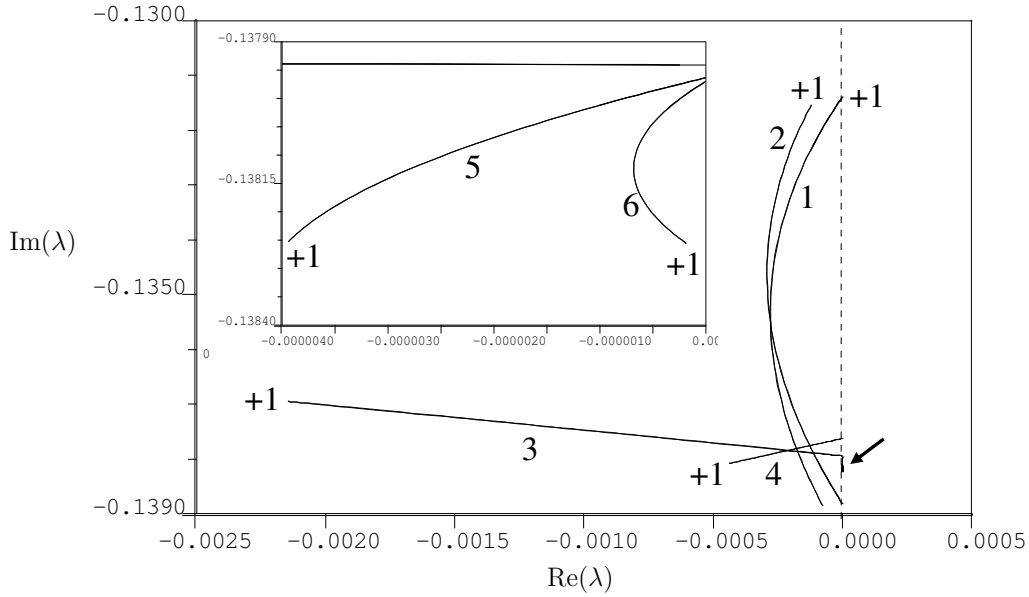
Figure 4.6: The spectral curves $\lambda_{\mathrm{Ho}}(\gamma, k)$, with '+1' denoting $\lambda_{\mathrm{Ho}}(+1, k)$, for the six values of k marked in Figure 4.5(a) using the same labels. The inset enlarges the region near the arrow head.

'belly' of the curve of spectrum lies on the imaginary axis. We find that for given k it has $A \leq \max(A_\pm(k))$ so that it always lies in the unstable region. We discuss more details of this belly dance in the next subsection.

4.3.4 The belly dance

As mentioned several times before, the fact that the $\mathcal{H}_{\pm 1}$ curves always yield the entire stability boundary is related to the change in curvature of the critical branch of spectral curve associated to the Hopf destabilization. Instead of investigating this along the stability boundary, we consider here A fixed at 0.01 and compare $\lambda_{\mathrm{Ho}}(\gamma, 0.01, k)$ for $\gamma \in \{+1, \mathrm{i}, -1\}$ as k decreases. For convenience we denote

$$\lambda_*(\gamma, L) := \lambda_{\mathrm{Ho}}^+(\gamma, 0.01, 2\pi/L).$$

We observe the same rotation and geometry as in Figure 4.6, but this choice of curve simplifies some of the computations. In Figure 4.7(a), we plot the two curves

$$\mathrm{Re}(\lambda_*(+1, L) - \lambda_*(-1, L))\exp(0.253L), \quad \mathrm{Re}(\lambda_*(\mathrm{i}, L) - \lambda_*(-1, L))\exp(0.253L), \tag{3.1}$$

in blue and red, respectively. We obtain a periodic graph up to an exponential factor, and infer that $\lambda_*(\mathrm{i}, L)$ is always more stable than either $\lambda_*(+1, L)$ or $\lambda_*(-1, L)$. This
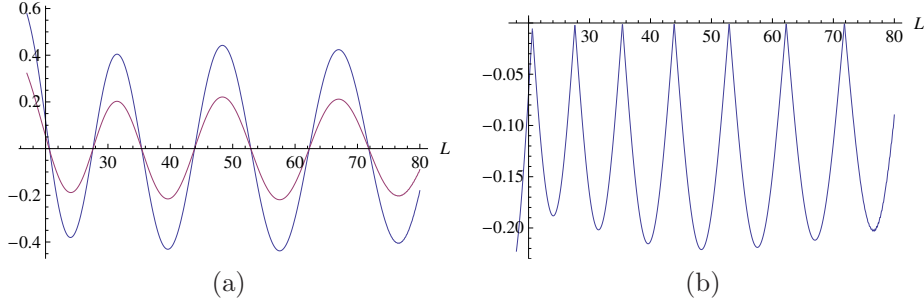
Figure 4.7: (a) Plot of the two graphs of (3.1); the first in blue, the second in red. (b) Plot of the graph of (3.2).

is further illustrated in Figure 4.7(b) where we plot

$$(\mathrm{Re}(\lambda_*(i, L) - \max\{\mathrm{Re}(\lambda_*(\gamma, L)) : \gamma = \pm 1\}) \exp(0.253L), \qquad (3.2)$$

which clearly always is negative. Geometrically, the line connecting $\lambda_*(+1, L)$ with $\lambda_*(-1, L)$, i.e. the leading order approximation of the entire spectral curve, is vertical at the roots of the blue curve in Figure 4.7(a). This occurs at every half-cycle of the rotation of the curve of spectrum as considered in Figure 4.6. Figure 4.7(b) establishes that at these values of L the point $\lambda_*(\mathrm{i}, L)$ lies to the left of this line in the complex plane. In other words, the belly of the spectral curves always points into the stable half plane. In fact, this also implies that the belly oscillates with twice the frequency of the rotation of the spectral curve (which can also checked directly from the numerical data). These numerical findings are all once more confirmed by the analysis of the normal form model presented in section §4.5.2 and especially in Figure 4.9.

4.3.5   Relation to the literature and to the normal form

In order to relate the computations presented in this section to the analytical literature on the Gray-Scott model (see for instance [16, 18, 48, 49, 56, 58]), we first need to decide upon the asymptotic magnitudes of parameters A and B with respect to ε. Since $\varepsilon^4 = 0.001$, i.e. $\varepsilon \approx 0.18$, and $B = 0.26$, it is natural to set $B = b\varepsilon$ with $b \approx 1.46$. An overlap between our computations and the analytical literature is formed by the (de)stabilization of homoclinic and nearly-homoclinic patterns, i.e. patterns with $k = 0$, or close to 0. Since the curve sn_2 represents the onset of pulse self-replication, see §4.3.1, which is known to be (just) outside the region of asymptotic analysis [16, 48, 57], we need to focus on the curves sn_1 and $\mathcal{H}_{\pm 1}$ in the (inset of) Figure 4.2(a) near $k = 0$. Since $\varepsilon^4 = 0.001$, it is thus natural to scale A as $a\varepsilon^4$.

As for the general model (1.5), the pulses in the Gray-Scott model do not have a $\mathcal{O}(1)$ amplitude. Following [16, 18], and as we did in §4.1.2, we scale U and V in (1.1), $\tilde{U} = U/(\varepsilon\sqrt{\varepsilon})$, $\tilde{V}(x,t) = \sqrt{\varepsilon}V$. Moreover, we introduce $\tilde{t} = \varepsilon$ and $\tilde{x} = x/\sqrt{\varepsilon}$

and obtain (after dropping all tildes),

$$
\begin{cases}
\varepsilon^2 U_t = U_{xx} - a\varepsilon^3\sqrt{\varepsilon}(1 - \varepsilon\sqrt{\varepsilon}U) - UV^2 \\
V_t = \varepsilon^2 V_{xx} - bV + UV^2
\end{cases}.
\tag{3.3}
$$

This version of the Gray-Scott model is very similar to (1.4) and therefore suitable to explain the differences between the Gray-Scott model in the parameter range considered here and the normal form model. Of course, an a priori important difference is the fact that the background state in (1.1) or (3.3) is not $(U(x,t), V(x,t)) \equiv (0,0)$. This is – however – not significant. The fact that the slow component does not remain $\mathcal{O}(1)$ in between two 'fast' V-pulses is much more relevant: in (3.3) it varies from being $\mathcal{O}(1)$ near a fast pulse to $\mathcal{O}(1/(\varepsilon\sqrt{\varepsilon}))$ in between two fast pulses (hence the scaling of $\tilde{U}$). Moreover, the linear term in the U-equation is not of $\mathcal{O}(\varepsilon^2)$, but smaller, $\mathcal{O}(\varepsilon^3\sqrt{\varepsilon})$.

Together, these two differences between (3.3) and (1.4) have as effect that the distance between two successive fast V-pulses is much longer in (3.3) than in (1.4). In (1.4), $U_{xx} = \varepsilon^2 U$ between two fast (stationary) pulses (V is exponentially small). Since the total variation in U is $\mathcal{O}(1)$, this implies that the natural wavelength of periodic patterns is $\mathcal{O}(1/\varepsilon)$ – i.e. $\mathcal{O}(1/\varepsilon^2)$ in the fast spatial scale ξ, see §4.4 and especially Theorem 4.1. In contrast, in the normalized Gray-Scott model (3.3), $U_{xx} = \varepsilon^{7/2}U$ to leading order, while the variation in U must be $\mathcal{O}(\varepsilon^{-3/2})$, hence the wavelength is of a periodic pattern in (3.3) is $\mathcal{O}(\varepsilon^{-5/2}) \gg O(\varepsilon^{-1})$.

Thus, the Gray-Scott model (3.3) is singular in the sense that the wavelength of 'typical' periodic patterns is much larger than in the 'normal' case (1.4). As a consequence, the length of the spectral branches Λ associated to the stability of the periodic patterns is much smaller than in the normal case, see §4.4 and §4.5. In fact, the branches Λ_h, i.e. the ones that are responsible for the Hopf dance (§4.5), are not of $\mathcal{O}(1)$ (as is the case for (1.4)), but asymptotically small in ε. In the Evans function approach to the stability of singular spatially periodic patterns developed in [68], the effect of the higher order corrections has been proved to be asymptotically small, and thus no attention has been paid to the higher order terms. However, this means that in the context of the 'singular' Gray-Scott model (3.3), the approach of [68] only gives the leading order position of the branch Λ_h as a point (a point that was already determined by the formal analysis presented in [16]). Thus, the leading order methods of [68] do not give any information on the geometry of the spectral branch Λ_h for the 'singular' Gray-Scott system, contrary to the 'normal' system (1.4) in which both the Hopf dance and the belly dance can be deduced analytically from the general frame work developed in [68].

The fact that the singular Gray-Scott system nevertheless exhibits the same Hopf dance behavior as the normal form model is another strong indication that the Hopf dance, i.e. snaking of the two Hopf bifurcation curves $\mathcal{H}_{\pm 1}$ near the homoclinic tip of a Busse balloon, indeed is a very robust phenomenon.

Remark 3.2 We refer to [16, 56, 48, 49] for analytical results on the existence and stability of spatially periodic patterns in the Gray-Scott model and their relations with explicit numerical simulations.

4.4   Preliminaries II: Periodic patterns in the normal form model (1.4)

In this section, we formulate the results on the existence and stability of a (class of) periodic pattern solutions to (1.4) that have originally been obtained in [22] and [68].

4.4.1   The existence of periodic pulse patterns

Stationary spatially periodic patterns in (1.4) correspond to periodic solutions in the 4-dimensional system,

$$\begin{cases} \dot{u} & = & \varepsilon p \\ \dot{p} & = & -\varepsilon u^{\alpha_1} v^{\beta_1} + \varepsilon^3 \mu u \\ \dot{v} & = & q \\ \dot{q} & = & v - u^{\alpha_2} v^{\beta_2} \end{cases} \tag{4.1}$$

where the dot denotes the derivative with respect to the fast spatial coordinate $\xi = x/\varepsilon$. The fast reduced limit,

$$u = \bar{u}, \ p = \bar{p}, \ \ddot{v} = v - \bar{u}^{\alpha_2} v^{\beta_2},$$

has the homoclinic solution,

$$v_{\mathrm{h}}^{r}(\xi; \bar{u}) = \bar{u}^{-\frac{\alpha_2}{\beta_2-1}} w_{\mathrm{h}}^{r}(\xi) \ \text{ with } \ w_{\mathrm{h}}^{r}(\xi) = \left(\frac{\beta_2+1}{2}\right)^{\frac{1}{\beta_2-1}} \left(\operatorname{sech}\left(\frac{1}{2}(\beta_2-1)\xi\right)\right)^{\frac{2}{\beta_2-1}}. \tag{4.2}$$

For large ξ, v and $q = \dot{v}$ are exponentially small. In that case, the (spatial) dynamics are driven by the (linear) slow reduced system,

$$v = q = 0, \ \ddot{u} = \varepsilon^4 \mu u. \tag{4.3}$$

We can now state the main existence theorem, where we introduce the parameter $\ell = \varepsilon^2 L$.

Theorem 4.1 [22] *Let $\mu, \alpha_1, \alpha_2, \beta_1, \beta_2$ satisfy (1.8). Then, there is an $\varepsilon_0 > 0$ such that for all $0 < \varepsilon < \varepsilon_0$, (4.1) possesses a family of periodic orbits $\gamma_{\mathrm{p}}(\xi; L)$ parametrized by their wavelength $L \stackrel{\text{def}}{=} 2\ell/\varepsilon^2$, with*

$$\ell \in [\ell_{\mathrm{sn}}, \infty) \ \text{ and } \ \ell_{\mathrm{sn}} = \frac{1}{\sqrt{\mu}} \operatorname{arccosh} \sqrt{\frac{\beta_2 - 1 + d}{d}} + \mathcal{O}(\varepsilon)$$

(1.7), (1.8).   The solutions $\gamma_{\mathrm{p}}(\xi; L)$ have positive u_{p}- and v_{p}-coordinates and two internal reflection symmetry points at distance $L = 2\ell/\varepsilon^2$ apart (in ξ) at which $p_{\mathrm{p}} =$

$q_{\mathrm{p}} = 0$. *They consist of a slow pieces on which $\gamma_{\mathrm{p}}(\xi; L)$ is exponentially close to a* cosh-*type solution of (4.3), alternated by fast parts in which $\gamma_{\mathrm{p}}(\xi; L)$ is $\mathcal{O}(\varepsilon)$ close to* $(\bar{u}_{\ell}, 0, v_{\mathrm{h}}^r(\xi; \bar{u}_{\ell}), \dot{v}_{\mathrm{h}}^r(\xi; \bar{u}_{\ell}))$ *(4.2), with*

$$\bar{u}_{\ell} = (2\sqrt{\mu}\tanh\sqrt{\mu}\ell)^{\frac{\beta_2-1}{d}} \left(\int_{-\infty}^{\infty} (w_{\mathrm{h}}^r(\xi))^{\beta_1} d\xi\right)^{-\frac{\beta_2-1}{d}}.$$

In the limit $\ell \to \infty$, $\gamma_{\mathrm{p}}(\xi; L)$ merges with the solution $\gamma_{\mathrm{h}}(\xi)$ that is homoclinic to $(0, 0, 0, 0)$; $\gamma_{\mathrm{p}}(\xi; L)$ *undergoes a saddle node bifurcation at $\ell = \ell_{\mathrm{sn}}$.*

The orbits $\gamma_{\mathrm{p}}(\xi; L)$ correspond to a family of stationary, symmetric, spatially periodic patterns $(U_{\mathrm{p}}(\xi; L), V_{\mathrm{p}}(\xi; L))$ in (1.4) parametrized by their wavelength L.

This theorem is proved in [22] by the methods of geometric singular perturbation theory. It should be noted that there are many more families of periodic patterns in (1.4), see [22]. The patterns $(U_{\mathrm{p}}(\xi; L), V_{\mathrm{p}}(\xi; L))$ described here correspond to the A-type patterns studied in [68] and are the only periodic patterns among those constructed in [22] that may be stable as solutions of (1.4) [68]. Except for the obvious fact that the slow cosh-type U-pieces have their minimums (and not their maximums) in between two successive fast V-pulses, the $(U_{\mathrm{p}}(\xi; L), V_{\mathrm{p}}(\xi; L))$-patterns are very similar to the Gray-Scott patterns presented in Figure 4.1.

4.4.2 Stability by the Evans function approach

The spectral stability analysis of the periodic patterns $(U_{\mathrm{p}}(\xi; L), V_{\mathrm{p}}(\xi; L))$ given by Theorem 4.1 completely follows the lines sketched in §4.2. Thus, the stability is determined by an Evans function $\mathcal{D}(\lambda, \gamma; L)$. Based on the direct linearization of (1.4) about the periodic pattern $(U_{\mathrm{p}}(\xi; L), V_{\mathrm{p}}(\xi; L))$ of Theorem 4.1 in the fast spatial coordinate ξ,

$$\begin{cases} u_{\xi\xi} = -\varepsilon^2 \left[\alpha_1 U_{\mathrm{p}}^{\alpha_1-1} V_{\mathrm{p}}^{\beta_1} u + \beta_1 U_{\mathrm{p}}^{\alpha_1} V_{\mathrm{p}}^{\beta_1-1} v\right] + \varepsilon^4 (\mu + \lambda) u \\ v_{\xi\xi} + \left[\beta_2 U_{\mathrm{p}}^{\alpha_2} V_{\mathrm{p}}^{\beta_2-1} - (1+\lambda)\right] v = -\alpha_2 U_{\mathrm{p}}^{\alpha_2-1} V_{\mathrm{p}}^{\beta_2} u \end{cases}, \qquad (4.4)$$

the spectral problem can be written in the form (2.2). As for the existence problem, a central role is played by the fast reduced limit problem associated to (4.4),

$$u \equiv \hat{u}, \quad v_{\xi\xi} + \left[\beta_2(w_{\mathrm{h}}^r(\xi))^{\beta_2-1} - (1+\lambda)\right] v = -\alpha_2 \hat{u}(\bar{u}_{\ell})^{-\frac{\alpha_2+\beta_2-1}{\beta_2-1}} (w_{\mathrm{h}}^r(\xi))^{\beta_2}, \qquad (4.5)$$

that is obtained by taking the limit $\varepsilon \to 0$ in (4.4) using (4.2) and Theorem 4.1. We denote

$$\mathcal{L}(\xi; \beta_2) = \beta_2(w_{\mathrm{h}}^r(\xi))^{\beta_2-1} - 1.$$

Since (4.4) is a linear problem, we can choose the value of $\hat{u}$ (by scaling). There are only two significant choices possible, $\hat{u} = 0$, or $\hat{u} = 1$. In the former case, (4.5) corresponds to the stability of the singular pulse solution $v_{\mathrm{h}}^r(\xi; \bar{u}_{\ell})$ (4.2) as solution to the scalar reduction of (1.4) in the fast field, $V_t = V_{\xi\xi} - V + \bar{u}_{\ell}^{\alpha_2} V_2^{\beta}$. This problem, $(\mathcal{L}(\xi; \beta_2) - \lambda)v = 0$, has essentially been solved in [17]: there are $J + 1$ eigenvalues

$\lambda_j^r = \lambda_j^r(\beta_2)$, $j = 0, ..., J$, with $\lambda_0^r = \frac{1}{4}(\beta_2 - 1)^2 - 1$, $\lambda_1^r \equiv 0$, $\lambda_j^r \in (-1, 0)$ for $j \geq 2$ and $\lambda_{j+1}^r < \lambda_j^r$. Moreover, the general solutions, and thus the eigenfunctions $v_j^r(\xi)$ for $\lambda = \lambda_j^r$, can be determined explicitly; there also is an explicit expression for $J = J(\beta_2)$ [17]. This also means that the Evans function associated to this problem, which we denote here in terms of a transmission function $t_f(\lambda)$, can be considered as a known expression [17].

If $\hat{u} \neq 0$, we scale it to 1 and introduce $w_{\text{in}}(\xi; \lambda)$ as the bounded solution of the inhomogeneous problem,

$$(\mathcal{L}(\xi; \beta_2) - \lambda)w = (w_{\text{h}}^r(\xi))^{\beta_2}, \tag{4.6}$$

which is obtained from (4.5) by an appropriate scaling of v. Note that $w_{\text{in}}(\xi; \lambda) = (\mathcal{L}(\xi; \beta_2) - \lambda)^{-1}(w_{\text{h}}^r(\xi))^{\beta_2}$ is uniquely determined for $\lambda \neq \lambda_j^r$ and can be computed explicitly (using the general solutions of the homogeneous problem [17]). Moreover, it is straightforward to show that $\mathcal{L}(\xi; \beta_2) - \lambda$ cannot be inverted for $\lambda = \lambda_j^r$, j even, and that $w_{\text{in}}(\xi; \lambda)$ exists, but is non-unique, if $\lambda \neq \lambda_j^r$ and j odd [17].

Finally, we need one additional ingredient to formulate the main result of [68] that describes the spectrum $\sigma((U_{\text{p}}, V_{\text{p}}))$ associated to the stability of the periodic patterns $(U_{\text{p}}(\xi; L), V_{\text{p}}(\xi; L))$ of Theorem 4.1: for $\delta > 0$, the region $\mathbb{C}_r \subset \mathbb{C}$ is defined by

$$\mathbb{C}_r(\delta) = \mathbb{C}\backslash\left\{\{\lambda \in \mathbb{C} : \text{Re}[\lambda] < \max(-1, -\mu) + \delta, |\text{Im}[\lambda]| < \delta\} \bigcup \{\cup_{j=0,...,J-1} B(\lambda_j^r, \delta)\}\right\}. \tag{4.7}$$

Thus, $\mathbb{C}_r$ is $\mathbb{C}$, except for δ-neighborhoods of the reduced eigenvalues λ_j^r and of $\{\lambda \in \mathbb{R} : \lambda < \max(-1, -\mu)\}$ – the spectrum associated to the stability of the trivial state $(0, 0)$ (and thus the essential spectrum of pulse type solutions of (1.4)).

Theorem 4.2 [68] *Let $\mu, \alpha_1, \alpha_2, \beta_1, \beta_2$ satisfy (1.8) and let $\ell > \ell_{\text{sn}}$. There is a $\delta_0 > 0$ and an $\varepsilon_0 = \varepsilon_0(\delta) > 0$ such that for all $0 < \delta < \delta_0$ and $0 < \varepsilon < \varepsilon_0(\delta)$, $\mathcal{D}(\lambda, \gamma; L) \neq 0$ for $\lambda \in \{\mathbb{C}\backslash\mathbb{C}_r\} \cap \{\text{Re}[\lambda] > 0\}$, i.e. there are no unstable γ-eigenvalues outside $\mathbb{C}_r$. For $\lambda \in \mathbb{C}_r$ (and $0 < \delta < \delta_0$, $0 < \varepsilon < \varepsilon(\delta)$), the Evans function $\mathcal{D}(\lambda, \gamma; L)$ associated to the spectral problem (2.2) for the patterns $(U_{\text{p}}(\xi; L), V_{\text{p}}(\xi; L))$ of Theorem 4.1 can be decomposed into a product of a 'fast' and a 'slow' Evans function,*

$$\mathcal{D}(\lambda, \gamma; L) = \mathcal{D}_f(\lambda, \gamma; L)\mathcal{D}_s(\lambda, \gamma; \ell), \quad \lambda \in \mathbb{C}_r, \gamma \in \mathbb{S}^1,$$

where,

$$\mathcal{D}_f(\lambda, \gamma; L) = -\gamma t_f(\lambda) e^{2L\sqrt{1+\lambda}}(1 + \mathcal{O}(\varepsilon)), \tag{4.8}$$

in which $t_f(\lambda)$ is the transmission function associated to the limit problem (4.5) with $\hat{u} = 0$, and,

$$\mathcal{D}_s(\lambda, \gamma; \ell) = \gamma\left[2\gamma_{\text{r}} - \left(\frac{1}{E(\lambda, \ell)}t_{11}(\lambda, \ell) + E(\lambda, \ell)t_{22}(\lambda, \ell) + \mathcal{O}(\varepsilon)\right)\right] \tag{4.9}$$

with $\gamma_{\text{r}} = \text{Re}[\gamma] \in [-1, 1]$,

$$E(\lambda, \ell; \mu) = e^{-2\ell\sqrt{\mu+\lambda}} \in \mathbb{C}, \tag{4.10}$$

and $\ell = \frac{1}{2}\varepsilon^2 L = \mathcal{O}(1)$ as in Theorem 4.1. Moreover,

$$t_{11}(\lambda, \ell; \mu) = 1 - \mathcal{S}(\lambda; \mu) \tanh \ell \sqrt{\mu}, \quad t_{22}(\lambda, \ell; \mu) = 1 + \mathcal{S}(\lambda; \mu) \tanh \ell \sqrt{\mu}, \quad (4.11)$$

with the analytic functions (for $\lambda \in \mathbb{C}_r$),

$$\mathcal{S}(\lambda; \mu) = \frac{\sqrt{\mu}}{\sqrt{\mu + \lambda}} \left[\alpha_1 - \alpha_2 \beta_1 \mathcal{R}(\lambda) \right], \quad (4.12)$$

and

$$\mathcal{R}(\lambda; \beta_1, \beta_2) = \left(\int_{-\infty}^{\infty} w_{\mathrm{in}}(\xi; \lambda)(w_{\mathrm{h}}^r(\xi))^{\beta_1 - 1} d\xi \right) \Big/ \left(\int_{-\infty}^{\infty} (w_{\mathrm{h}}^r(\xi))^{\beta_1} d\xi \right), \quad (4.13)$$

(4.2), (4.6), that can be computed explicitly [17].

The proof of this result is given in [68]. It is based on the NLEP method developed in [17] for the decomposition and explicit approximation of the Evans function associated to the stability of homoclinic patterns $(U_{\mathrm{h}}(\xi), V_{\mathrm{h}}(\xi))$ in (1.4) that appear as the limit for $L \to \infty$, i.e. $k \downarrow 0$, from the periodic patterns $(U_{\mathrm{p}}(\xi; L), V_{\mathrm{p}}(\xi; L))$ (Theorem 4.1).

Note that $t_f(\lambda) \neq 0$ for $\lambda \in \mathbb{C}_r$ (by the definition of $\mathbb{C}_r$ (4.7)). Thus, it follows from this theorem that the stability of $(U_{\mathrm{p}}(\xi; L), V_{\mathrm{p}}(\xi; L))$ is determined by the solutions $\lambda(\gamma)$ of $\mathcal{D}_s(\lambda, \gamma; \ell) = 0$ (4.9). Moreover, Theorem 4.2 also establishes that the spectrum $\sigma(U_{\mathrm{p}}, V_{\mathrm{p}})$ cannot cross through $\lambda = 0$ as a parameter is varied (since $\mathcal{D}(\lambda, \gamma; L) \neq 0$ for λ in the positive half plane δ-close to 0). Hence, except for the saddle node bifurcation at $\ell = \ell_{\mathrm{sn}}$ (Theoreom 4.1), the pattern $(U_{\mathrm{p}}(\xi; L), V_{\mathrm{p}}(\xi; L))$ can only be (de)stabilized by a Hopf bifurcation. Due to the 'collapsed' character of the spectral branches $\Lambda(L, \mu)$ (§4.2.2), this implies that the ± 1-type Hopf bifurcations will play an important role in the bifurcation analysis of $(U_{\mathrm{p}}(\xi; L), V_{\mathrm{p}}(\xi; L))$, especially near the homoclinic limit.

4.5 Near the homoclinic pulse: patterns with long wavelengths

In this section we consider the stability and bifurcations of the periodic patterns $(U_{\mathrm{p}}(\xi; L), V_{\mathrm{p}}(\xi; L))$ of Theorem 4.1 for $\ell = \varepsilon^2 L$ large. It follows from [36, 77, 78] that for every discrete eigenvalue $\lambda_{\mathrm{h}, j} \in \mathbb{C}$ of the spectral stability problem associated to the limiting homoclinic pattern $(U_{\mathrm{h}}(\xi), V_{\mathrm{h}}(\xi)) = (U_{\mathrm{p}}(\xi; \infty), V_{\mathrm{p}}(\xi; \infty))$, there must be a spectral branch $\Lambda_{\mathrm{h}}(L) \in \mathbb{C}$ of the stability problem associated to the periodic pattern $(U_{\mathrm{p}}(\xi; L), V_{\mathrm{p}}(\xi; L))$ that approaches $\lambda_{\mathrm{h}, j}$ as $L \to \infty$ (see Remark 5.1). By the results of Theorem 4.2, we can explicitly approximate the branch $\Lambda_{\mathrm{h}}(L)$ for ℓ large, and thus obtain detailed information on the spectrum $\sigma((U_{\mathrm{p}}, V_{\mathrm{p}}))$ for large ℓ.

To investigate the structure of Λ_h for large ℓ, we introduce a second small parameter, δ, by setting $\ell = \frac{1}{\delta}$ – note that this is a slight abuse of notation, this δ is not related to the δ introduced in Theorem 4.2. We assume that $\delta = \mathcal{O}(1)$ w.r.t. ε, i.e. $0 < \varepsilon \ll \delta \ll 1$. In fact, we will consider all correction terms in ε – see Theorem 4.2 – as higher order effects in this section (and thus not even refer to these terms). Since a central expression as $E(\lambda, \ell; \mu)$ is exponentially small in δ in absolute value (4.10), this implies that we implicitly assume that ε is much smaller than exponentially small terms in δ in the forthcoming analysis. Note that this is mostly a technical issue, it does not influence the essence of our results.

Remark 5.1 In fact, the results in [78] also establish the exponential decay rate of $\sigma((U_\mathrm{p}, V_\mathrm{p}))$ as $L \to \infty$. Moreover, in [78] an expansion similar to the forthcoming one is given for the 'small' spectrum $\sigma((U_\mathrm{p}, V_\mathrm{p}))$, i.e. the part of the spectrum that is connected to the origin (and thus is associated to the translational eigenvalue $\lambda(+1) = 0$). Here, we consider the part of the spectrum associated to a 'nontrivial' eigenvalue of the homoclinic limit, more specifically, an eigenvalue associated to a Hopf instability.

4.5.1   The Hopf dance

Since $\lambda(\gamma)$ must be a zero of $\mathcal{D}_s(\lambda, \gamma; \ell)$, it follows from the expression (4.9) in Theorem 4.2 that a spectral branch $\Lambda = \{\lambda = \lambda(\gamma) : \gamma \in \mathbb{S}^1\} \in \mathbb{C}$ (§4.2.1) is implicitly determined by

$$t_{11}(\lambda, \ell) = 2\,\gamma_\mathrm{r} E(\lambda, \ell) - E^2(\lambda, \ell)\, t_{22}(\lambda, \ell), \tag{5.1}$$

(at leading order in ε). By (4.10), this condition reduces to $t_{11}(\lambda, \ell; \mu) = 0$ as $\ell \to \infty$. Moreover, by (4.11),

$$\lim_{\ell \to \infty} t_{11}(\lambda, \ell; \mu) = 1 - \mathcal{S}(\lambda; \mu) = t_2(\lambda; \mu). \tag{5.2}$$

Here $t_2(\lambda; \mu)$ is in fact the slow transmission function that was shown in [17] to govern the stability of the homoclinic pulse pattern $(U_\mathrm{h}(\xi), V_\mathrm{h}(\xi))$. Hence, we have explicitly recovered the above mentioned general results of [36, 78]. In fact, we have obtained a bit more: every spectral branch $\Lambda \subset \mathbb{C}_r$, see (4.7), associated to a periodic pattern $(U_\mathrm{p}(\xi; L), V_\mathrm{p}(\xi; L))$ limits on a non-zero eigenvalue λ_h associated to the limiting homoclinic pattern $(U_\mathrm{h}(\xi), V_\mathrm{h}(\xi))$ as $\ell \to \infty$. Note that it follows from (5.2) that $\mathcal{S}(\lambda_h; \mu) = 1$.

As mentioned above, the homoclinic pulse $(U_\mathrm{h}(\xi), V_\mathrm{h}(\xi))$ can only be (de)stabilized by a pair of complex conjugate eigenvalues $\lambda_\mathrm{h}(\mu), \overline{\lambda_\mathrm{h}}(\mu) \notin \mathbb{R}$, with by definition $\mathrm{Im}[\lambda_\mathrm{h}(\mu)] > 0$. At the bifurcation, the pulse must thus be destabilized by a Hopf instability. In this section we study the spectral curves that limit on these Hopf bifurcation eigenvalues for large but bounded ℓ. The associated critical values of parameter μ and λ_h are defined by,

$$\lambda_\mathrm{h}(\mu_\mathrm{H}) = \lambda_\mathrm{h,H} = i\lambda_\mathrm{h,H,i} \in i\mathbb{R} \ \ \text{with} \ \ \lambda_\mathrm{h,H,i} > 0. \tag{5.3}$$

Thus, by definition,

$$\mathcal{S}(\lambda_{\mathrm{h}}(\mu); \mu) \equiv 1. \tag{5.4}$$

Since we have assumed that $\ell = \frac{1}{\delta} \gg 1$, it follows that $|E(\lambda, \ell; \mu)|$ is exponentially small in δ (4.10). Therefore, we define

$$E_{\mathrm{h}} = E_{\mathrm{h}}(\ell; \mu) = E(\lambda_{\mathrm{h}}, \ell; \mu) = e^{-2\ell\sqrt{\mu+\lambda_{\mathrm{h}}}}, \quad E_0 = E_0(\ell; \mu) = E(0, \ell; \mu) = e^{-2\ell\sqrt{\mu}}. \tag{5.5}$$

and obtain the following expansion,

$$\tanh \ell\sqrt{\mu} = 1 - 2E_0 + 2E_0^2 + \mathcal{O}_E(3), \tag{5.6}$$

where the $\mathcal{O}_E(N)$ notation indicates the order in $|E|$, $\mathcal{O}_E(N) = \mathcal{O}_E(|E|^N)$ – note that this notation is somewhat ambiguous, since the magnitude of $|E|$ strongly depends on the values of λ and μ – see (5.11), (5.12) below. Since we know that λ must be close to λ_{h}, we expand $\mathcal{S}(\lambda; \mu)$ as a Taylor series in $(\lambda - \lambda_{\mathrm{h}})$,

$$\mathcal{S}(\lambda; \mu) = 1 + (\lambda - \lambda_{\mathrm{h}})\mathcal{S}'(\lambda_{\mathrm{h}}; \mu) + \frac{1}{2}(\lambda - \lambda_{\mathrm{h}})^2 \mathcal{S}''(\lambda_{\mathrm{h}}; \mu) + \mathcal{O}_E(3), \tag{5.7}$$

where we anticipate the forthcoming result that $\lambda - \lambda_{\mathrm{h}} = \mathcal{O}_E(|E|)$. The expression $E(\lambda; \mu)$ can be expanded in terms of both E_{h} and $(\lambda - \lambda_{\mathrm{h}})$,

$$E(\lambda, \ell; \mu) = E_{\mathrm{h}} - \ell(\lambda - \lambda_{\mathrm{h}})\frac{1}{\sqrt{\mu+\lambda_{\mathrm{h}}}}E_{\mathrm{h}} + \mathcal{O}_E(3), \tag{5.8}$$

where we have implicitly used that $\ell^k |E_{\mathrm{h}}^{m+1}| \ll |E_{\mathrm{h}}^m|$ for all $k \geq 0$. Substitution of the $\mathcal{O}_E(1)$ parts of these expansions into (5.1), using (4.11), yields a leading order approximation of Λ_{h},

$$-(\lambda - \lambda_{\mathrm{h}})\mathcal{S}'(\lambda_{\mathrm{h}}) + 2E_0 = 2E_{\mathrm{h}}\gamma_{\mathrm{r}} + \mathcal{O}_E(2).$$

We have thus obtained the following lemma.

Lemma 5.2 *There is a $\delta_0 > 0$ such that for all $\ell > 1/\delta_0$, the spectral branch $\Lambda_{\mathrm{h}}(\ell; \mu)$ is given by,*

$$\Lambda_{\mathrm{h}}(\ell; \mu) = \left\{\lambda(\gamma, \ell; \mu) = \lambda_{\mathrm{h}}(\mu) + \frac{2}{\mathcal{S}'(\lambda_{\mathrm{h}}; \mu)}\left(E_0(\ell; \mu) - \gamma_{\mathrm{r}}E_{\mathrm{h}}(\ell; \mu)\right) + \mathcal{O}_E(2), \gamma \in \mathbb{S}^1\right\}. \tag{5.9}$$

Thus, to leading order, $\Lambda_{\mathrm{h}}(\ell; \mu)$ is a straight interval at a distance of $|2E_0(\ell; \mu)/\mathcal{S}'(\lambda_{\mathrm{h}}; \mu)|$ from λ_{h}. Both this distance and the length of the interval decrease exponentially fast with ℓ. The endpoints of $\Lambda_{\mathrm{h}}(\ell; \mu)$ are given by

$$\partial_{\pm}\Lambda_{\mathrm{h}}(\ell; \mu) = \lambda_{\mathrm{h}}(\mu) + \frac{2}{\mathcal{S}'(\lambda_{\mathrm{h}}; \mu)}\left(E_0(\ell; \mu) \mp E_{\mathrm{h}}(\ell; \mu)\right). \tag{5.10}$$

Recall that $\partial_+\Lambda_{\mathrm{h}}(\mu)$ corresponds to the $\mathcal{H}_{+1}-$Hopf bifurcation, in which all extrema of the pattern $(U_{\mathrm{p}}(\xi; L), V_{\mathrm{p}}(\xi; L))$ start to oscillate exactly in phase at the bifurcation, and $\partial_+\Lambda_{\mathrm{h}}(\mu)$ to the $\mathcal{H}_{-1}-$Hopf bifurcation, in which extrema that are one period $(= 2L)$ away from each other begin to oscillate exactly out of phase (§4.2.2).

Remark 5.3 A result similar to Lemma 5.2 has been presented in [68] (Lemma 6.1). However, there the presence of the term $E_0(\ell; \mu)$ in (5.9) has been overlooked.

Next we infer more geometric information about Λ_{h}. By the lemma, the length of Λ_{h} is to leading order given by $2|E_{\mathrm{h}}/\mathcal{S}'|$, and the distance to λ_{h} is to leading order given by $2|E_0/\mathcal{S}'|$. The relative magnitude of these quantities is thus determined by

$$|E_{\mathrm{h}}(\ell; \mu)/E_0(\ell; \mu)| = e^{-2\ell\left(\mathrm{Re}\sqrt{\mu+\lambda_{\mathrm{h}}}-\sqrt{\mu}\right)}, \qquad (5.11)$$

which is exponentially small in δ if $\mu > 0$ and $\lambda = \lambda_{\mathrm{r}} + i\lambda_{\mathrm{i}}$ are such that

$$2\mu\lambda_{\mathrm{r}} + \lambda_{\mathrm{i}}^2 > 0. \qquad (5.12)$$

Note that this is satisfied if $\lambda_{\mathrm{r}} \geq 0$. Since $\lambda_{\mathrm{h}}(\mu_H) = i\lambda_{\mathrm{h,H,i}}$ with $\lambda_{\mathrm{h,H,i}} > 0$ due to (5.3), (5.12) also holds near the bifurcation at which $(U_{\mathrm{p}}(\xi; L), V_{\mathrm{p}}(\xi; L))$ destabilizes. Hence, near the destabilization, and in general when (5.12) holds, the length of Λ_{h} is much shorter than its distance to λ_{h}. On the other hand, the orientation of Λ_{h} with respect to λ_{h} is to leading order governed by

$$\frac{E_{\mathrm{h}}(\ell; \mu)}{\mathcal{S}'(\lambda_{\mathrm{h}}; \mu)} = \frac{e^{-2\ell\nu_{\mathrm{h,r}}}}{\rho_{\mathrm{h}}} \left[\cos\left(2\ell\nu_{\mathrm{h,i}} - \theta_{\mathrm{h}}\right) - i\sin\left(2\ell\nu_{\mathrm{h,i}} - \theta_{\mathrm{h}}\right)\right], \qquad (5.13)$$

in which

$$\begin{aligned} \nu_{\mathrm{h}}(\mu) &\overset{\mathrm{def}}{=} +\sqrt{\mu + \lambda_{\mathrm{h}}(\mu)} = \nu_{\mathrm{h,r}} + i\nu_{\mathrm{h,i}} \ \ \text{with} \ \ \arg\left[\nu_{\mathrm{h}}(\mu)\right] \in (0, \pi), \\ \mathcal{S}'(\lambda_{\mathrm{h}}; \mu) &\overset{\mathrm{def}}{=} \rho_{\mathrm{h}}(\mu)e^{i\theta_{\mathrm{h}}(\mu)} \ \ \text{with} \ \ \rho_{\mathrm{h}} \in \mathbb{R}^+, \theta_{\mathrm{h}} \in [0, 2\pi) \end{aligned} \qquad (5.14)$$

(Lemma 5.2). Combined, the above observations imply that

$$\mathrm{Re}[\lambda(\gamma)] \gtrless \mathrm{Re}[\lambda_{\mathrm{h}}] \ \ \text{for all} \ \ \gamma \in \mathbb{S}^1 \ \Leftrightarrow \ \mathrm{Re}[\mathcal{S}'(\lambda_{\mathrm{h}}; \mu)] \gtrless 0 \qquad (5.15)$$

if (5.12) holds – see Figure 4.8. It thus follows that the homoclinic pattern $(U_{\mathrm{h}}(\xi), V_{\mathrm{h}}(\xi))$ is the last 'periodic' pattern to destabilize if and only if $\mathrm{Re}[\mathcal{S}'(\lambda_{\mathrm{h,H}}; \mu_H)]$, the value of $\mathrm{Re}[\mathcal{S}'(\lambda_{\mathrm{h}}; \mu)]$ at the Hopf bifurcation (5.3), is positive. Or, vice versa, there exist stable periodic patterns $(U_{\mathrm{p}}(\xi; L), V_{\mathrm{p}}(\xi; L))$ with $L = 2\ell/\varepsilon^2$ and $\ell = 1/\delta$, when $(U_{\mathrm{h}}(\xi), V_{\mathrm{h}}(\xi))$ has already been destabilized if $\mathrm{Re}[\mathcal{S}'(\lambda_{\mathrm{h,H}}; \mu_H)] < 0$ – see again Figure 4.8.

Remark 5.4 It has been conjectured by Wei-Ming Ni in [60] that the homoclinic solution $(U_{\mathrm{h}}(\xi), V_{\mathrm{h}}(\xi))$ is the last pattern to become unstable in the generalized Gierer-Meinhardt equation (1.4) as μ approaches a Hopf bifurcation value. Here, we have thus shown that Ni's conjecture reduces to a conjecture on the sign of $\mathrm{Re}[\mathcal{S}'(\lambda_{\mathrm{h,H}}; \mu_H)]$. It follows from the analysis of the expression $\mathcal{S}'(\lambda_{\mathrm{h}}; \mu)$ in [17] that $\mathrm{Re}[\mathcal{S}'(\lambda_{\mathrm{h,H}}; \mu_H)] > 0$ for the classical Gierer-Meinhardt case ($\alpha_1 = 0, \beta_1 = 2, \alpha_2 = -1, \beta_2 = 2$), hence it follows that Ni's conjecture holds for this case. For a general proof of Ni's conjecture one needs to analyse $\mathrm{Re}[\mathcal{S}'(\lambda_{\mathrm{h,H}}; \mu_H)]$ as function of the parameters $\alpha_1, \alpha_2, \beta_1, \beta_2$. It is to be expected that one will encounter behavior that differs significantly from
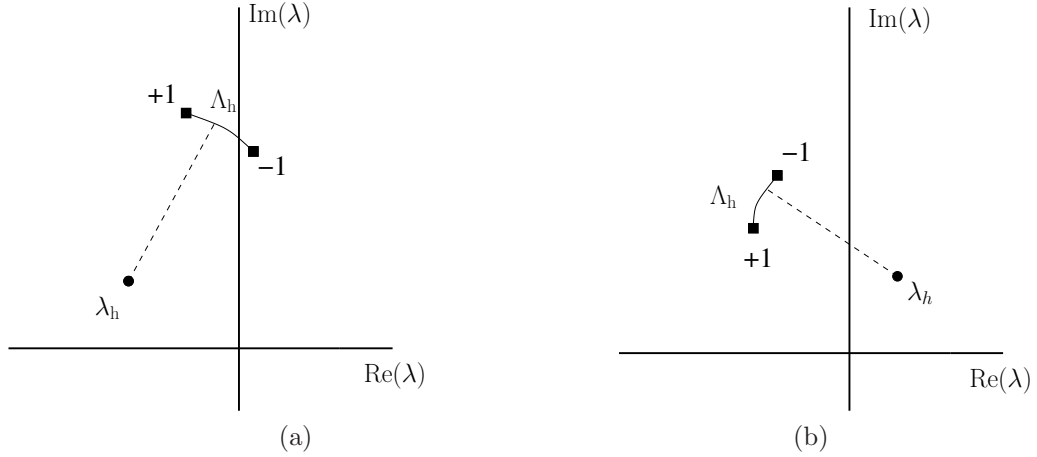
Figure 4.8: (a) A schematic picture of a spectral branch for the case that $\text{Re}[\mathcal{S}'(\lambda_{\text{h,H}}; \mu_{\text{H}})] > 0$ for some fixed $\mu > \mu_{\text{H}}$: the homoclinic pattern is the last periodic pattern to destabilizes as $\mu \downarrow \mu_{\text{H}}$. (b) The case that $\text{Re}[\mathcal{S}'(\lambda_{\text{h,H}}; \mu_{\text{H}})] < 0$ for some fixed $\mu < \mu_{\text{H}}$: the homoclinic limit is unstable, while there still exist stable long wavelength periodic patterns.

that of the classical case. In fact, in [24] the character of λ_{h} as function of μ for the special case $\alpha_1 = 5/4, \beta_1 = 2, \alpha_2 = -3, \beta_2 = 2$ has been considered (as an example): in this case $\text{Re}[\lambda_{\text{h}}(\mu)]$ changes signs twice as μ increases from 0, i.e. there are two (homoclinic) Hopf bifurcations, at $\mu_{\text{H,1}}$ and $\mu_{\text{H,2}}$: $(U_{\text{h}}(\xi), V_{\text{h}}(\xi))$ is stable for $\mu \in (\mu_{\text{H,1}}, \mu_{\text{H,2}})$. It is straightforward to check from the information in [24] that $\text{Re}[\mathcal{S}'(\lambda_{\text{h}}(\mu_{\text{H,1}}); \mu_{\text{H,1}})] > 0$ and $\text{Re}[\mathcal{S}'(\lambda_{\text{h}}(\mu_{\text{H,2}}); \mu_{\text{H,2}})] < 0$. Hence, there still exist stable periodic patterns $(U_{\text{p}}(\xi; L), V_{\text{p}}(\xi; L))$ as $(U_{\text{h}}(\xi), V_{\text{h}}(\xi))$ is destabilized by μ crossing through $\mu_{\text{H,2}}$ (in the case $\alpha_1 = 5/4, \beta_1 = 2, \alpha_2 = -3, \beta_2 = 2$). However, this example not necessarily disproves Ni's conjecture, since one could argue that Ni's conjecture concerns only the first bifurcation (for increasing μ) at which stable patterns are created (i.e. $\mu = \mu_{\text{H,1}}$ at which $\text{Re}[\mathcal{S}'(\lambda_{\text{h}}(\mu_{\text{H,1}}); \mu_{\text{H,1}})] > 0$).

The Hopf bifurcation curves $\mathcal{H}_{\pm 1} = \{\mu = \mu_{\pm}(\ell) \in \mathbb{C}\}$ are determined by the values of ℓ and μ at which the endpoints $\partial_{\pm}\Lambda_{\text{h}}(\ell; \mu)$ cross through the imaginary axis, i.e. by the condition

$$\text{Re}\left[\partial_{\pm}\Lambda_{\text{h}}(\ell; \mu_{\pm}(\ell))\right] = 0. \tag{5.16}$$

Since we have seen that $\Lambda_{\text{h}}(\ell; \mu)$ is exponentially close to λ_{h}, we expect that both $\mu_{\pm}(\ell)$ are exponentially close – i.e. $\mathcal{O}(|E|) = \mathcal{O}_E(1)$ – to μ_{H} (5.3). Therefore, we expand $\lambda_{\text{h}}(\mu)$ around μ_{H},

$$\lambda_{\text{h}}(\mu) = \lambda_{\text{h,H}} + (\mu - \mu_{\text{H}})\lambda_{\text{h}}'(\mu_{\text{H}}) + \frac{1}{2}(\mu - \mu_{\text{H}})^2 \lambda_{\text{h}}''(\mu_{\text{H}}) + \mathcal{O}_E(3), \tag{5.17}$$

once more anticipating on the expectation that $\mu - \mu_{\mathrm{H}} = \mathcal{O}_E(1)$. Note that $\lambda'_{\mathrm{h}}(\mu_{\mathrm{H}})$ and $\lambda''_{\mathrm{h}}(\mu_{\mathrm{H}})$ can be expressed in terms of $\mathcal{S}'(\lambda_{\mathrm{h,H}}; \mu_{\mathrm{H}})$ and $\mathcal{S}''(\lambda_{\mathrm{h,H}}; \mu_{\mathrm{H}})$ (5.7) by a straightforward expansion of (5.4). For instance,

$$\lambda'_{\mathrm{h}}(\mu_{\mathrm{H}}) = -\frac{1}{\mathcal{S}'(\lambda_{\mathrm{h,H}}; \mu_{\mathrm{H}})} \frac{\partial \mathcal{S}}{\partial \mu}(\lambda_{\mathrm{h,H}}; \mu_{\mathrm{H}}) = -\frac{1}{2} \frac{\lambda_{\mathrm{h,H}}}{\mu_{\mathrm{H}}(\mu_{\mathrm{H}} + \lambda_{\mathrm{h,H}})\mathcal{S}'(\lambda_{\mathrm{h,H}}; \mu_{\mathrm{H}})}, \qquad (5.18)$$

where we have used that

$$\frac{\partial \mathcal{S}}{\partial \mu}(\lambda; \mu) = \left[\frac{\partial}{\partial \mu} \frac{\sqrt{\mu}}{\sqrt{\mu + \lambda}} \right] [\alpha_1 - \alpha_2 \beta_1 \mathcal{R}(\lambda)] = \frac{1}{2} \frac{\lambda}{\mu(\mu + \lambda)} \mathcal{S}(\lambda; \mu)$$

(4.12), and that $\mathcal{S}(\lambda_{\mathrm{h,H}}; \mu_{\mathrm{H}}) = 1$. The derivation of the expression for $\lambda''_{\mathrm{h}}(\mu_{\mathrm{H}})$ is similar, but more involved. The combination of (5.17) with Lemma 5.2 (5.9) yields the following leading order approximation of $\Lambda_{\mathrm{h}}(\ell; \mu))$ for $\mu \; \mathcal{O}_E(1)$ close μ_{H},

$$\lambda(\gamma, \ell; \mu) = \lambda_{\mathrm{h,H}} + (\mu - \mu_{\mathrm{H}})\lambda'_{\mathrm{h}}(\mu_{\mathrm{H}}) + \frac{2}{\mathcal{S}'(\lambda_{\mathrm{h,H}}; \mu_{\mathrm{H}})} \left(E_0(\ell; \mu_{\mathrm{H}}) - \gamma_{\mathrm{r}} E_{\mathrm{h}}(\ell; \mu_{\mathrm{H}}) \right) + \mathcal{O}_E(2).$$

The application of condition (5.16) implies that,

$$0 = (\mu_{\pm} - \mu_{\mathrm{H}})\mathrm{Re}\left[\lambda'_{\mathrm{h}}(\mu_{\mathrm{H}})\right] + \mathrm{Re}\left[\frac{2}{\mathcal{S}'(\lambda_{\mathrm{h,H}}; \mu_{\mathrm{H}})} \left(E_0(\ell; \mu_{\mathrm{H}}) \mp E_{\mathrm{h}}(\ell; \mu_{\mathrm{H}}) \right) \right] + \mathcal{O}_E(2),$$

since $\lambda_{\mathrm{h,H}} \in i\mathbb{R}$ (5.3). Hence by (5.5) and (5.14),

$$\mu_{\pm}(\ell) = \mu_{\mathrm{H}} - \frac{2}{\mathrm{Re}\left[\lambda'_{\mathrm{h}}(\mu_{\mathrm{H}})\right]} e^{-2\ell\sqrt{\mu_{\mathrm{H}}}} \mathrm{Re}\left[\frac{1 \mp e^{-2\ell((\nu_{\mathrm{h,r}}(\mu_{\mathrm{H}}) - \sqrt{\mu_{\mathrm{H}}}) + i\nu_{\mathrm{h,i}}(\mu_{\mathrm{H}}))}}{\mathcal{S}'(\lambda_{\mathrm{h,H}}; \mu_{\mathrm{H}})} \right] + \mathcal{O}_E(2),$$

where $\lambda'_{\mathrm{h}}(\mu_{\mathrm{H}})$ is determined by (5.18). The above analysis can be summarized as follows.

Corollary 5.5 *There is a $\delta_0 > 0$ such that for all $\ell > 1/\delta_0$, the Hopf bifurcation curves $\mathcal{H}_{\pm 1}$ are to leading order given by*

$$\mu_{\pm}(\ell) = \mu_{\mathrm{H}} - \frac{2}{\rho_{\mathrm{h}}(\mu_{\mathrm{H}})\mathrm{Re}\left[\lambda'_{\mathrm{h}}(\mu_{\mathrm{H}})\right]} e^{-2\ell\sqrt{\mu_{\mathrm{H}}}} \left[\cos\theta_{\mathrm{h}}(\mu_{\mathrm{H}}) \mp e^{-2\ell(\nu_{\mathrm{h,r}}(\mu_{\mathrm{H}}) - \sqrt{\mu_{\mathrm{H}}})} \cos\left(2\ell\nu_{\mathrm{h,i}}(\mu_{\mathrm{H}}) - \theta_{\mathrm{h}}(\mu_{\mathrm{H}})\right) \right].$$

with $\rho_{\mathrm{h}}(\mu), \theta_{\mathrm{h}}(\mu), \nu_{\mathrm{h,r}}(\mu),$ and $\nu_{\mathrm{h,i}}(\mu)$ as defined in (5.14) and $\lambda'_{\mathrm{h}}(\mu_{\mathrm{H}})$ given by (5.18). The curves $\mathcal{H}_{\pm 1}$ 'snake' among each other and have infinitely many intersection points as $\ell \to \infty$ that accumulate on μ_{H}. These intersection points represent co-dimension 2 bifurcations, they are given by $\mu = \mu_{+1}(\ell_2(k)) = \mu_{-1}(\ell_2(k))$ with

$$\ell_2(k) = \frac{\pi + 2\theta_{\mathrm{h}}(\mu_{\mathrm{H}})}{4\nu_{\mathrm{h,i}}(\mu_{\mathrm{H}})} + \frac{\pi}{2\nu_{\mathrm{h,i}}(\mu_{\mathrm{H}})} k > \frac{1}{\delta_0}, \quad k \in \mathbb{N}.$$

Thus this corollary confirms the structure of the the sinusoidally oscillating and exponentially converging snaking curves $\mathcal{H}_{+1}$ and $\mathcal{H}_{-1}$ as found numerically for the Gray-Scott problem in section §4.3.

It should be noted that one could also define the curves $\mathcal{H}(\gamma)$, $\gamma \in \mathbb{S}^1$, that describe the relation between μ and ℓ for which the point $\lambda(\gamma)$ on the spectral branch $\Lambda_{\mathrm{h}}(\ell; \mu)$ crosses the imaginary axis (5.9). It is straightforward to check that these curves are all inside the (infinitely many) regions bounded by $\mathcal{H}_{\pm 1}$. This implies that neither of these curves can correspond to a (de)stabilizing Hopf bifurcation, and thus reconfirms the fact that all bifurcations near μ_{H} must be of $\mathcal{H}_{\pm 1}-$type. Moreover, it also implies that *all* $\mathcal{H}(\gamma)$ curves pass through the co-dimension 2 intersection points determined by $\mathcal{H}_{+1} \cap \mathcal{H}_{-1}$. This is of course a very degenerate but also artificial phenomenon, it is caused by the fact that the spectral branch $\Lambda_{\mathrm{h}}(\ell; \mu)$ is *to leading order* a straight interval that coincides with the imaginary axis at the intersection points $\mathcal{H}_{+1} \cap \mathcal{H}_{-1}$. A more accurate approximation of $\Lambda_{\mathrm{h}}(\ell; \mu)$ will show that it is in general bent, as we shall show in the upcoming section. Note that the orientation of the associated 'belly' with respect to the imaginary axis decides whether the pattern $(U_{\mathrm{p}}(\xi; L), V_{\mathrm{p}}(\xi; L))$ indeed may undergo a co-dimension 2 bifurcation caused by both $\mathcal{H}_{+1}$ and $\mathcal{H}_{-1}$, or whether there is no co-dimension 2 bifurcation since it is preceded by and 'interior' $\mathcal{H}(\gamma)-$bifurcation, as described in §4.2.2.

4.5.2 The effect of bending: the belly dance

To study the next order parabolic correction to $\Lambda_{\mathrm{h}}(\ell; \mu)$, we need to determine the next order correction to expression (5.9) in Lemma 5.2. As in §4.5.1, we first consider the spectral branch $\Lambda_{\mathrm{h}}(\ell; \mu)$ for general μ, i.e. μ not necessarily close to μ_{H}. By (4.10), (5.8), (4.11), (5.6), (5.7),

$$E^2(\lambda, \ell; \mu)\, t_{22}(\lambda, \ell; \mu, 0) = [E_{\mathrm{h}}(\ell; \mu) + \mathcal{O}_E(2)]^2 [1 + (1 + \mathcal{O}_E(1))(1 + \mathcal{O}_E(1))] = 2E_{\mathrm{h}}^2(\ell; \mu) + \mathcal{O}_E(3),$$

and we thus find as next order approximation to (5.1),

$$\begin{aligned}
-(\lambda - \lambda_{\mathrm{h}})\mathcal{S}'(\lambda_{\mathrm{h}}) &= 2\gamma_{\mathrm{r}}E_{\mathrm{h}} - 2E_0 - \tfrac{1}{2}(\lambda - \lambda_{\mathrm{h}})^2 \mathcal{S}''(\lambda_{\mathrm{h}}; \mu) - 2E_0(\lambda - \lambda_{\mathrm{h}})\mathcal{S}'(\lambda_{\mathrm{h}}) \\
&\quad + 2E_0^2 - 2(\lambda - \lambda_{\mathrm{h}})\tfrac{\ell}{\sqrt{\mu + \lambda_{\mathrm{h}}}} E_{\mathrm{h}} - 2E_{\mathrm{h}}^2 + \mathcal{O}_E(3),
\end{aligned}$$

where we have once again used (4.10), (4.11), (5.6), (5.7), and (5.8). We can now substitute the leading order approximation of $(\lambda - \lambda_{\mathrm{h}})$ (5.9) into the right hand side of this identity, to obtain

$$\begin{aligned}
(\lambda - \lambda_{\mathrm{h}})\mathcal{S}'(\lambda_{\mathrm{h}}) &= 2(E_0 - \gamma_{\mathrm{r}}E_{\mathrm{h}}) + 2(E_{\mathrm{h}}^2 - E_0^2) + 4\tfrac{\ell}{\mathcal{S}'(\lambda_{\mathrm{h}})\sqrt{\mu + \lambda_{\mathrm{h}}}}\gamma_{\mathrm{r}}E_{\mathrm{h}}(E_0 - \gamma_{\mathrm{r}}E_{\mathrm{h}}) \\
&\quad + 4E_0(E_0 - \gamma_{\mathrm{r}}E_{\mathrm{h}}) - 2\tfrac{\mathcal{S}''(\lambda_{\mathrm{h}})}{(\mathcal{S}'(\lambda_{\mathrm{h}}))^2}(E_0 - \gamma_{\mathrm{r}}E_{\mathrm{h}})^2 + \mathcal{O}_E(3).
\end{aligned}$$

We have thus obtained,

Lemma 5.6 *There is a $\delta_0 > 0$ such that for all $\ell > 1/\delta_0$, the spectral branch $\Lambda_{\mathrm{h}}(\ell; \mu)$ is given by the quadratic approximation,*

$$\Lambda_{\mathrm{h}}(\ell; \mu) = \left\{\lambda(\gamma, \ell; \mu) = \lambda_{\mathrm{h}}(\mu) + \mathcal{G}_0(\ell; \mu) + \mathcal{G}_1(\ell; \mu)\,\gamma_{\mathrm{r}} + \mathcal{G}_2(\ell; \mu)\,\gamma_{\mathrm{r}}^2 + \mathcal{O}_E(3), \gamma \in \mathbb{S}^1\right\},$$

$$\tag{5.19}$$

with

$$
\begin{array}{rcl}
\mathcal{G}_0(\ell;\mu) &=& \frac{2}{\mathcal{S}'(\lambda_{\mathrm{h}})}\left[E_0 + \left(1 - \frac{\mathcal{S}''(\lambda_{\mathrm{h}})}{(\mathcal{S}'(\lambda_{\mathrm{h}}))^2}\right)E_0^2 + E_{\mathrm{h}}^2\right] + \mathcal{O}_E(3),\\[2mm]
\mathcal{G}_1(\ell;\mu) &=& -\frac{2}{\mathcal{S}'(\lambda_{\mathrm{h}})}\left[1 + 2\left(1 - \frac{\ell}{\mathcal{S}'(\lambda_{\mathrm{h}})\sqrt{\mu+\lambda_{\mathrm{h}}}} - \frac{\mathcal{S}''(\lambda_{\mathrm{h}})}{(\mathcal{S}'(\lambda_{\mathrm{h}}))^2}\right)E_0\right]E_{\mathrm{h}} + \mathcal{O}_E(3),\\[2mm]
\mathcal{G}_2(\ell;\mu) &=& -\frac{2}{(\mathcal{S}'(\lambda_{\mathrm{h}}))^2}\left[\frac{2\ell}{\sqrt{\mu+\lambda_{\mathrm{h}}}} + \frac{\mathcal{S}''(\lambda_{\mathrm{h}})}{\mathcal{S}'(\lambda_{\mathrm{h}})}\right]E_{\mathrm{h}}^2 + \mathcal{O}_E(3).
\end{array}
$$

$$(5.20)$$

Of course, $\Lambda_{\mathrm{h}}(\ell;\mu)$ is at leading order still an interval that rotates as function of ℓ, its rotation is to leading order still determined by (5.13). Nevertheless, as function of $\gamma_{\mathrm{r}} \in [-1,1]$, $\Lambda_{\mathrm{h}}(\ell;\mu)$ is a parabola (up to corrections of $\mathcal{O}_E(3)$). Moreover, up to a non-rotating factor, the orientation of the parabolic belly is to leading order determined by,

$$
\left(\frac{E_{\mathrm{h}}(\ell;\mu)}{\mathcal{S}'(\lambda_{\mathrm{h}};\mu)}\right)^2 = \frac{e^{-4\ell\nu_{\mathrm{h,r}}}}{\rho_{\mathrm{h}}^2}\left[\cos\left(4\ell\nu_{\mathrm{h,i}} - 2\theta_{\mathrm{h}}\right) - i\sin\left(4\ell\nu_{\mathrm{h,i}} - 2\theta_{\mathrm{h}}\right)\right].
$$

(5.20). Thus, the parabolic belly indeed 'dances' around the leading order linear approximation of $\Lambda_{\mathrm{h}}(\ell;\mu)$ with a frequency that is twice the frequency of the rotation of $\Lambda_{\mathrm{h}}(\ell;\mu)$ (5.13). More precisely: in a coordinate frame that rotates along with the linear leading order approximation so that $\Lambda_{\mathrm{h}}(\ell;\mu)$ remains vertical, the $\mathcal{O}_E(2)$ parabolic correction indeed performs a 'belly dance' from left to right. This is in full agreement with the numerical observations for the Gray-Scott model in section §4.3.

In general, the parabolic correction will not have an influence on the destabilization of the periodic pattern $(U_{\mathrm{p}}(x;L),V_{\mathrm{p}}(x;L))$, it will be caused by one of the endpoints $\partial_{\pm}\Lambda_{\mathrm{h}}(\ell;\mu) = \lambda(\pm 1,\ell;\mu)$ (5.19), (5.10). However, near the co-dimension 2 points, where $\Lambda_{\mathrm{h}}(\ell;\mu)$ is almost vertical and $\mathrm{Re}[\partial_{+}\Lambda_{\mathrm{h}}(\ell;\mu)]$ and $\mathrm{Re}[\partial_{-}\Lambda_{\mathrm{h}}(\ell;\mu)]$ are close to 0, the parabolic 'belly' may play a role: the orientation of the parabola with respect to the imaginary axis determines whether and endpoint $\partial_{\pm}\Lambda_{\mathrm{h}}(\ell;\mu)$ is the first to cross through the imaginary axis, or an interior point. Note that $\Lambda_{\mathrm{h}}(\ell;\mu)$ would be tangent to the imaginary axis in this latter case, i.e. $\mathrm{Re}[\lambda(\gamma_{\mathrm{r}}^{\mathrm{int}},\ell;\mu)] = 0$ for some $\gamma_{\mathrm{r}}^{\mathrm{int}} \neq \pm 1$, while $\mathrm{Re}[\lambda(\gamma_{\mathrm{r}}^{\mathrm{int}},\ell;\mu)] < 0$ for all $\gamma_{\mathrm{r}} \in [-1,+1]\backslash\{\gamma_{\mathrm{r}}^{\mathrm{int}},\overline{\gamma_{\mathrm{r}}^{\mathrm{int}}}\}$. However, this does not happen.

Corollary 5.7 *Let $(U_{\mathrm{p}}(x;L),V_{\mathrm{p}}(x;L))$ be a periodic pattern, let $\ell = \varepsilon^2 L = 1/\delta$ be large enough, and assume that $(U_{\mathrm{p}}(x;L),V_{\mathrm{p}}(x;L))$ is destabilized by $\Lambda_{\mathrm{h}}(\ell;\mu)$ as μ crosses through the critical value $\mu_{\mathrm{dest}} = \mu_{\mathrm{dest}}(\ell)$. This destabilization either is a Hopf bifurcation of $\mathcal{H}_{+1}-$ or $\mathcal{H}_{-1}-$type, i.e. the destabilization must be caused by one of the endpoints $\partial_{\pm}\Lambda_{\mathrm{h}}(\ell;\mu)$, or it is a co-dimension 2 bifurcation, i.e. μ_{dest} corresponds to an intersection of the $\mathcal{H}_{+1}-$ and $\mathcal{H}_{-1}-$curves.*

Note that this corollary establishes that the boundary of the Busse balloon near a homoclinic tip indeed must be formed by the two 'snaking' $\mathcal{H}_{+1}-$ and $\mathcal{H}_{-1}-$curves – see Figure 4.10(a).

Since the parabolic correction to $\Lambda_h(\ell; \mu)$ only is of $\mathcal{O}_E(2)$ (Lemma 5.6), $(U_p(x; L), V_p(x; L))$ must be destabilized by a Hopf bifurcation of $\mathcal{H}_{\pm 1}$-type if $\Lambda_h(\ell; \mu)$ is not $\mathcal{O}_E(1)$ close to being vertical. The corollary can thus be proved by only considering the near-vertical case, with $\Lambda_h(\ell; \mu)$ in the stable part of the complex plane. It will be shown that in this case the parabolic belly is pointing away from the imaginary axis.

Proof. In leading order, the orientation of $\Lambda_h(\ell; \mu)$ is determined by (5.9) and especially by (5.13). It follows that $\Lambda_h(\ell; \mu)$ is vertical up to $\mathcal{O}_E(1)$ corrections if

$$\frac{E_h(\ell; \mu)}{\mathcal{S}'(\lambda_h; \mu)} = i\mathcal{Q} + \mathcal{O}_E(1), \mathcal{Q} \in \mathbb{R} \ (\mathcal{Q} \neq 0),$$

Thus, by (5.13), $2\ell\nu_{h,i} - \theta_h = \frac{1}{2}\pi + k\pi + \mathcal{O}_E(1)$, with $k \in \mathbb{Z}$ and k large enough. Hence, $\Lambda_h(\ell; \mu)$ is to leading order vertical for ℓ $\mathcal{O}_E(1)$ close to

$$\ell_{vert}(\mu) = \frac{\pi + 2\theta_h}{4\nu_{h,i}} + \frac{\pi}{2\nu_{h,i}}k. \tag{5.21}$$

By (5.20), (5.13), and (5.21), the quadratic deformation of $\Lambda_h(\ell; \mu)$ is determined by $\mathcal{G}_2(\ell_{vert}, \mu)\gamma_r^2$ (5.19), with

$$\mathcal{G}_2(\ell_{vert}, \mu) = \frac{2}{\rho_h^2}\left[\frac{2\ell_{vert}}{\sqrt{\mu + \lambda_h}} + \frac{\mathcal{S}''(\lambda_h)}{\mathcal{S}'(\lambda_h)}\right]e^{-4\ell_{vert}\nu_{h,r}} + \mathcal{O}_E(3), \tag{5.22}$$

The assumption $\ell = \frac{1}{\delta} \gg 1$, implies that the orientation of the parabolic 'belly' with respect to its leading order vertical configuration is determined by the real part of $1/\sqrt{\mu + \lambda_h}$.

Since $\text{Im}[\lambda_h] > 0$ by definition (5.3), it follows that $\arg[\mu + \lambda_h] \in (0, \pi)$, so that $\arg[\sqrt{\mu + \lambda_h}] \in (0, \frac{1}{2}\pi)$ (see (5.14)) and $\arg[1/\sqrt{\mu + \lambda_h}] \in (-\frac{1}{2}\pi, 0)$. Hence, $\text{Re}[1/\sqrt{\mu + \lambda_h}] > 0$, so that

$$\text{Re}[\mathcal{G}_2(\ell_{vert}, \mu)\gamma_r^2]|_{\gamma_r = \pm 1} > \text{Re}[\mathcal{G}_2(\ell_{vert}, \mu)\gamma_r^2]|_{\gamma_r = 0} = 0,$$

which implies that the parabolic belly of $\Lambda_h(\ell_{vert}, \mu)$ points to the left, that is, away from the imaginary axis if $\Lambda_h(\ell_{vert}, \mu)$ is contained in the stable complex half plane. Therefore, it is impossible for interior points of $\Lambda_h(\ell, \mu_{dest})$ to cross through the imaginary axis before the endpoints $\partial_\pm \Lambda_h(\ell, \mu_{dest})$ do. Since $\Lambda_h(\ell, \mu)$ rotates as function of ℓ, there must be values of $\mu_{dest}(\ell)$ for which both endpoints $\partial_\pm \Lambda_h(\ell, \mu_{dest})$ are on the imaginary axis. Such situations correspond to the co-dimension 2 bifurcation at which $\mathcal{H}_{+1}$ and $\mathcal{H}_{-1}$ intersect.

Finally, we note that the higher order, non-quadratic, corrections to the shape of $\Lambda_h(\ell, \mu_{dest})$ – see Lemma 5.6 – cannot have an effect on the above considerations. $\square$

The fact that the parabolic belly always points away from the imaginary axis indeed is quite intriguing. In Figure 4.9, a sketch is given of the combined Hopf and belly dance: the belly 'dances' with twice the frequency of the rotation of the spectral
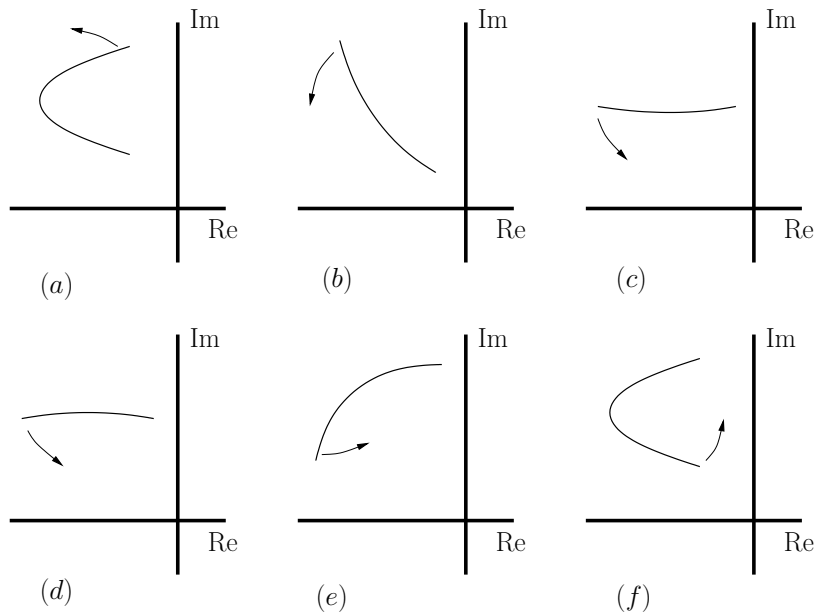
Figure 4.9: A sketch of the combined Hopf and belly dances of the spectral curve Λ_h for values of μ and k inside the Busse balloon. Wavenumber k decreases in a series of snapshots from (a) to (f), the picture shows a series of snapshots of Λ_h. The arrow indicate the direction of the rotation. Notice that this sketch does not include the exponential decay of the scale of the curve as k decreases and that (the higher order effect of) its bending has been exaggerated. Compare to Figure 4.6.

curve. The belly dances causes the boundary of the Busse balloon to be as sketched in Figure 4.10(a). Although we have just shown that this does not occur in equations of the type (1.2)/(1.4), it would a priori have been natural to expect that also the situation as presented in Fig 4.10(b) could occur. Here the boundary of a Busse balloon is sketched in the hypothetical situation that parabolic belly is oriented towards the imaginary axis near the bifurcation: ($\mathcal{O}(1)$) close to the intersections of $\mathcal{H}_{+1}$ and $\mathcal{H}_{-1}$ there is a small region in which the pattern $(U_p(\xi; L), V_p(\xi; L))$ is destabilized by an 'internal Hopf bifurcation' at $\gamma_r^{int} \neq \pm 1$. In the final section we discuss whether this scenario indeed is impossible (especially in the light of Remark 1.4).

4.6   Discussion

In this chapter we have found, by numerical means, that the Busse balloon associated to periodic patterns in the Gray-Scott model (with $\varepsilon^4 = 0.001$ and $B = 0.026$) has a fine structure consisting of a Hopf dance of snaking bifurcation curves $\mathcal{H}_{\pm 1}$ with many co-dimension 2 intersections. This phenomenon has been established as a
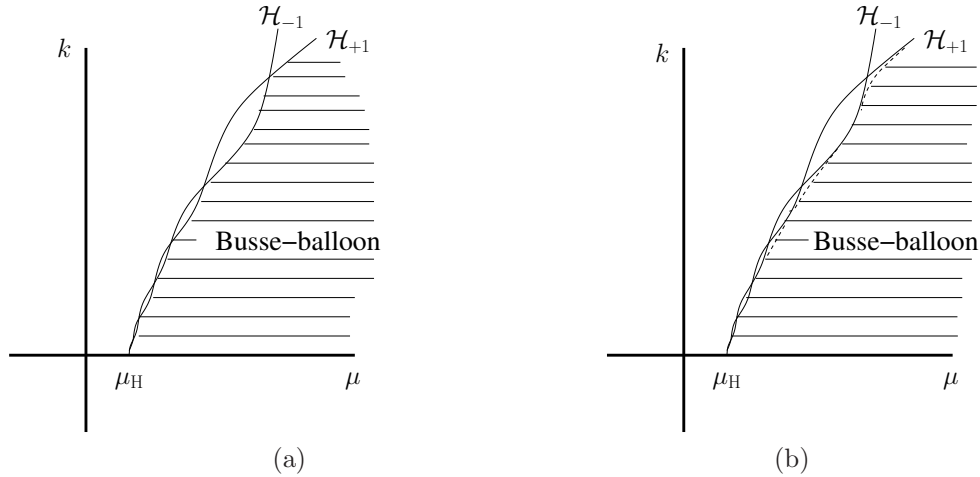
Figure 4.10: A typical sketch of the snaking curves $\mathcal{H}_{+1}$ and $\mathcal{H}_{-1}$.(a) The situation as established by the analysis: the belly of Λ_{h} always points into the stable half plane near the intersections of $\mathcal{H}_{\pm}$ (b) The hypothetical scenario in which the belly would be oriented towards the unstable half plane: there are no co-dimension 2 bifurcations near the homoclinic tip, but the intersection of $\mathcal{H}_{\pm 1}$ are preceded by 'interior' Hopf bifurcations as the spectral branch Λ_{h} crosses the imaginary axis for some γ-eigenvalue with $\gamma \notin \{\pm 1\}$.

generic destabilization mechanism by a detailed analysis of the destabilization of long wavelength, nearly localized, stationary, reversible spatially periodic patterns in the class of two component, singularly perturbed reaction-diffusion systems represented by the normal form model (1.4).

The main open question of course is: *'Does the Hopf dance destabilization mechanism persist beyond the range of singularly perturbed two component reaction-diffusion systems?'* We strongly believe that this is the case. Since the destabilization mechanism concerns the behavior of nearly homoclinic patterns, it is expected that it is possible to establish the validity of the Hopf dance mechanism for non-singularly perturbed N-component reaction-diffusion equations by extending the methods developed in [36, 78]. We do have to be a careful, though. A first look into the applicability of the methods of [36, 78] to this problem suggests that it is possible to establish the persistence of the stretching and rotating behavior of the (collapsed) spectral curves near the homoclinic limit. By the general theory presented in section §4.2, this would imply that the Hopf dance mechanism indeed also appears as a generic feature is this much larger class of systems.

However, at this point it is not at all clear whether or not the belly dance also persists, and more importantly: in what way it persists. We expect that the boundary of the

Busse balloon near the homoclinic limit does not necessarily have to be of the type sketched in Figure 4.10 (a), i.e. the structure associated to the Gray-Scott system and to the normal form. This feature may be related to the character of the models (1.1) and (1.4). It follows from a detailed re-examination of the proof of Corollary 5.7 that the orientation of the belly is in essence determined by the exponential terms $E(\lambda, \ell)$ in the expression for the Evans function given in Theorem 4.2. In general, we do not expect such exponential terms in the Evans function associated to the stability of stationary patterns. In fact, it is for this reason to be expected that the belly dance may already change orientation in the class of singularly perturbed two component models presented in Remark 1.4: the results to be presented in [13] seem to imply that the role of the exponential expressions $E(\lambda, \ell)$ may be taken over by more general expressions. These expressions may cause the orientation of the belly in the Hopf dance to change. Note that this (so far quite formal) observation does not 'destroy' the genericity of the Hopf dance, it only shows that the orientation of the belly dance may change if one considers a larger class of models. In fact, it shows that the two Hopf dance scenarios shown in Figure 4.10 may both occur (and thus not only the one given in Figure 4.10(a)). Of course, this all is at present not yet established as a rigorous mathematical result: it is the subject of work in progress.

Chapter 5

Outlook for ecologists

In ecology, we are interested in many features of semi-arid ecosystems, not the least among which are pattern formation from a homogeneously vegetated state and early-warning signs for desertification [41, 46, 74, 91]. For example, for the GKGS-model (0.5) we have derived parameter combinations for which the homogeneously vegetated state (U_+, V_+) destabilizes and a patterned state appears. Since the Ginzburg-Landau equation serves to describe the patterns if the precipitation rate is slightly below threshold, we can perfectly describe the appearance of patterns in the GKGS-model (0.5). On the other hand, in this thesis we did not at all consider the determination of early warning signs captured by the GKGS-model.

More generally, despite recent field studies that revealed a power-law in the patch-size distribution of the vegetation [45] that were successful in explaining the distribution by the use of cellular automata, profound insight in ecological signs of imminent desertification is basically lacking. Moreover, although reaction-diffusion(-advection) models are used extensively to model semi-arid ecosystems, early warning mechanisms have neither been consistently described nor studied by these models.

This chapter aims at describing the relevant ecological consequences of the results of this thesis, as well as at a description of possible future work. It will be argued that the Busse balloons that have been constructed in chapter 3 will be of vital importance in further analyses of desertification in the GKGS-model.

5.1   Discussion of results

In original nondimensional parameters, the GKGS-model reads

$$\begin{array}{rclclclclclcl}
u_t &=& u_{xx} &+& \nu u_x &+& a &-& Lu &-& Muv^2 \\
v_t &=& d_v v_{xx} &-& bv &+& Nuv^2 &&&&
\end{array} \tag{1.1}$$

with $u(x,t), v(x,t) : \mathbb{R} \times \mathbb{R}_+ \rightarrow \mathbb{R}$ and $a, b, \nu \geq 0$, $d_v \geq 0$. Now, u can can be directly interpreted as the water infiltration and w is the vegetation density. No-

tice that, following the results of chapters 2 and 3, we model the spread of water infiltration with diffusion and not with porous media flow / nonlinear diffusion. From [46] we quote estimates for the case that the vegetation consists of grass: $\nu = 365$ m year^{-1} (it increases from 0 m year^{-1}), $a = 250$ to 750 kg H$_2$O m^{-2} year^{-1}, $L = 4$ year^{-1}, $M = 100$ kg H$_2$O m^{-2} year^{-1} kg dry mass m^{-2}, $b = 1.8$ year^{-1}, $d_v = 1.0$ m^2 year^{-1}, $N = 0.3$ kg dry mass m^{-2} year^{-1}.

The three homogeneous background states or equilibria from system (1.1) can now be written as

$$u_\pm = \frac{1}{2}[a \pm \sqrt{a^2 - 4b^2}] \quad \text{and} \quad v_\pm = \frac{1}{2b}[a \mp \sqrt{a^2 - 4b^2}] \tag{1.2}$$

and the desert state $(u_0, v_0) = (\frac{a}{L}, 0)$. Of course, just as in the GKGS-system (0.5), the desert state (u_0, v_0) and the vegetated equilibrium (u_+, v_+) are stable with respect to homogeneous perturbations; the vegetated equilibrium (u_-, v_-) is always unstable.

Just as before, the stable periodic patterns appear at a supercritical Turing-Hopf bifurcation at $a = a_{\text{TH}}(\nu)$. Near the Turing-Hopf bifurcation at a_{TH}, they form an Eckhaus band of stable patterns. When the condition $0 < a_{\text{TH}} - a \ll 1$ breaks down, we can no longer derive a modulation equation to obtain insight in the dynamics of (1.1) and we have to resort to continuation methods. So, we have constructed two Busse balloons for (1.1), one for $\nu = 0$ m year^{-1} and one for $\nu = 365$ m year^{-1} with the further parameters drawn from [46]: $a = 250$ to 750 kg H$_2$O m^{-2} year^{-1}, $L = 4$ year^{-1}, $M = 100$ kg H$_2$O m^{-2} year^{-1} kg dry mass m^{-2}, $b = 1.8$ year^{-1}, $d_v = 1$ m^2 year^{-1}, $N = 0.3$ kg dry mass m^{-2} year^{-1}. However, we have to choose a rate for the diffusion coefficient d_u as well (Klausmeier's model does not include diffusion of water). We assume $d_v = 1000$. This way, the diffusion coefficients of both d_v and d_u differ by a factor 1000. Though it may at first sight seem as if with this choice the diffusion of water ($d_v = 1000$) outranges the advection of water ($\nu = 365$), this is not the case. To see this, we rescale d_v to $d_v = 1$. This can be done by rescaling x with $x = \sqrt{1000}\,\tilde{x}$, which gives rescaled parameters $\tilde{d}_v = 1$ and $\tilde{\nu} = 11.5$ and $\tilde{d}_u = 0.001$, as is the standard setting in chapter 2. Thus, advection clearly dominates diffusion. The constructed Busse balloons are shown in Figures 5.1(a) and 5.1(b) and 5.2.

5.2   Ecological interpretation of results

From Figure 5.1, one derives that $a_{\text{TH}}(0) \approx 1.05 \cdot 10^3$ kg H$_2$O m^{-2} year^{-1} and $a_{\text{TH}}(365) \approx 1.13 \cdot 10^3$ kg H$_2$O m^{-2} year^{-1}. Therefore, we deduce that the background state (u_+, v_+) destabilizes at a (slightly) higher precipitation rate when the gradient slope of the terrain is steeper. We interpret this as follows: on terrains with a nontrivial gradient slope, the water runs downhill without infiltrating the soil. Therefore, the homogeneous vegetation state (u_+, v_+) at terrains with a nontrivial gradient slope destabilizes into a patterned state at a higher precipitation rate than homogeneous vegetation on flat terrains, where water slowly infiltrates the soil without running off.
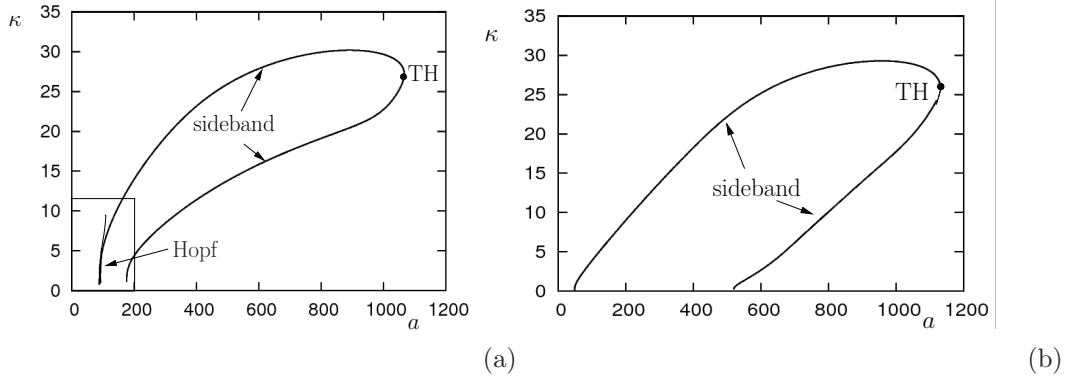
(a)   (b)

Figure 5.1: (a) Busse balloon for the GKGS-system in ecologically meaningful parameters (1.1) with $\nu = 0$ m year^{-1} and $b = 1.8$ year^{-1}. An enlargement of the indicated rectangle is presented in Figure 5.2. (b) Busse balloon for the GKGS-system in ecologically meaningful parameters (1.1) with $\nu = 365$ m year^{-1} and $b = 1.8$ year^{-1}. Both Busse balloons have been depicted on the same scale.

5.2.0.1   Near desertification   An other striking fact observed in the Busse balloons for the GKGS-model (1.1) is that the upper branch of sideband instabilities crosses the a-axis for positive $a > 0$, both for $\nu = 0$ m year^{-1} and for $\nu = 365$ m year^{-1}. Notice that this is a difference with the Busse balloons that we found for the GKGS-system in the scaling of (0.5) that have been constructed in chapter 3, where the critical value of a quickly dropped to 0 for ν increased slightly above 0 (see section 4.3.2). Numerical checks for other ν have confirmed that for each ν, there exists a precipitation rate $a = a_0^-(\nu) > 0$ such that there is no spatially periodic pattern (for any wavenumber κ).

When a is smaller than a_{TH}, the boundary of the Busse balloons in Figure 5.1 consists of sideband instabilities. For $\nu = 0$ m year^{-1}, the upper curve of sideband instabilities is crossed by the Hopf dance that has been discussed in chapter 4. See Figure 5.1(a)[1]. Therefore, spatially periodic patterns on a flat terrain destabilize into the desert state through a Hopf instability, while, at the other hand, spatially periodic patterns on a terrain with a nontrivial gradient slope destabilize into the desert state through a sideband instability. This yields one of the most intriguing ecological questions induces by our mathematical analysis: is it possible to observe from a patterned state whether it is close to a sideband instability or whether it is close to a Hopf instability?

Also, $a_0^-(\nu)$ is a decreasing function of ν: if the gradient slope increases, there are stable spatially periodic patterns for ever smaller precipitation rates. From Figure 5.1 we deduce that $a_0^-(0) \approx 8.8 \cdot 10^1$ kg H$_2$O m^{-2} year^{-1} and $a_0^-(365) \approx$

---

[1]In Figure 5.1(a), we have traced out an 'approximate' Hopf dance: the Hopf curve depicted in Figure 5.1(a) does not consist of γ-eigenvalues for fixed γ
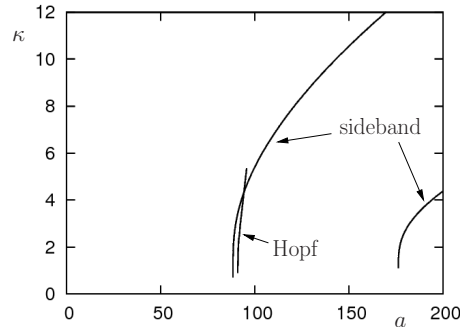
Figure 5.2: Hopf curve for the GKGS-system in ecologically meaningful parameters with $\nu = 0$ m year^{-1} and $b = 1.8$ year^{-1}. Enlargement of the inset of the Busse balloon from Figure 5.1)(a).

$5.0 \cdot 10^1$ kg H$_2$O m^{-2} year^{-1}. Loosely formulated, this means that desertification for systems with a nontrivial gradient slope happens at a *lower* precipitation rate than for systems that are flat. This may be understood by the following arguments. If the precipitation rate is small, then in the bare areas soil tends to dry out and becomes impermeable for water infiltration, so that precipitation that falls down in the bare areas eventually evaporates. The (scarce) vegetated areas are penetrated by roots that moisturize the soil, which entails that water from precipitation that falls down in vegetated areas infiltrates the soil. In systems with a nontrivial gradient slope, water runs downhill until it reaches a vegetated spot where it is taken up by the roots. In a flat system, water cannot run and will evaporate in the course of time, leaving only the water that falls on the vegetated areas to be taken up by plant roots. Therefore, if the precipitation rate is low, in flat systems there is more stress on vegetation growth than in systems that have nontrivial gradient slope.

Thus, we conclude that a steeper gradient considerably increases the total area of the Busse balloon: for each wavenumber κ, there is a considerable larger interval (a_κ^-, a_κ^+) for which stable spatially periodic patterns exist (compare Figure 5.1(a) to 5.1(b)).

An initially stable spatially periodic pattern will for decreasing a in principle not change its wavenumber, as long as (a, κ) remains inside the Busse balloon. When an initially stable pattern gradually approaches the boundary of the Busse balloon, it will, at a further decrease of the precipitation rate a, eventually destabilize. However, at the lower precipitation rate a the specific shape of the Busse balloon depicted in Figure 5.1 generally allows for stable periodic patterns with a smaller wavenumber. See Figure 5.3. Therefore, if the decrease in a is not too fast, it is expected that the original stable spatially periodic pattern is adapted such that its wavenumber becomes smaller. Note that this mechanism of decreasing the wavenumber as a consequence
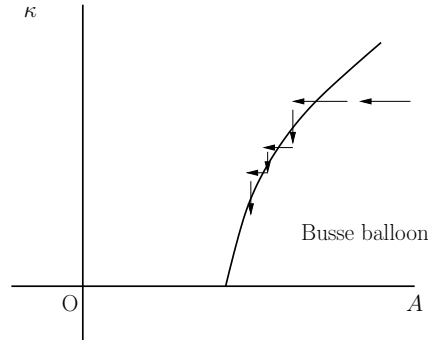
Figure 5.3: Part of a (schematic) Busse balloon for slowly changing parameters. Schematic depiction of a path that a spatially periodic pattern may follow during decreasing precipitation, after it crosses the boundary of the Busse balloon.

of decreasing a cannot work if the left boundary $k_l(a)$ of the Busse balloon is not an increasing function of a. It is remarkable that all Busse balloons constructed in this work have a boundary $k_l(a)$ that is an increasing function of a up to the point where k achieves its maximal value. Now, since the left boundary of the Busse balloons for the GKGS-system have this specific shape (see Figure 5.1), the internal dynamics will force the pattern to decrease its wavenumber a little and cross the boundary of the Busse balloon for this smaller wavenumber, so that a new (stable) spatially periodic pattern with a smaller wavenumber appears. This is confirmed by numerical simulations [87].

See Figure 5.1. Homoclinic patterns come as limit cases for spatially periodic patterns for small wavenumbers (homoclinic patterns have wavenumber $\kappa = 0$). From the Busse balloons in Figure 5.1 one deduces that also for the GKGS-system (1.1) in realistic parameters, the homoclinic pattern is the last pattern destabilizing for decreasing a. This once more confirms Ni's conjecture [60] that has been discussed in chapter 5. Therefore, we conclude that 'oasis'-like patterns, i.e. small patches of vegetation without any other vegetation in a large area surrounding, are the last remaining vegetated patterns and can no longer adapt to any other pattern at the rim of desertification.[2] On the other hand, it is in principle possible that oasis-like patterns are *not* at the edge of desertification, as there exists a range $(a_0^-(\nu), a_0^+(\nu))$ of precipitation rates for which homoclinic patterns exist. Since homoclinic patterns are stable for each $a \in (a_0^-(\nu), a_0^+(\nu))$, oasis-like patterns appear naturally in realistic settings (although we are aware that there are many other mechanisms that may explain the appearance of oasis states – such as the existence of a local water well).

---

[2]See also the discussion in §5.3.

5.3   Future work

The Busse balloons depicted in Figure 5.1 give a complete overview of the stable spatially periodic patterns described by the GKGS-model (1.1). By depicting all wavenumbers for all possible choices of a system parameter, they are in fact a graphically displayed parametrization of all stable spatially periodic patterns that solve the system under study. Their boundaries are associated to destabilization mechanisms of the (stable) spatially periodic patterns. By a (numerical) scrutiny of the spectrum associated to the linearization of a solution at the boundary of the Busse balloon, one generally specifies the type of instability that the pattern undergoes when it crosses the boundary.

One crucial assumption made throughout this thesis is that all other[3] parameters of the system are constant in time. In reality, of course, this is never the case. For example, the evaporation rate L in (1.1) depends on temperature, humidity and other environmental factors that are not constant in time, even not when one averages over longer periods of time, and therefore L itself is not constant in time.

As indicated in section 5.2.0.1, when a pattern with some fixed wavenumber reaches the boundary of the Busse balloon while the precitation rate a is slowly decreasing, it will change to a stable pattern with a smaller wavenumber. Exactly *how* this happens is not completely clear and needs further analysis.

If the precipitation rate L decreases even further, and the wavenumber of the pattern has been adapted several times, the pattern gradually aproaches the axis $\kappa = 0$. Future research should at least in part focus on the specific characteristics of the dynamics at the boundary of the Busse balloon that lead to desertification. This way, one may be able to deduce early warning signals if desertification is imminent.

An other very relevant question arises when we add a second spatial coordinate y to the model. Notice Klausmeier's original model naturally incorporates two spatial coordinates x and y. In the GKGS-model with two spatial coordinates, a more realistic description of vegetation patterns can be given. Two-dimensional spotted patterns, striped patterns and other coherent structures may then be described, as well as their instabilities.

---

[3]That is, all parameters different from the one used to construct the Busse balloon.

Chapter 6

Derivation of the Ginzburg-Landau Equation

In this appendix, we outline the derivation of the Ginzburg Landau Equation for the amplitude $\mathcal{A}$ of the pattern that appears at the Turing-Hopf bifurcation. Each of the four different cases of Figure 1.1 can be derived from the expressions given in this appendix by considering either $\gamma = 1$ or $c = 0$, or both.

In §6.0.1 we derive the Ginzburg-Landau Equation for the special case that $\gamma = 1$ and $c = \sqrt{\frac{2}{3}}b$ which was presented in §2.1.5.3.

The Ginzburg-Landau Ansatz for patterns that emerge at the Turing-Hopf instability can, for the rescaled GKGS-system (1.38), be written as

$$+ \varepsilon \begin{pmatrix} X_{02} \\ Y_{02} \end{pmatrix} + \dots$$

$$\begin{pmatrix} U \\ V \end{pmatrix} = \mathcal{A} \begin{pmatrix} 2b \\ \eta_{\gamma,c} \end{pmatrix} e^{i(k_* x + \omega_* t)} + \varepsilon \begin{pmatrix} X_{12} \\ Y_{12} \end{pmatrix} e^{i(k_* x + \omega_* t)} + \varepsilon^2 \begin{pmatrix} X_{22} \\ Y_{22} \end{pmatrix} e^{2i(k_* x + \omega_* t)} + \text{c.c.} + \dots$$

$$+ \varepsilon \begin{pmatrix} X_{13} \\ Y_{13} \end{pmatrix} e^{i(k_* x + \omega_* t)} + \text{c.c.} + \dots \tag{0.1}$$

where $\mathcal{A}$ and X_{ij} are functions of $\xi = \varepsilon x$ and $\tau = \varepsilon^2(x - c_g t)$ and c_g the group velocity defined by (1.26). Substituting this expansion in the GKGS-system (1.38) and collecting terms of equal powers of ε and the Fourier modes $e^{i(k_* x + \omega_* t)}$, we derive expressions for $X_{02,12,22,13}$ and $Y_{02,12,22,13}$ subsequently. Notice that the scaling in (1.38) has the advantage that the terms of order ε^2 only play a role in the equations for X_{13} and Y_{13}.

As mentioned in paragraph 2.1.4, the solvability condition can be applied to solve an equation of the form

$$\mathcal{M}_{i\omega_*}(a_*, k_*, c)x = y. \tag{0.2}$$

The equations for $X_{1j}, Y_{1j}, j = 2, 3$ are of this form, with

$$\mathcal{M}_{i\omega_*}(a_*, k_*, c) = \begin{pmatrix} -\Gamma k_*^2 - \frac{a_*^2}{b^2} + ick_* & -2b \\ \frac{a_*^2}{b^2} & -k_*^2 + b - i\omega_* \end{pmatrix}. \tag{0.3}$$

We briefly point out the construction of the set of solutions for (0.2). The construction for $c = 0$ differs from that for $c \neq 0$.

If $c \neq 0$, the matrix in (0.3) has two eigenvalues, $\lambda_+ = 0$ and

$$\lambda_- = -\Gamma k_*^2 - \frac{a_*^2}{b^2} + ick_* - k_*^2 + b - i\omega_*. \tag{0.4}$$

If $y \in \mathrm{Rg}\, \mathcal{M}_{i\omega_*}(a_*, k_*, c)$ and $c \neq 0$, the set of solutions to (0.2) is given by

$$x = \frac{1}{\lambda_-} y + \ker \mathcal{M}_{i\omega_*}(a_*, k_*, c).$$

On the other hand, if $c = 0$, we know from Proposition 1 in section 2.1.3 that

$$a_*^{\gamma+1} = \gamma g b^{2\gamma+1} \quad \text{and} \quad k_*^2 = \frac{1}{2}(1 - g).$$

It is then straightforward to show that

$$\mathcal{M}_{i\omega_*}(a_*, k_*, 0) = \begin{pmatrix} -\frac{1}{2}(g - 7)\left(\frac{g\gamma}{b}\right)^{\frac{2}{\gamma+1}} b^2 & -2b \\ \left(\frac{g\gamma}{b}\right)^{\frac{2}{\gamma+1}} b^2 & \frac{1}{2}b(1 + g) \end{pmatrix}, \tag{0.5}$$

and that $\lambda_- = 0$ if $\gamma = 1$. It is also straightforward to show that both columns of $\mathcal{M}_{i\omega_*}(a_*, k_*, 0)$ span the range. We call the second column v_1. So if y from (0.2) lies in the range, there exists an $\alpha \in \mathbb{R}$ such that $y = \alpha v_1$. Hence, if $c = 0$, the set of solutions to (0.2) can be presented as

$$x = \alpha \cdot \begin{pmatrix} 0 \\ 1 \end{pmatrix} + \ker \mathcal{M}_{i\omega_*}(a_*, k_*, 0). \tag{0.6}$$

By plugging in the expansion (0.1) into (1.38) one obtains at order $\mathcal{O}(\varepsilon)$ an equation for $(X_{02}, Y_{02})^T$,

$$\begin{pmatrix} X_{02} \\ Y_{02} \end{pmatrix} = \left[-2\frac{b^4}{a_*^3}|\eta_{\gamma,c}|^2 - 8\frac{b^2}{a_*}\mathrm{Re}(\eta_{\gamma,c}) \right] \begin{pmatrix} 1 \\ 0 \end{pmatrix} |\mathcal{A}^2|. \tag{0.7}$$

We will use shorthands x_{02}, y_{02} for $X_{02} = x_{02}|\mathcal{A}|^2$, $Y_{02} = y_{02}|\mathcal{A}|^2$. The values for x_{02} and y_{02} can be read from (0.7). At order $\mathcal{O}(\varepsilon E)$, we find equations of the form

$$\mathcal{M}_{i\omega_*}(a_*, k_*, c) \begin{pmatrix} X_{12} \\ Y_{12} \end{pmatrix} = \begin{pmatrix} x_{12} \\ y_{12} \end{pmatrix} \mathcal{A}_\xi$$

which can be solved if $(x_{1j}, y_{1j})^T \in \operatorname{Rg} \mathcal{M}_{i\omega_*}(a_*, k_*, c)$. We find

$$
\begin{array}{rcl}
x_{12} & = & [-4bi\Gamma k_* - 2bc]/\lambda_-; \\
y_{12} & = & [-\eta_{\gamma,c} c_{\mathrm{g}} - 2ik_* \eta_{\gamma,c}]/\lambda_-.
\end{array}
\tag{0.8}
$$

It can be checked that, indeed, $(x_{1j}, y_{1j})^T \in \operatorname{Rg} \mathcal{M}_{i\omega_*}(a_*, k_*, c)$. At order $\mathcal{O}(\varepsilon E^2)$ we find

$$
\begin{pmatrix} X_{22} \\ Y_{22} \end{pmatrix} = \begin{pmatrix} x_{22} \\ y_{22} \end{pmatrix} \mathcal{A}^2.
$$

with

$$
\begin{array}{rcl}
x_{22} & = & \left(\frac{b}{a_*}\right)^2 (4k_*^2 + 2i\omega_* - b)y_{22} - \left(\frac{b}{a_*}\right)^2 \left(\frac{b^2}{a_*}\eta_{\gamma,c}^2 + 4a_*\eta_{\gamma,c}\right) \\[2mm]
y_{22} & = & \dfrac{\frac{b^2}{a_*}\eta_{\gamma,c}^2 + 4a_*\eta_{\gamma,c} + 8b^2 k_*^2 \gamma(\gamma-1)\left(\frac{b^2}{a_*}\right)^{\gamma-2} + \left(\frac{b}{a_*}\right)^2\left(\frac{b^2}{a_*}\eta_{\gamma,c}^2 + 4a_*\eta_{\gamma,c}\right)\left(-4\Gamma k_*^2 - \left(\frac{a_*}{b}\right)^2 + 2ick_*\right)}{\left(\frac{b^2}{a_*}\right)^2(4k_*^2 + 2i\omega_* - b)\left(-4\Gamma k_*^2 - \left(\frac{a_*}{b}\right)^2 + 2ick_*\right) - 2b}
\end{array}
\tag{0.9}
$$

At order $\varepsilon^2 E$, we obtain equations for X_{13} and Y_{13}. These equations can be written as

$$
\mathcal{M}_{\omega_*}(a_*, k_*, c) \begin{pmatrix} X_{13} \\ Y_{13} \end{pmatrix} = \begin{pmatrix} I_1 \\ I_2 \end{pmatrix},
\tag{0.10}
$$

The right-hand sides I_1, I_2 are built up by several terms. The nonlinear terms from the reaction kinetics generate:

$$
\begin{array}{rcl}
2\dfrac{a_*}{b}UV & \to & 2\dfrac{a_*}{b}[2by_{22} + \eta_{\gamma,c}x_{02} + \bar{\eta}_{\gamma,c}x_{22}] \\[2mm]
\dfrac{b^2}{a_*}V^2 & \to & \dfrac{b^2}{a_*}[2\bar{\eta}_{\gamma,c}y_{22}] \\[2mm]
UV^2 & \to & 4b|\eta_{\gamma,c}|^2 + 2b\eta_{\gamma,c}^2
\end{array}
$$

We define L_{tot} as the sum of these expressions:

$$
L_{\mathrm{tot}} := (2\bar{\eta}_{\gamma,c}\frac{b^2}{a_*} + 4a_*)y_{22} + 2\frac{a_*}{b}(\eta_{\gamma,c}x_{02} + \bar{\eta}_{\gamma,c}x_{22}) + 2b(2|\eta_{\gamma,c}|^2 + \eta_{\gamma,c}^2)
\tag{0.11}
$$

The nonlinear terms that appear from working out the nonlinear diffusion terms generate:

$$U_{xx}U \quad \rightarrow \quad -2bk_*^2(x_{02} + 5x_{22})\gamma(\gamma - 1)\left(\frac{b^2}{a_*}\right)^{\gamma-2}$$

$$(U_x)^2 \quad \rightarrow \quad 8bk_*^2 x_{22}\gamma(\gamma - 1)\left(\frac{b^2}{a_*}\right)^{\gamma-2}$$

$$\frac{1}{2}U_{xx}U^2 \quad \rightarrow \quad -12b^3 k_*^2\gamma(\gamma - 1)(\gamma - 2)\left(\frac{b^2}{a_*}\right)^{\gamma-3}$$

$$(U_x)^2 U \quad \rightarrow \quad 8b^3 k_*^2\gamma(\gamma - 1)(\gamma - 2)\left(\frac{b^2}{a_*}\right)^{\gamma-3}$$

$$U_{xx} \quad \rightarrow \quad -2bk_*^2$$

From this we define:

$$L_{\mathrm{NLD}} \quad = \quad -2bk_*^2(x_{22} + x_{02})\gamma(\gamma - 1)\left(\frac{b^2}{a_*}\right)^{\gamma-2} - 4b^3 k_*^2\gamma(\gamma - 1)(\gamma - 2)\left(\frac{b^2}{a_*}\right)^{\gamma-3}$$

$$L_{\mathcal{A},\mathrm{NLD}} \quad = \quad -k_*^2\gamma(\gamma - 1)\frac{2b}{a_*}\left(\frac{b^2}{a_*}\right)^{\gamma-2}.$$

We then obtain for the right-hand side of the system

$$I_1 \quad = \quad (-4\frac{a_*}{b} - L_{\mathcal{A},\mathrm{NLD}})\mathcal{A} + (L_{\mathrm{tot}} - L_{\mathrm{NLD}})|\mathcal{A}|^2\mathcal{A} - (cx_{12} + 2b\Gamma + 2ik_*\Gamma x_{12})\mathcal{A}_{\xi\xi}$$

$$I_2 \quad = \quad 4\frac{a_*}{b}\mathcal{A} - L_{\mathrm{tot}}|\mathcal{A}|^2\mathcal{A} - (c_{\mathrm{g}}y_{12} + \eta_{\gamma,c} + 2ik_*y_{12})\mathcal{A}_{\xi\xi} + \eta_{\gamma,c}\mathcal{A}_\tau \qquad (0.12)$$

To derive the Ginzburg-Landau Equation, we impose the solvability condition (1.42) to (0.10):

$$2bI_2 - (k_*^2 + i\omega_* - b)I_1 = 0, \qquad (0.13)$$

and obtain,

$$\begin{aligned}
2b\eta_{\gamma,c}\mathcal{A}_\tau \quad = \quad & \left[2b(c_{\mathrm{g}}y_{12} + \eta_{\gamma,c} + 2ik_*y_{12}) - (k_*^2 + i\omega_* - b)(cx_{12} + 2b\Gamma + 2ik_*\Gamma x_{12})\right]\mathcal{A}_{\xi\xi} \\
& - \left[4\frac{a_*}{b}(k_*^2 + i\omega_* + b) + (k_*^2 + i\omega_* - b)L_{\mathcal{A},\mathrm{NLD}}\right]\mathcal{A} \\
& + \left[(k_*^2 + i\omega_* + b)L_{\mathrm{tot}} - (k_*^2 + i\omega_* - b)L_{\mathrm{NLD}}\right]|\mathcal{A}|^2\mathcal{A}.
\end{aligned}$$

6.0.1 The special case that $\gamma = 1$ and $c = \sqrt{\frac{2}{3}b}$

In this section we present the expressions for x_{ij}, y_{ij}, $ij = 02, 12, 22$ for the special case that $\gamma = 1$ and $c = \sqrt{\frac{2}{3}b}$. In Proposition 2 we computed that for $\gamma = 1$ and $c = \sqrt{\frac{2}{3}b}$ one has

$$k_*^2 = \frac{1}{3}b, \quad a_*^2 = \frac{1}{3}b^3, \quad \omega_* = -\frac{1}{3}b\sqrt{2} \quad \text{and} \quad c_g = -\sqrt{\frac{2}{3}b}.$$

Also, one computes the second component of a basis vector of the kernel of $\mathcal{M}_{\omega_*}(a_*, k_*, c)$ and the nonzero eigenvalue of $\mathcal{M}_{\omega_*}(a_*, k_*, c)$ as

$$\eta_{1,\sqrt{\frac{2}{3}b}} = \frac{1}{3}b\left(-2 + i\sqrt{2}\right) \quad \text{and} \quad \lambda_+ = \frac{2}{3}bi\sqrt{2}.$$

These values are used to derive

$$
\begin{aligned}
x_{02} &= 4b\sqrt{\frac{b}{3}} \\
y_{02} &= 0 \\
x_{12} &= -\frac{1}{2}\sqrt{6b}\,(2 - i\sqrt{2}) \\
y_{12} &= \frac{1}{2}\sqrt{6b} \\
x_{22} &= \frac{2}{33}b\sqrt{\frac{b}{3}}(23 + 26i\sqrt{2}) \\
y_{22} &= -\frac{2}{33}b\sqrt{\frac{b}{3}}(20 + 14i\sqrt{2})
\end{aligned}
$$

The nonlinear terms from the reaction kinetics are

$$
\begin{aligned}
2\frac{a_*}{b}UV &\rightarrow -\frac{4}{99}b^3(82 + 31i\sqrt{2}) \\
\frac{b^2}{a_*}V^2 &\rightarrow \frac{48}{99}b^3(1 + 4i\sqrt{2}) \\
UV^2 &\rightarrow \frac{4}{9}b^3(7 - 2i\sqrt{2})
\end{aligned}
$$

The sum of these expressions is

$$L_{\text{tot}} := \frac{4}{99}(7 - 5i\sqrt{2}).$$

The nonlinear diffusion terms are, of course, zero, so $L_{\text{NLD}} = L_{\mathcal{A},\text{NLD}} = 0$. We get for the right hand components as in equations (0.10):

$$
\begin{aligned}
\frac{b}{3}I_1 &= -4\sqrt{\frac{3}{b}}\mathcal{A} + \frac{4}{33}b^2(7 - 5i\sqrt{2})|\mathcal{A}|^2\mathcal{A} + (6 + 3i\sqrt{2})\mathcal{A}_{\xi\xi} \\
\frac{b}{3}I_2 &= 4\sqrt{\frac{3}{b}}\mathcal{A} - \frac{4}{33}b^2(7 - 5i\sqrt{2})|\mathcal{A}|^2\mathcal{A} + (5 - 4i\sqrt{2})\mathcal{A}_{\xi\xi} - (2 - i\sqrt{2})\mathcal{A}_\tau
\end{aligned}
$$

These give the Ginzburg-Landau Equation in (1.51):

$$\mathcal{A}_\tau = \frac{1}{3}(8 + i\sqrt{2})\mathcal{A}_{\xi\xi} + \frac{2}{9}\sqrt{\frac{3}{b}}(5 + i\sqrt{2})\mathcal{A} - \frac{2}{33}(5 - 2i\sqrt{2})b^2|\mathcal{A}|^2\mathcal{A}.$$

6.0.2   Derivation of the Ginzburg-Landau equation for the GKGS-system with $c = 0$

In this section we present the expressions for $x_{ij}, y_{ij}, ij = 02, 12, 22$ for the special case that $c = 0$. In Proposition 1 we computed that for $c = 0$ one has

$$k_*^2 = \frac{1}{2}(1 - g)b, \quad \text{and} \quad a_*^{\gamma+1} = g\gamma b^{2\gamma+1}.$$

Also, one computes the second component of a basis vector of the kernel of $\mathcal{M}_{\omega_*}(a_c, k_c, c)$ and the nonzero eigenvalue of $\mathcal{M}_{\omega_*}(a_c, k_c, c)$ as

$$\eta_{\gamma,0} = \frac{1}{2}(g - 7)\frac{a_*^2}{b^2} \quad \text{and} \quad \lambda_- = \frac{1}{2}(g - 7)\frac{a_*^2}{b^2} + \frac{1}{2}(1 + g)b$$

These values are used to derive

$$
\begin{aligned}
x_{02} &= 4a_* \\
y_{02} &= 0 \\
x_{12} &= 0 \\
y_{12} &= 2\mathrm{i}(6 - g)\frac{a_*^2}{b^3}k_* \\
x_{22} &= \frac{2}{9}[9 - 2(3 + g)\gamma]a_* \\
y_{22} &= -\frac{4}{9}(5 - g)\gamma\frac{a_*^3}{b^3}
\end{aligned}
$$

The sum of the nonlinear terms from the kinetics is

$$L_{\text{tot}} := \left[\frac{8}{9}(18 - 2g)\gamma + 6(5 - g)\right]\frac{a_*^4}{b^3}.$$

And we have

$$
\begin{aligned}
L_{\text{NLD}} &= -2bk_*^2(x_{02} + x_{22})\gamma(\gamma - 1)\left(\frac{b^2}{a_*}\right)^{\gamma-2} - 4b^3k_*^2\gamma(\gamma - 1)(\gamma - 2)\left(\frac{b^2}{a_*}\right)^{\gamma-3} \\
L_{\text{NLD},\mathcal{A}} &= -(1 - 5g)(\gamma - 1)\frac{a_*}{b}
\end{aligned}
$$

This gives the Ginzburg-Landau Equation in (1.49):

$$\mathcal{A}_\tau = 2\sqrt{2}\,\mathcal{A}_{\xi\xi} + b_1(\gamma)\mathcal{A} + \mathcal{L}_1(\gamma)|\mathcal{A}|^2\mathcal{A}$$

with

$$
\begin{aligned}
b_1(\gamma) &= \left[-39 + 27\sqrt{2} + (41 - 29\sqrt{2})\,\gamma\right]\left(\frac{g\gamma}{b}\right)^{\frac{1}{\gamma+1}} \\
\mathcal{L}_1(\gamma) &= -\frac{1}{9}(2 - \sqrt{2})\left[18(3 + 2\sqrt{2}) + 12(2 + \sqrt{2})\gamma + (-8 + 3\sqrt{2})\gamma^2\right]\left(\frac{g\gamma}{b}\right)^{\frac{2}{\gamma+1}}b^3
\end{aligned}
$$

6.0.3 Derivation of the Ginzburg-Landau equation for the case $c \gg 1$: the Klausmeier model and the GKGS-model for $c \gg 1$

This appendix to §2.1.6 deals with three themes: first, we give an elaborate account on the scalings introduced in 2.1.6 that were used to derive the Klausmeier system (1.53) from the GKGS-system. Secondly, we derive the GLE for the Klausmeier system (0.33).

Scaling analysis for the Klausmeier system as a limit case of the GKGS system. We remark that the equilibria for both systems (0.5) and (1.53) are the same. Patterns close to the equilibrium (U_+, V_+) can be described as

$$
\begin{aligned}
U &= \delta^{2\beta-\alpha}(\hat{U}_+ + \varepsilon\hat{U}(x,t)); \\
V &= \delta^{\alpha-\beta}(\hat{V}_+ + \varepsilon\hat{V}(x,t)).
\end{aligned}
\tag{0.14}
$$

Substitution of these expansions in (0.5) gives the leading order formulation (1.38). We are interested in the behaviour of the GKGS-model for $0 < 1/\sqrt{c} \ll \varepsilon \ll 1$. Since we know from Proposition 2 that $a_c = \mathcal{O}(\sqrt{c})$, we put $a_* = \bar{a}_*\sqrt{c}$ and obtain for (1.38),

$$
\begin{aligned}
\delta^{3\beta-2\alpha}U_t &= c^{-\frac{1}{2}(\gamma-1)}\gamma\left(\frac{b^2}{\bar{a}_*}\right)^{\gamma-1}U_{xx} + cU_x - [c\frac{\bar{a}_*^2}{b^2}U + 2bV] \\
&\quad + \varepsilon\left[\gamma(\gamma-1)\left(\frac{b^2}{\bar{a}_*\sqrt{c}}\right)^{\gamma-2}[U_{xx}U + (U_x)^2] - \frac{b^2}{\bar{a}_*}\sqrt{c}V^2 - 2\frac{\bar{a}_*}{b}\sqrt{c}UV\right] \\
&\quad + \varepsilon^2\left[\gamma(\gamma-1)(\gamma-2)\left(\frac{b^2}{\bar{a}_*\sqrt{c}}\right)^{\gamma-3}[U(U_x)^2 + \frac{1}{2}U^2U_{xx}]\right. \\
&\qquad\qquad \left. + \gamma(\gamma-1)\frac{1}{\bar{a}_*\sqrt{c}}\left(\frac{b^2}{\bar{a}_*\sqrt{c}}\right)^{\gamma-1}U_{xx} + 2r\frac{\bar{a}_*}{b^2}\sqrt{c}U - UV^2\right] \\
V_t &= V_{xx} + \left[\frac{\bar{a}_*^2c}{b^2}U + bV\right] + \varepsilon\left[\frac{b^2}{\bar{a}_*\sqrt{c}}V^2 + 2\frac{\bar{a}_*}{b}\sqrt{c}UV\right] - \varepsilon^2\left[2r\frac{\bar{a}_*}{b^2}\sqrt{c}U - UV^2\right].
\end{aligned}
\tag{0.15}
$$

In order to derive the Klausmeier model, we must scale the components U and V such that the diffusion coefficient in the first component of (1.38) is of higher order in $1/\sqrt{c}$ than the other terms in the equations. The other terms must balance at the same, highest order. In order to obtain this, we scale U, V and r such that

$$
U = \frac{\bar{U}}{\sqrt{c}}, \quad V = \sqrt{c}\bar{V} \quad \text{and} \quad r = \bar{r}\sqrt{c}.
\tag{0.16}
$$

With these scalings we obtain for (0.15), by neglecting higher orders of δ and $1/\sqrt{c}$,

$$
\begin{aligned}
0 &= \bar{U}_{\tilde{x}} - [\frac{\bar{a}_*^2}{b^2}\bar{U} + 2\bar{V}] \\
&\quad -\varepsilon\left[\frac{b^2}{\bar{a}_*}\bar{V}^2 + 2\frac{\bar{a}_*}{b}\bar{U}\bar{V}\right] + \varepsilon^2\left[2\bar{r}\frac{\bar{a}_*}{b^2}\bar{U} - \bar{U}\bar{V}^2\right] \\
\bar{V}_{\bar{t}} &= \bar{V}_{\bar{x}\bar{x}} + [\frac{\bar{a}_*^2}{b^2}\bar{U} + \bar{V}] \\
&\quad +\varepsilon\left[\frac{b^2}{\bar{a}_*}\bar{V}^2 + 2\frac{\bar{a}_*}{b}\bar{U}\bar{V}\right] - \varepsilon^2\left[2\bar{r}\frac{\bar{a}_*}{b^2}\bar{U} - \bar{U}\bar{V}^2\right].
\end{aligned}
\tag{0.17}
$$

We can now scale out b by putting

$$\bar{U} = \tilde{U}b^{3/4}; \quad \bar{V} = \tilde{b}^{1/4}V; \quad \bar{a}_c = \tilde{a}_c b^{5/4};$$
$$x = b^{-1/2}\tilde{x}; \quad t = b^{-1/4}\tilde{t}; \quad \bar{r} = \tilde{r}b^{5/4}, \tag{0.18}$$

and obtain, to leading order in ε and neglecting higher order terms of δ and $\frac{1}{\sqrt{c}}$,

$$
\begin{aligned}
0 &= \tilde{U}_{\tilde{x}} - [\tilde{a}_*^2\tilde{U} + 2\tilde{V}] \\
&\quad -\varepsilon\left[\tfrac{1}{\tilde{a}_*}\tilde{V}^2 + 2\tilde{a}_*\tilde{U}\tilde{V}\right] + \varepsilon^2\left[2\tilde{r}\tilde{a}_*\tilde{U} - \tilde{U}\tilde{V}^2\right] \\
\tilde{V}_{\tilde{t}} &= \tilde{V}_{\tilde{x}\tilde{x}} + [\tilde{a}_*^2\tilde{U} + \tilde{V}] \\
&\quad +\varepsilon\left[\tfrac{1}{\tilde{a}_*}\tilde{V}^2 + 2\tilde{a}_*\tilde{U}\tilde{V}\right] - \varepsilon^2\left[2\tilde{r}\tilde{a}_*\tilde{U} - \tilde{U}\tilde{V}^2\right].
\end{aligned}
\tag{0.19}
$$

This system is the one presented in (1.55).

Derivation of the GLE for the Klausmeier system: the regime $0 < 1/\sqrt{c} \ll \varepsilon \ll 1$.   From (0.19) one derives the dispersion relation associated to the linearization about the background state (U_+, V_+) in the Klausmeier model, neglecting higher orders of ε,

$$\det \mathcal{M}_\lambda(\tilde{a}_*, i\tilde{k}) := \det\begin{pmatrix} -\tilde{a}_*^2 + i\tilde{k} & -2 \\ \tilde{a}_*^2 & 1 - \tilde{k}^2 - \tilde{\lambda} \end{pmatrix} = 0. \tag{0.20}$$

We apply conditions (1.7) to derive critical parameters. Working out the dispersion relation (0.20) using condition $(1.7)_1$,

$$
\begin{aligned}
i\tilde{\omega}\tilde{a}_*^2 + i\tilde{k}(1 - \tilde{k}^2) &= 0; \\
\tilde{\omega}\tilde{k} + (\tilde{k}^2 - 1)\tilde{a}_*^2 + 2\tilde{a}_*^2 &= 0.
\end{aligned}
\tag{0.21}
$$

From these relations one derives

$$\tilde{k}^2(\tilde{k}^2 - 1) + \tilde{a}_*^4(\tilde{k}^2 + 1) = 0. \tag{0.22}$$

and by solving equation $(0.21)_1$ for $\tilde{\omega}$ we get

$$\tilde{\omega}_* = \tilde{k}_*(\tilde{k}_*^2 - 1)\frac{1}{\tilde{a}_*^2}, \tag{0.23}$$

and thus

$$\frac{\partial\tilde{\omega}}{\partial\tilde{k}} = \frac{1}{\tilde{a}_*^2}(3\tilde{k}^2 - 1). \tag{0.24}$$

Differentiating (0.24) with respect to $\tilde{k}$ and substituting equation $(0.21)_2$ into the result, we get

$$2\tilde{k}^2 - 1 + \tilde{a}_*^4 = 0. \tag{0.25}$$

Solving (0.22) and (0.25) for $\tilde{a}$ and $\tilde{k}$ then gives

$$\tilde{a}_*^2 = \sqrt{2} - 1 \quad \text{and} \quad \tilde{k}_*^2 = \sqrt{2} - 1, \tag{0.26}$$

which are the expressions for large c that we had derived in Proposition 2. From these expressions for $\tilde{a}_*$ and $\tilde{k}_*$ we further derive the critical frequency and the group speed

$$\begin{aligned}
\tilde{\omega}_* &= -\sqrt{2}\sqrt{\sqrt{2} - 1}; \\
\tilde{c}_{\mathrm{g}} &= -\frac{\partial \tilde{\omega}}{\partial \tilde{k}}\big|_{k=k_*} = -2 + \sqrt{2}.
\end{aligned} \tag{0.27}$$

From (0.20) it follows that the kernel and range of the linearization about the equilibrium $(\tilde{U}_+, \tilde{V}_+)$ equal

$$\ker \mathcal{M}_{\mathrm{i}\tilde{\omega}_*}(\tilde{a}_*, \tilde{k}_*) = \begin{pmatrix} 2 \\ -\tilde{a}_*^2 + \mathrm{i}k_* \end{pmatrix} \tag{0.28}$$

and

$$\mathrm{Rg}\,\mathcal{M}_{\mathrm{i}\tilde{\omega}_*}(\tilde{a}_*, \tilde{k}_*) = \begin{pmatrix} -2 \\ 1 - \tilde{k}_*^2 - \mathrm{i}\tilde{\omega}_* \end{pmatrix}$$

From the expression for the range of $\mathcal{M}_{\mathrm{i}\tilde{\omega}_*}(\tilde{a}_*, \tilde{k}_*)$ we derive that the equations

$$\mathcal{M}_{\mathrm{i}\tilde{\omega}}(\tilde{a}_*, \tilde{k}_*)x = f$$

can be solved for x if and only if $f \in \mathrm{Rg}\,\mathcal{M}_{\mathrm{i}\tilde{\omega}_*}(\tilde{a}_*, \tilde{k}_*)$, that is, if f fullfills the *solvability condition*

$$2f_2 + [1 - \tilde{k}_*^2 - \mathrm{i}\tilde{\omega}_*]f_1 = 0. \tag{0.29}$$

Since $\mathrm{Det}\,\mathcal{M}_{\mathrm{i}\tilde{\omega}_*}(\tilde{a}_*, \tilde{k}_*) = 0$, it follows that the unique solution to the equation $\mathcal{M}_{\mathrm{i}\tilde{\omega}_*}(\tilde{a}_*, \tilde{k}_*)x = f$ is

$$x = \frac{1}{\lambda_-}f$$

with λ_- the nonzero eigenvalue of $\mathcal{M}_{i\tilde{\omega}_*}(\tilde{a}_*, \tilde{k}_*)$,

$$\lambda_- := \mathrm{Tr}\,\mathcal{M}_{\mathrm{i}\tilde{\omega}}(\tilde{a}_*, \tilde{k}_*) = -\tilde{a}_*^2 + \mathrm{i}k_* + 1 - \tilde{k}_*^2 - \mathrm{i}\tilde{\omega}_*. \tag{0.30}$$

By using (0.28), the expansion (U, V) that describes the pattern near its onset (i.e. for $\tilde{a} = \tilde{a}_* - \tilde{r}\varepsilon^2$) can be written out as

$$\begin{pmatrix} U \\ V \end{pmatrix} = \mathcal{A}(\xi, \tau)\begin{pmatrix} 2 \\ \eta \end{pmatrix} e^{\mathrm{i}(\tilde{k}_* x + \tilde{\omega}_* t)} + \mathrm{c.c.} + \mathrm{h.o.t.}, \tag{0.31}$$

with the shorthand

$$\eta := -\tilde{a}_*^2 + \mathrm{i}\tilde{k}_*.$$

As pointed out in at the begin of Appendix 6, in the Ginzburg-Landau formalism

one subsequently derives equations of the form $X_{02} = x_{02}\mathcal{A}^2, Y_{02} = y_{02}\mathcal{A}^2, X_{12} = x_{12}\mathcal{A}_\xi, Y_{12} = y_{12}\mathcal{A}_\xi, X_{22} = x_{22}|\mathcal{A}|^2, Y_{22} = y_{22}|\mathcal{A}|^2$. The formulas for x_{ij} and y_{ij} are derived by substituting the expansion (0.31) in the leading order system (0.19) and collecting terms of order $\varepsilon^{j-1}E^i$ (with shorthand $E = e^{i(\tilde{k}_c x + \tilde{\omega}_c t)}$) and solving them for X_{ij} and Y_{ij}:

$$
\begin{aligned}
x_{02} &= -2\frac{1}{\tilde{a}_*^3}|\eta|^2 - 4\frac{1}{\tilde{a}_*}(\bar{\eta}+\eta) \\
y_{02} &= 0 \\
x_{12} &= \frac{-2}{\lambda_-} \\
y_{12} &= \frac{1}{\lambda_-}(\eta c_g - 2\eta i \tilde{k}_c) \\
x_{22} &= \frac{2i\tilde{k}_*[\frac{1}{\tilde{a}_*}\eta^2 + 4\tilde{a}_*\eta]}{[-\tilde{a}_*^2 + 2i\tilde{k}_*]\cdot[4\tilde{k}_*^2 + 2i\tilde{\omega}_* - 1] - 2\tilde{a}_*^2} \\
y_{22} &= \frac{1}{\tilde{a}_*^2}[4\tilde{k}_*^2 + 2i\tilde{\omega} - 1]x_{22} - \frac{1}{\tilde{a}_*^2}[\frac{1}{\tilde{a}_*}\eta^2 + 4\tilde{a}_*\eta]
\end{aligned}
\tag{0.32}
$$

The Ginzburg-Landau Equation that describes the onset of patterns in the Klausmeier system (0.19) reads

$$
\begin{aligned}
2\eta A_\tau &= -[2(v_g y_{12} - \eta - 2i\tilde{k}_* y_{12}) - x_{12}(1 - \tilde{k}_*^2 - i\tilde{\omega}_*)]A_{\xi\xi} \\
&\quad - 4\tilde{r}\tilde{a}_*[1 + \tilde{k}_* + i\tilde{\omega}]A + [1 + \tilde{k}_* + i\tilde{\omega}]L_{\text{tot}}|A|^2 A
\end{aligned}
\tag{0.33}
$$

with

$$
L_{\text{tot}} = \frac{2\bar{\eta}}{\tilde{a}_*}y_{22} + 4\tilde{a}_*^2 y_{22} + 2\tilde{a}_*\eta x_{02} + 2\tilde{a}_*\bar{\eta}x_{22} + 4|\eta|^2 + 2\eta^2.
$$

If one works out the parameter values for $\tilde{a}_*^2 = \sqrt{2} - 1$ and $\tilde{k}_*^2 = \sqrt{2} - 1$, the leading order system (0.19) becomes

$$
\begin{aligned}
0 &= \tilde{U}_{\tilde{x}} - [(\sqrt{2}-1)\tilde{U} + 2\tilde{V}] \\
&\quad - \varepsilon\left[\frac{1}{\sqrt{\sqrt{2}-1}}\tilde{V}^2 + 2\sqrt{\sqrt{2}-1}\tilde{U}\tilde{V}\right] + \varepsilon^2\left[2\tilde{r}\sqrt{\sqrt{2}-1}\tilde{U} - \tilde{U}\tilde{V}^2\right] \\
\tilde{V}_{\tilde{t}} &= \tilde{V}_{\tilde{x}\tilde{x}} + [(\sqrt{2}-1)\tilde{U} + \tilde{V}] \\
&\quad + \varepsilon\left[\frac{1}{\sqrt{\sqrt{2}-1}}\tilde{V}^2 + 2\sqrt{\sqrt{2}-1}\tilde{U}\tilde{V}\right] - \varepsilon^2\left[2\tilde{r}\sqrt{\sqrt{2}-1}\tilde{U} - \tilde{U}\tilde{V}^2\right].
\end{aligned}
\tag{0.34}
$$

The matrix that describes the linear leading order part of this system is then

$$
\mathcal{M}_\lambda(\tilde{a}_*, k) := \begin{pmatrix} -\sqrt{2} + 1 + i\sqrt{\sqrt{2}-1} & -2 \\ \sqrt{2} - 1 & 2 - \sqrt{2} + i\sqrt{2}\sqrt{\sqrt{2}-1} \end{pmatrix},
\tag{0.35}
$$

Working out the levels for the different expressions (0.32), we get

$$
\begin{aligned}
x_{02} &= (4 - 2\sqrt{2})\sqrt{\sqrt{2} - 1} \\
y_{02} &= 0 \\
x_{12} &= -\tfrac{1}{41}\left[10 - 3\sqrt{2} - \mathrm{i}(40 + 29\sqrt{2})\sqrt{\sqrt{2} - 1}\right] \\
y_{12} &= \tfrac{1}{82}\left[78\sqrt{2} - 96 + \mathrm{i}(16\sqrt{2} - 108)\sqrt{\sqrt{2} - 1}\right] \\
x_{22} &= \tfrac{1}{69}\left[(61\sqrt{2} + 40)\sqrt{\sqrt{2} - 1} + 2\mathrm{i}(67\sqrt{2} - 13)\right] \\
y_{22} &= -\tfrac{2}{69}\left[(10\sqrt{2} + 42)\sqrt{\sqrt{2} - 1} + \mathrm{i}(5\sqrt{2} - 2)\right]
\end{aligned}
\tag{0.36}
$$

and

$$
L_{\mathrm{tot}} = -44 + 32\sqrt{2} + \mathrm{i}[-20 + 18\sqrt{2}]\sqrt{\sqrt{2} - 1}.
$$

The Ginzburg-Landau equation then becomes

$$
\begin{aligned}
-2[\sqrt{2} - 1 + \mathrm{i}\sqrt{\sqrt{2} - 1}]\mathcal{A}_\tau ={}& -\tfrac{1}{41}[594 - 416\sqrt{2} + \mathrm{i}(330 - 304\sqrt{2})\sqrt{\sqrt{2} - 1}]\mathcal{A}_{\xi\xi} \\
& - 4\tilde{r}\left[\sqrt{2}\sqrt{\sqrt{2} - 1} - i(2 - \sqrt{2})\right]\mathcal{A} \\
& + \tfrac{4}{69}\left[-885 + 637\sqrt{2} + \mathrm{i}(183 - 170\sqrt{2})\sqrt{\sqrt{2} - 1}\right]|\mathcal{A}|^2\mathcal{A}
\end{aligned}
$$

or equivalently,

$$
\begin{aligned}
\mathcal{A}_\tau ={}& \tfrac{1}{41}\left[(66 - 56\sqrt{2}) - \mathrm{i}(63 - 23\sqrt{2})\sqrt{\sqrt{2} - 1}\right]\mathcal{A}_{\xi\xi} \\
& + \tilde{r}\left[4\sqrt{\sqrt{2} - 1} + i(4 - 2\sqrt{2})\right]\mathcal{A} \\
& + \tfrac{4}{69}\left[-807 + 534\sqrt{2} + \mathrm{i}(418 - 286\sqrt{2})\sqrt{\sqrt{2} - 1}\right]|\mathcal{A}|^2\mathcal{A}
\end{aligned}
$$

The GLE for the GKGS model for $c \gg 1$: the regime $0 < \varepsilon \ll 1/\sqrt{c} \ll 1$.
As in the previous section, we scale the leading order system of the GKGS model according to (1.54). We then obtain the leading order system (1.57). To first order in ε, the leading order system (1.57) reads

$$
\mathcal{M}_\lambda^c(\tilde{a}_*, \mathrm{i}\tilde{k}) := \begin{pmatrix} -\gamma a_*^{1-\gamma}c^{-\frac{1}{2}\gamma}b^{\frac{3}{4}\gamma - \frac{1}{4}}\tilde{k}^2 + c^{1/2}[i\tilde{k} - \tilde{a}_*^2] & -2c^{1/2} \\ \tilde{a}_*^2 & 1 - \tilde{k}^2 - \tilde{\lambda} \end{pmatrix}.
\tag{0.37}
$$

First, we remark that for $\gamma \geq 1$ the linear part of the nonlinear diffusion in the GKGS-model is in leading order $\leq \mathcal{O}(c^{-1/2})$. Secondly, we remark that to leading order in c, it holds that

$$
\det \mathcal{M}_\lambda^c(\tilde{a}_*, \mathrm{i}\tilde{k}) = c^{1/2}\mathcal{M}_\lambda(\tilde{a}_*, \mathrm{i}\tilde{k}) + \mathcal{O}(c^{\frac{1}{2}(1-\gamma)})
$$

with $\mathcal{M}_\lambda(\tilde{a}_*, i\tilde{k})$ as defined in (0.20). Therefore, the critical $\tilde{k}_*$, $\tilde{a}_*$, $\tilde{\omega}_*$ and $\tilde{c}_g$ are to leading order in c as in (0.26) and (0.27).

The solvability condition is as in (0.29). Using the leading order system (1.57), we compute

$$
\begin{aligned}
x_{02} &= -2\tfrac{1}{\tilde{a}_*^3}|\eta|^2 - 4\tfrac{1}{\tilde{a}_*}(\bar{\eta} + \eta) \\
y_{02} &= 0 \\
x_{12} &= \frac{l_0 \cdot c^{-\frac{1}{2}\gamma} - 2}{\lambda_-} \\
y_{12} &= \frac{1}{\lambda_-}(\eta c_g - 2\eta i\tilde{k}_c) \\
x_{22} &= \frac{1}{\tilde{a}_*^2}[4\tilde{k}_*^2 + 2i\tilde{\omega} - 1]y_{22} - \frac{1}{\tilde{a}_*^2}\left[\tfrac{1}{\tilde{a}_*}\eta^2 + 4\tilde{a}_*\eta\right] \\
y_{22} &= \frac{-l_1 c^{-\theta_1} - l_2 c^{-\theta_2}\frac{1}{\tilde{a}_*}\eta^2 + 4\tilde{a}_*\eta + \frac{1}{a^2}[-l_3 c^{-\theta_2} - a^2 + 2i\tilde{k}][\tfrac{1}{a}\eta^2 + 4a\eta]}{[l_4 \cdot c^{-\theta_4} - \tilde{a}_*^2 + 2i\tilde{k}_*] \cdot [4\tilde{k}_*^2 + 2i\tilde{\omega}_* - 1] - 2\tilde{a}_*^2}
\end{aligned}
\qquad (0.38)
$$

In (0.38) it is understood that all l_i, $i = 0, \ldots, 4$ do not depend on c and that $\theta_i \geq 0$ for $i = 0, \ldots, 4$. We have not computed the l_i and θ_i explicitly. This gives for the GLE of the GKGS-model in general form

$$
\begin{aligned}
2\eta\mathcal{A}_\tau &= -\left[2(c_g y_{12} - \eta - 2i\tilde{k}_* y_{12}) - (x_{12} + \text{const} \cdot c^{-\frac{1}{2}\gamma})(1 - \tilde{k}_*^2 - i\tilde{\omega}_*)\right]\mathcal{A}_{\xi\xi} \\
&\quad - \left[4\tilde{r}\tilde{a}_*(1 + \tilde{k}_*^2 + i\tilde{\omega}) + (\tilde{k}_*^2 + i\tilde{\omega} - 1)L_{\mathcal{A},\text{NLD}}\right]\mathcal{A} \\
&\quad + \left[(1 + \tilde{k}_*^2 + i\tilde{\omega})L_{\text{tot}} - (\tilde{k}_*^2 + i\tilde{\omega} - 1)L_{\text{NLD}}\right]|\mathcal{A}|^2\mathcal{A}
\end{aligned}
$$

$$(0.39)$$

with

$$
\begin{aligned}
L_{\text{NLD}} &= -\tilde{k}_*^2(x_{22} + x_{02}) \cdot \text{const} \cdot c^{-\frac{1}{2}(1+\gamma)} - 4\tilde{k}_*^2 \cdot \text{const} \cdot c^{-\frac{1}{2}(1+\gamma)} \\
L_{\mathcal{A},\text{NLD}} &= -\tilde{k}_* \cdot \text{const} \cdot c^{-\frac{1}{2}\gamma}
\end{aligned}
$$

We have not bothered about calculating the constant denoted by "const", since for asymptotically large c the associated expressions only play a role at higher order. That is, for asymptotically large $c \gg 1$ it is immediate that (0.39) reduces to (0.33). Using the expressions (0.38) for $\tilde{k}$, $\tilde{a}$, $\tilde{\omega}$ and c_g one obtains the GLe for the Klausmeier system (0.33).

Bibliography

[1] I. Aranson and L. Kramer [2002], The world of the Ginzburg-Landau equation, *Rev. Modern Phys.* **74**, 99-143.

[2] P. Atela, C.Golé, S. Hotton [2002], A dynamical system for plant pattern formation: a rigorous analysis, *J. Nonlinear Sc.* **12**, 641-676.

[3] F. Borgogno, P. D'Odorico, F. Laio, L. Ridolfi [2008] Mathematical Models of vegetation Pattern Formation in Ecohydrology, *Reviews of Geophysics* **47**.

[4] F.H. Busse [1978], Nonlinear properties of thermal convection, *Rep. Prog. Phys.* **41**, 1929-1967.

[5] W. Chen and M.J. Ward [2009], Oscillatory instabilities and dynamics of multi-spike patterns for the one-dimensional Gray-Scott model, *European J. Appl. Math.* **20** no. 2, 187214.

[6] P. Chossat and G. Iooss [1994] *The Couette-Taylor problem.* Applied Mathematical Sciences **102**, Springer-Verlag.

[7] P. Collet, J.-P. Eckmann [1990], The time dependent amplitude equation for the Swift-Hohenberg problem, *Comm. Math. Phys.* **132**, no. 1, 139153.

[8] V. Deblauwe, N. Barbier, P. Couteron, et al. [2008], The global biogeography of semi-arid periodic vegetation patterns, *Global Ecology and Biogeography* **17**(6), 715-723.

[9] R.L Devaney, Reversible Diffeomorphisms and Flows [1976], *Trans. Am. Math. Soc.* **218**, 89-113.

[10] E.J. Doedel. AUTO-07P: Continuation and bifurcation software for ordinary differential equations, http://cmvl.cs.concordia.ca/auto.

[11] A. Doelman [1990]. *On the Nonlinear Evolution of Patterns. Modulation Equations and their Solutions..* PhD thesis, Rijksuniversiteit Utrecht.

[12] A. Doelman [1996], Breaking the hidden symmetry in the Ginzburg-Landau equation, *Physica D* **97**(4), 398-428.

[13] A. Doelman [2012], An explicit theory for pulses in two component singularly perturbed reaction-diffusion equations, in preparation.

[14] A. Doelman and W. Eckhaus [1991], Periodic and quasi-periodic solutions of degenerate modulation equations, *Physica D* **53**, 249-266.

[15] A. Doelman, R.A. Gardner, and C.K.R.T. Jones [1995], Instability of quasiperiodic solutions of the Ginzburg-Landau equation, *Proc. Roy. Soc. Edinburgh Sect. A* **125**(3), 501-517.

[16] A. Doelman, R.A. Gardner and T.J. Kaper [1998], Stability analysis of singular patterns in the 1-D Gray–Scott model: a matched asymptotics approach, *Physica D* **122**(1-4), 1-36.

[17] A. Doelman, R. A. Gardner and T.J. Kaper [2001], Large stable pulse solutions in reaction-diffusion equations, *Ind. Univ. Math. J.* **50**, 443-507.

[18] A. Doelman, R. A. Gardner and T.J. Kaper [2002], A stability index analysis of 1-D patterns of the Gray–Scott model, *Memoirs AMS* **155**, (737).

[19] A. Doelman, T. J. Kaper and P. Zegeling [1997], Pattern formation in the one-dimensional Gray-Scott model, *Nonlinearity* **10**, 523-563.

[20] A. Doelman, G. Schneider [2001]. *The complex Ginzburg-Landau equation.* Unpublished notes.

[21] A. Doelman, J.D.M. Rademacher and S. van der Stelt [2012], Hopf dances near the tips of Busse balloons, *Discr. Cont. Dyn. Syst. (S)* **5**(1), 61-92.

[22] A. Doelman, T.J. Kaper, H. van der Ploeg [2001], Spatially periodic and aperiodic multi-pulse patterns in the one-dimensional Gierer-Meinhardt equation, *Methods Appl. Anal.* **8**, no. 3, 387414.

[23] A. Doelman, T. J. Kaper and P. Zegeling [1997], Pattern formation in the one-dimensional Gray-Scott model, *Nonlinearity* **10**, 523-563.

[24] A. Doelman and H. van der Ploeg [2002], Homoclinic stripe patterns, *SIAM J. Appl. Dyn. Syst.* **1**(1), 65–104.

[25] A. Doelman, B. Sandstede, A. Scheel and G. Schneider [2009], The dynamics of modulated wave trains, *Memoirs of the AMS* **199** (2009), (934).

[26] S. Douady, Y. Couder [1996], Phyllotaxis as a Self-Organizing Iterative Process, Part I, *J. Theor. Biol.* **178**, 255-274.

[27] S. Douady, Y. Couder [1996], Phyllotaxis as a Self-Organizing Iterative Process, Part II, *J. Theor. Biol.* **178**, 275-294.

[28] S. Douady, Y. Couder [1996], Phyllotaxis as a Self-Organizing Iterative Process, Part III, *J. Theor. Biol.* **178**, 295-312.

[29] W. Eckhaus [1979]. *Asymptotic analysis of singular perturbations.* Studies in Mathematics and its Applications **9**, North-Holland Publishing Co., Amsterdam-New York.

[30] W. Eckhaus and G. Iooss [1989], *Strong selection or rejection of spatially periodic patterns in degenerate bifurcations*, Physica D **39**, 124-146.

[31] L. Edelstein-Keshet [1988]. *Mathematical Models in Biology.* Random House, New York, 1988.

[32] E. G. Eszter [1999], *Evans function analysis of the stability of periodic traveling wave solutions of the FitzHugh-Nagumo system.* PhD thesis, U. of Massachusetts in Amherst.

[33] L.C. Evans [1998]. *Partial Differential Equations.* Amer. Math. Soc..

[34] T. Gallay [1995], *Periodic patterns and traveling fronts for the Ginzburg-Landau equation*, Proceedings of the IUTAM/ISIMM Symposium on Structure and Dynamics of Nonlinear Waves in Fluids, volume 7 of Adv. Ser. Nonlinear. Dynam. 230-238, World Sci. Publishing, River Edge NJ, 1995.

[35] R.A. Gardner [1993], On the structure of the spectra of periodic travelling waves, *J. Math. Pure Appl.* **72**, 415-439.

[36] R.A. Gardner [1997], Spectral analysis of long wavelength periodic waves and applications, *J. Reine Angew. Math.* **491**, 149-181.

[37] A. Gierer and H. Meinhardt [1972], A theory of biological pattern formation, *Kybernetik* **12**, pp. 3039.

[38] James Gleick [1987]. *Chaos: Making a new science.* Viking Penguin, 1987.

[39] D. Henry [1981]. *Geometric Theory of semilinear parabolic equations.* Lecture notes in Mathematics **840**, Springer, Berlin.

[40] A. Hodges [1983]. *Alan Turing: the enigma*, Simon & Schuster, New York.

[41] R. HilleRisLambers, M. Rietkerk, F. van den Bosch, H.H.T. Prins, H. de Kroon [2001], Vegetation pattern formation in semi-arid grazing systems, *Ecology* **81**(1) 50-61.

[42] IPCC[2007]. *IPCC Fourth Assessment Report: Climate Change 2007.* http://www.ipcc.ch/

[43] D. Iron and M.J. Ward [2002], The dynamics of multi-spike solutions to the one-dimensional Gierer–Meinhardt model, *SIAM J. Appl. Math.* **62**(6), 1924-1951.

[44] D. Iron, M.J. Ward and J. Wei [2001], The stability of spike solutions to the one-dimensional Gierer-Meinhardt model, *Physica D* **150**, 25-62.

[45] S. Kefi, M. Rietkerk, C.L. Alados, Y. Pueyo, V.P. Papanastasis, A. ElAich, P.C. de Ruiter [2007], Spatial vegetation patterns and imminent desertification in Mediterranean arid ecosystems, *Nature 449* **7159** 213-217.

[46] C.A. Klausmeier [1999], Regular and irregular patterns in semi-arid vegetation, *Science* **284** 1826-1828.

[47] R. Knutti [2008], Should we believe model predictions of future climate change?, *Philosophical Transactions* **366** 4647-4664.

[48] T. Kolokolnikov, M. Ward and J. Wei [2005], The existence and stability of spike equilibria in the one-dimensional Gray-Scott model: the pulse-splitting regime, *Physica D* **202**, 258-293.

[49] T. Kolokolnikov, M.J. Ward and J. Wei [2005], The existence and stability of spike equilibria in the one-dimensional Gray-Scott model: the low feed-rate regime, *Stud. Appl. Math.* **115** (2005), 21-71.

[50] M. Kunz [2001], Dynamical Models of Phyllotaxis, *Physica D* **157**, 147-165.

[51] R. Levefer and O. Lejeune [1997], On the origin of tiger bush, *Bulletin of Mathematical Biology* **59** 263-294.

[52] W.A. Macfadyan [1950a], Soil and vegetation in British Somaliland, *Nature* **165** 121.

[53] W.A. Macfadyan [1950b], Vegetation patterns in the semi-desert planes of British Somaliland, *Geographical Journal* **71** 107-130.

[54] B. J. Matkowsky and V. A. Volpert [1993], Stability of plane wave solutions of complex Ginzburg-Landau equations, *Quart. Appl. Math.* **51**, 265-281.

[55] A. Mielke [2002], The Ginzburg-Landau equation in its role as modulation equation, *Handbook of Dynamical Systems, II* (ed. B. Fiedler), Elsevier, pp. 759-835.

[56] D.S. Morgan, A. Doelman and T.J. Kaper [2002], Stationary periodic patterns in the 1D Gray-Scott model, *Meth. Appl. Anal.* **7**(1), 105-150.

[57] C. B. Muratov and V. V. Osipov [2001], Traveling spike autosolitons in the Gray-Scott model, *Physica D* **155**(1-2), 112–131.

[58] C. Muratov and V.V. Osipov [2002], Stability of the static spike autosolitons in the Gray-Scott model, *SIAM J. Appl. Math.* **62**(5), 1463-1487.

[59] A. Newell, J. Whitehead [1969], Finite bandwidth, finite amplitude convection, *J. Fluid Mech.* **38**, 279-303.

[60] W.-M. Ni [1998], Diffusion, cross-diffusion, and their spike-layer steady states, *Notices AMS*, **45**(1), 9-18.

[61] Y. Nishiura [2002]. *Far-from-equilibrium Dynamics*. Am. Math. Soc., Providence, Rhode Island.

[62] Y. Nishiura and D. Ueyama [1999], A skeleton structure for self-replication dynamics, *Physica D* **130**, 73-104.

[63] Y. Nishiura and D. Ueyama [2001], Spatio-temporal chaos for the Gray-Scott model, *Physica D* **150**, 137-162.

[64] M. Oh and K. Zumbrun [2003], Stability of periodic solutions of conservation laws with viscosity: Analysis of the Evans function, *Arch. Rational Mech. Anal.* **166**, 99-166.

[65] N. Oreskes, K. Shrader-Frechette, K. Belitz [1994], Verification, Validation, and Confirmation of Numerical Models in the Earth Sciences, *Science* **263**, 641-646.

[66] J. E. Pearson [1993], Complex patterns in a simple system, *Science*, **261**, 189-192.

[67] V. Petrov, S. K. Scott and K. Showalter [1994], Excitability, wave reflection, and wave splitting in a cubic autocatalysis reaction-diffusion system, *Phil. Trans. Roy. Soc. Lond., Series A* **347**, 631-642.

[68] H. van der Ploeg and A. Doelman [2005], Stability of spatially periodic pulse patterns in a class of singularly perturbed reaction-diffusion equations, *Indiana Univ. Math. J.* **54**(5), 1219-1301.

[69] K.Popper [1992]. *The Logic of scientific Discovery*. Hurchinson & Co., London.

[70] J.D.M. Rademacher, B. Sandstede and A. Scheel [2007], Computing absolute and essential spectra using continuation, *Physica D* **229**(2), 166-183.

[71] J.D.M. Rademacher and A. Scheel [2006], Instabilities of wave trains and Turing patterns in large domains, *Int. J. Bif. Chaos*, **17**(8), 2679-2691.

[72] J.D.M. Rademacher and A. Scheel [2006], The saddle-node of nearly homogeneous wave trains in reaction-diffusion systems, *J. Dyn. Diff. Eq.* **19**(2), 479-496.

[73] W. N. Reynolds, J. E. Pearson and S. Ponce-Dawson [1994], Dynamics of self-replicating patterns in reaction diffusion systems, *Phys. Rev. Lett.* **72**, 2797-2800.

[74] M. Rietkerk, M. Boerlijst, F. van Langevelde, H.H.T. J. van de Koppel, L. Kumar, H.H.T. Prins, A.M. de Roos [2001], Self-organization of vegetation in arid ecosystems, *The American Naturalist* **160**(4) 524-530.

[75] W. Rudin [1966]. *Real and Complex Analysis*. McGraw-Hill Book Co.

[76] B. Sandstede [2002], Stability of travelling waves, *Handbook of Dynamical Systems, II* (ed. B. Fiedler), Elsevier, 983-1055.

[77] B. Sandstede and A. Scheel [2000], Absolute and convective instabilities of waves on unbounded and large dounded domains, *Physica D* **145**, 233-277.

[78] B. Sandstede and A. Scheel [2001], On the stability of periodic travelling waves with large spatial period, *J. Diff. Eq.* **172**, 134-188.

[79] P.J. Saunders (ed.) [1992]. *The collected works of A.M. Turing: Morphogenesis.* Amsterdam: North Holland, 1992.

[80] A. Scheel [2003], Radially symmetric patterns of reaction-diffusion systems, *Mem. Amer. Math. Soc.* **165**.

[81] G. Schneider [1998], Nonlinear diffusive stability of spatially periodic solutions - Abstract theorem and higher space dimensions -, *Tohoku Math. Publ.* **8**, 159-168.

[82] L.A. Seghel [1969], Distant sidewalls cause slow amplitude modulation of cellular convection, *J. Fluid Mech.* **38**, 203-224.

[83] A. Shepeleva [1997], On the validity of the degenerate Ginzburg-Landau equation, *Math. Methods Appl. Sci.* **20**, 1239-1256.

[84] A. Shepeleva [1998], Modulated modulations approach to the loss of stability of periodic solutions for the degenerate Ginzburg-Landau equation, *Nonlinearity* **11**, 409-429.

[85] J.A. Sherrat [2005], An analysis of vegetation stripe formation in semi-arid landscapes, *J. Math. Biol* **51** 183-197.

[86] J.A. Sherratt [2010]. Pattern solutions of the Klausmeier model for banded vegetation in semi-arid environments I, *Nonlinearity* **23** 2657-2675.

[87] J.A. Sherratt and G.J Lord [2007], Nonlinear dynamics and pattern bifurcations in a model for vegetation stripes in semi-arid environments, *J. Pop. Biol.* **71** 1-11.

[88] L.A. Smith [2002], What might we learn from climate forecasts?, PNAS *99*, 2487-2492.

[89] M.J. Smith and J.A. Sherratt [2007], The effects of unequal diffusion coefficients on periodic travelling waves in oscillatory reaction-diffusion systems, *Physica D* **236**(2), 90-103.

[90] K. Stewartson, J.T. Stuart [1971], A nonlinear instability theory for a wave system in a plane Poiseuille flow, *J. Fluid Mech.* **48**, 529-545.

[91] J.M. Thiery, J.M. D'Herbes and C. Valentin [1995], A model simulating the genesis of banded vegetation patterns in Niger. *Journal of Ecology* **83** 497-507.

[92] A.M. Turing [1950], The chemical basis of morphogenesis, *Phil. Trans. Roy. Soc. B* **237**, 37-72, reproduced in [79].

[93] A. van Harten [1991], On the validity of the Ginzburg-Landau equation, *J. Nonlinear Sci.* **1** no. 4, 397422.

[94] W. van Saarloos, P.C. Hohenberg [1992], Fronts, pulses, sources and sinks in generalized complex Ginzburg-Landau equations, *Phys. Rev. Lett.* **79**, 213-216.

[95] F. Verhulst [1990]. *Nonlinear Differential Equations and Dynamical Systems.* Springer Verlag.

[96] A.I. Volpert, V.A. Volpert and V.A. Volpert [1994]. *Traveling waves solution of parabolic systems.* Transl. Math. Mono. **140**, Am. Math. Soc., Providence.

[97] M.J. Ward and J. Wei [2003], Hopf bifurcations and oscillatory instabilities of spike solutions for the one-dimensional Gierer-Meinhardt model, *J. Nonl. Sc.* **13**(2), 209-264.

[98] J. Wei and M. Winter [2003], Existence and stability of multiple-spot solutions for the Gray-Scott model in $\mathbb{R}^2$, *Physica D* **176**(3-4), 147-180.

[99] J. Wei and M. Winter [2004], Existence and stability analysis of asymmetric patterns for the Gierer-Meinhardt system, *J. Math. Pures Appl.* **(9) 83**(4), 433-476.

[100] P.L. White [1970]. Brousses tigrés patterns in Southern Niger. *Journal of Ecology* **58** 549-553.

[101] E.P. Wigner [1960]. The unreasonable effectiveness of mathematical models in natural sciences. *Commun. Pure Appl. Math.* **13**.

Summary

Semi-arid ecosystems, ecosystems with an annual precipitation between 250 mm and 500 mm, cover about 30% of the earth's crust. In the fifties, when the first pictures of the earth's surface were taken from outer space, one discovered patterns in many of these ecosystems. Because of their scale, they were often hard to see from the ground. During the last twenty years, theoretical ecologists have become convinced that these vegetation may reveal the imminent threat of desertification – a process that has dramatic ecological and humanitarian consequences.

In 1999, C.A. Klausmeier proposed a model to describe the water infiltration and the vegetation density of semi-arid ecosystems. His model was a reaction-advection-diffusion-system. This thesis generalizes this model and studies the existence and stability of periodic patterns. We call it the *generalized Klausmeier-Gray-Scott model*, since it is a generalization of the Gray-Scott system as well as of the Klausmeier system. The generalized Klausmeier-Gray-Scott system is a so-called *partial differential equation*: the components that are described by it depend on time as well as on space.

More precisely, the generalized Klausmeier-Gray-Scott model describes two components that both depend of time and space: the vegetation density and the water infiltration. The change in time of each of the components depends on different mechanisms. Some of these describe the nonlinear diffusion of water or the 'diffusion' of the vegetation density, an other describes the advection of water, and others describe the uptake of water through the roots of plants. Despite the existence of other (linear) mechanisms that may influence the change of the components in time, these systems are called *reaction-advection-diffusion systems*.

This thesis contributes to the study of periodic patterns described by the Klausmeier-Gray-Scott model. It mainly consists of three parts. The first part deals with the appearance ('rise') of these patterns in a Turing(-Hopf) bifurcation when a system parameter (such as the rainfall or the grazing pressure we mostly consider the rainfall) passes a critical value. The second part deals with the disappearance ('fall') of periodic patterns when the system parameter decreases considerably. The third part describes a novel destabilization mechanism for a class of reaction-diffusion equations.

The appearance of periodic patterns from a homogeneous state can be dealt with

by the derivation of a so-called modulation equation that describes the slow spatial and temporal variation of the amplitude of the periodic patterns near the critical value. The modulation equation that describes this behaviour is called the Ginzburg-Landau equation. In this thesis a Ginzburg-Landau equation is derived for the full Klausmeier-Gray-Scott system with nonlinear diffusion (see chapter 2). We show that the Turing(-Hopf) bifurcation is supercritical for some parameter values of the parameter describing nonlinear diffusion, while it is subcritical for other parameter values. However, the values for which the Turing(-Hopf) bifurcation is supercritical, are not realistic.

The description of periodical patterns when the system parameter is no longer asymptotically close to the critical value for the Turing(-Hopf) bifurcation, can, so far, only be done by very limited analytical methods. However, a thorough study of the instabilities of periodical patters can be done by the application of recently developed numerical methods (see chapter 3). These methods enable us to determine the spectrum of periodic patterns locally near the origin. In this thesis we set out to construct so-called Busse balloons. A Busse balloon is an area in (parameter, wavenumber)-space that consists of stable patterns. The limits are drawn by the instabilities of the periodic pattern. In this thesis we demonstrate that the boundary of Busse balloons for the generalized Klausmeier-Gray-Scott system always consists of either sideband instabilities or Hopf bifurcations, and only in the case of the model for flat ecosystems (no incline) it can also be a fold.

In the third section of this thesis (chapter 4) we deal with the so-called Hopf dance, a novel destabilization mechanism that destabilizes periodical patterns for small values of the rainfall parameter, such that the desert is the only stable state. The Hopf dance is a type of instability that consists of two intertwining Hopf bifurcations. We show that the Hopf dance can be constructed numerically in the Gray-Scott model, and we prove the existence of the Hopf dance in the case of the Gierer-Meinhardt system.

Samenvatting

Semi-aride ecosystemen, ecosystemen met een jaarlijkse regenval tussen de 250 mm en de 500 mm, bedekken 30% van het landoppervlak van de aarde. Toen in de jaren vijftig de eerste luchtfoto's vanuit de ruimte gemaakt werden, ontdekte men dat de vegetatie van veel van deze ecosystemen patronen vertoont, die door de soms grote schaal lastig te zien is op de grond. In laatste decennia zijn theoretisch ecologen er steeds meer van overtuigd geraakt dat deze patronen kunnen wijzen op woestijnvorming – een proces dat zowel ecologisch als humanitair grote gevolgen heeft.

In 1999 formuleerde C.A. Klausmeier een model om de hoeveelheid water en de hoeveelheid biomassa in deze ecosystemen te beschrijven. Het model dat hij voorstelde valt binnen de klasse van reactie-advectie-diffusie systemen. In dit proefschrift wordt dit model gegeneraliseerd, en vervolgens bestuderen we de existentie en stabiliteit van periodieke patronen die dit model beschrijft. Het gegeneraliseerde model noemen wij het *generalized Klausmeier-Gray-Scott model*, omdat het zowel een generalisatie is van het Gray-Scott systeem als van het Klausmeier systeem. Het generalized Klausmeier-Gray-Scott systeem is een zogenaamde *partiële differentiaalvergelijking*: de grootheden die door het systeem beschreven worden hangen af van zowel de tijd als de ruimte.

Preciezer geformuleerd, het generalized Klausmeier-Gray-Scott model beschrijft twee componenten of grootheden, die beide van tijd en ruimte afhangen: de vegetatiedichtheid en de water infiltratie. De verandering van elk van deze componenten in de tijd hangt af van verschillende bijdragen. Sommige hiervan beschrijven de niet-lineaire diffusie van water of de 'diffusie' van vegetatiedichtheid, een andere beschrijft de advectie van water, en weer andere bijdragen beschrijven de opname van water door de wortels van de planten. Omdat de lineaire termen die voor de verandering van de componenten een rol spelen, voor het gemak even vergeten worden, heten deze systemen daarom *reactie-advectie-diffusie-systemen*.

In dit proefschrift valt de studie van de periodieke patronen die beschreven worden door het generalized Klausmeier-Gray-Scott model grosso modo uiteen in drie delen. Het eerste deel betreft het ontstaan van deze patronen in een Turing(-Hopf) bifurcatie als een systeemparameter (bijv. de regenval of de begrazingsdruk – in dit proefschrift met name de regenval) een kritische waarde passeert. Het tweede deel heeft van doen met het verdwijnen van de periodieke patronen als deze parameter vervolgens (veel)

verder afneemt. Het derde deel beschrijft een nieuw instabiliteitsmechanisme voor een klasse van reactie-diffusie vergelijkingen.

Het ontstaan van de periodieke patronen uit een homogene toestand wordt behandeld door het afleiden van een zogenaamde modulatievergelijking die het langzaam variëren van de amplitude van de ontstane patronen beschrijft asymptotisch dichtbij de kritieke waarde. De modulatievergelijking die dit gedrag beschrijft heet de Ginzburg-Landau vergelijking. In dit proefschrift wordt een Ginzburg-Landau vergelijking afgeleid voor het volledige Klausmeier-Gray-Scott systeem met niet-lineaire diffusie (zie hoofstuk 3). We laten zien dat de Turing(-Hopf) bifurcatie voor sommige waarden van de parameter voor niet-lineaire diffusie superkritisch is en voor andere waarden van de parameter voor niet-lineaire diffusie subkritisch. Echter, de waarden voor gamma waarvoor de Turing(-Hopf) bifurcatie superkritisch is, zijn niet realistisch.

Het beschrijven van periodieke patronen als de systeemparameter niet langer asymptotisch dicht bij de kritieke waarde voor de Turing(-Hopf) bifurcatie is, kan vooralsnog maar zeer beperkt middels analytische methoden plaatsvinden. Een grondige studie van de instabiliteiten van periodieke patronen kan echter wel gedaan worden door het aanwenden van recent ontwikkelde numerieke methoden (zie hoofdstuk 3). Deze methoden stellen ons in staat om lokaal (dat wil zeggen, in de buurt van de oorsprong) het spectrum van periodieke patronen te bepalen. In dit proefschrift leggen wij ons toe op de constructie van zogenaamde Busse ballonnen. Een Busse ballon is een gebied in (parameter, golfgetal)-ruimte dat bestaat uit stabiele patronen. De grenzen ervan worden gevormd door instabiliteiten van de periodieke patronen. In dit proefschrift laten we zien dat de instabiliteiten die de rand vormen van Busse ballons voor het generalized Klausmeier-Gray-Scott system altijd ofwel sideband instabiliteiten zijn ofwel Hopf bifurcaties, en alleen in het geval van het model voor vlakke ecosystemen (geen helling) ook een fold.

In derde deel van dit proefschrift (hoofdstuk 4) behandelen we de zogenaamde Hopf dans, een type instabiliteit waardoor periodieke patronen kunnen destabiliseren bij lage regenval, zodat de woestijn de enige stabiele toestand is. De Hopf dans is een type instabiliteit dat bestaat uit twee in en uit elkaar vlechtende Hopf bifurcaties. We laten zien dat de Hopf dans numeriek geconstrueerd kan worden in het Gray-Scott model en we bewijzen het bestaan van de Hopf dans in het geval van het Gierer-Meinhardt systeem.

Dankwoord

Arjen, allereerst mijn woord aan jou. Mijn proefschrift had nooit het huidige niveau bereikt zonder jouw hulp en ik heb veel van je geleerd op wiskundig vlak. Je bent behalve een goed en zeer creatief wiskundige ook een aimabel mens en hoewel je zelf eens grapte dat je ook maar "eenoog in het land der blinden" bent toen we het sociaal verkeer tussen wiskundigen onderling bespraken, weet jij denk ik ook wel dat dat onzin is. Om dit te illustreren wil ik je graag herinneren aan een andere gevleugelde uitspraak van jou, namelijk dat je "nog altijd niet weet wat je wilt worden". Want ofschoon dit misschien zelfs wel een beetje waar is, begreep je goed dat iemand als ik niet een carrière in de wiskunde moet ambiëren, omdat academisch onderzoek in de wiskunde nu eenmaal meer tijd en inspanning van iemand vergt dan *ik* daarvoor willens ben te geven. Een van jouw grootste verdiensten aan mij is dat je me hebt laten zien dat je moet kiezen voor wat je ècht wil, in plaats van alleen het pad te volgen dat voor je ligt. Dank je daarvoor.

Jens, first I want to express my gratitude for your patience in explaining me the same concepts two (or more) times and your endurance during the long AUTO-sessions that we embarked upon together. I think that two people working together in math could hardly have been any more different than you and I, but I hope we have benefited from our cooperation. I certainly have.

Geertje, allereerst vind ik het spijtig – het moet me toch even van het hart – dat we niet onze resultaten over singuliere storingen hebben uitgebreid tot een artikel. Maar hopelijk kan een toekomstige AIO of afstudeerder nog wat met ons materiaal. Ik dank je voor de prettige Skypesessies en de vlijt waarmee je alle fouten uit mijn Ginzburg-Landau berekeningen hebt gevist. Het heeft even geduurd, maar ik ben er nu gerust op dat alles correct is.

Max Rietkerk wil ik graag danken voor de altijd enthousiaste discussies in Utrecht. Ik hoop dat het inmiddels gehonoreerde NWO-project *Critical Transitions and early-warning Signals in Spatial Ecosystems* met Arjen en Jens, dat als vervolg van dit proefschrift gezien kan worden, tot interessante nieuwe inzichten mag leiden.

Ook wil ik hierbij mijn dank uitdrukken voor de prettige werksfeer die dankzij vele collega's op het Korteweg-de Vries Instituut heerst. In het bijzonder gaat mijn dank

Curriculum vitae

Sjors van der Stelt ging van 1992 tot 1998 naar het vwo op Scholengemeenschap Godelinde te Naarden, later Casparus College en thans Vechtstedecollege geheten. In het studiejaar 1998-1999 studeerde hij aanvankelijk natuurkunde en na het eerste trimester wiskunde aan de Universiteit van Amsterdam. Na het behalen van de propedeuse wiskunde in 1999 vervolgde hij een studie in de wiskunde. Hij liep stage bij hedgefund Newtrade N.V. en schreef vervolgens een scriptie onder begeleiding van dr. R.G. de Vilder en dr. A.A. Balkema. Zijn afstudeerscriptie heette: *Modelling Stock Prices*. In augustus 2004 behaalde hij het doctoraal diploma in de wiskunde (cum laude) met bijvakken geschiedenis, natuurkunde, Frans en filosofie. Hij ontving vervolgens een Talentenbeurs van het Ministerie van Onderwijs, Wetenschap en Cultuur en een VSB beurs van het VSB Fonds om een jaar in Parijs colleges te volgen binnen de DEA in de Processus Stochastiques georganiseerd door het Laboratoire de Probabilités et Modèles Aléatoires. Bij terugkomst in Nederland in augustus 2005 werd hij docent aan het Korteweg-de Vries Instituut van de Wiskunde aan de Universiteit van Amsterdam. In 2006 behaalde hij tevens een Master in Teaching of Mathematics aan de Universiteit van Amsterdam.

Vanaf maart 2007 heeft Sjors van der Stelt, tot september 2008 in deeltijd naast zijn functie als docent, en vanaf september 2008 in voltijd, gewerkt aan een onderzoek van wiskundige modellen voor vegetatiepatronen in semi-aride ecosystemen, dat heeft geleid tot het onderhavige proefschrift. Hij heeft dit gedaan onder begeiding van prof. dr. A. Doelman, dr. G.M. Hek en dr. J.D.M. Rademacher. In het kader hiervan gaf hij voordrachten tijdens de Dynamics of Patterns Days in mei 2009 en november 2010, de SIAM Conference on Applications of Dynamical Systems ("Snowbird") in mei 2009, de Workshop Nonlinear Dynamics of Natural Systems in april 2010 en het Nederlands Mathematisch Congres 2011. In de studiejaren 2007-2008 en 2008-2009 organiseerde hij mede het AIO Seminarium.

Vanaf mei 2008 tot mei 2011 was hij daarnaast in functie als secretaris (tot maart 2010) en voorzitter (tot mei 2011) van het bestuur van Woningvereeniging "Het Nieuwe Huis" dat in deze periode een grondige renovatie van het flatgebouw 'Het Nieuwe Huis' aan het Amsterdamse Roelof Hartplein heeft begeleid. Bovendien heeft hij van oktober 2006 tot augustus 2010 gewerkt aan de herziening van de tekst en de financiering middels fondsen van de tweede druk van het boek *De Bomen in Artis en Hortus*,

dat in september 2010 verscheen. Ook was hij tijdens de periode van september 2008 tot oktober 2010 op donderdagavond werkzaam als klepper bij brasserie Harkema. Daarnaast volgde hij aan de Schrijversvakschool te Amsterdam op zaterdagen tijdens de lente van 2010 een cursus Proza. Vanaf mei 2011 is hij halve weken en vanaf oktober 2011 fulltime werkzaam als quantitatief risico analist bij ABN AMRO N.V.